RESEARCH & DEVELOPMENT

Implementation of Shadow Performance-Related Specifications for an Asphalt Paving Project

Y. Richard Kim, Ph.D., P.E., F. ASCE

Jaehoon Jeong

Dept. of Civil, Construction, & Environmental Engineering

North Carolina State University

NCDOT Project 2017-29

FHWA/NC/2017-29

July 2020

Implementation of Shadow Performance-Related Specifications for an Asphalt Paving Project

FINAL REPORT

Submitted to:

North Carolina Department of Transportation
(Project No. HWY-2017-29)

Submitted by:

Y. Richard Kim, Ph.D., P.E., F.ASCE
Jimmy D. Clark Distinguished University Professor
Campus Box 7908
Department of Civil, Construction & Environmental Engineering
North Carolina State University
Raleigh, NC 27695-7908
Tel: 919-515-7758, Fax: 919-515-7908
kim@ncsu.edu

Jaehoon Jeong
Graduate Research Assistant

Department of Civil, Construction, and Environmental Engineering
North Carolina State University
Raleigh, NC

July 2020

TECHNICAL REPORT DOCUMENTATION PAGE

1. Report No. FHWA/NC/2017-29	2. Government Accession No.	3. Recipient's Catalog No.
4. Title and Subtitle North Carolina Department of Transportation Shadow Project for the Development of Performance-Related Specifications		5. Report Date July 14, 2020 6. Performing Organization Code:
7. Author(s) Y. Richard Kim, Ph.D., P.E., Jaehoon Jeong		8. Performing Organization Report No.
9. Performing Organization Name and Address Box 7908, Dept. of Civil, Construction, & Environmental Engineering, NC State University, Raleigh, NC 27695		10. Work Unit No. 11. Contract or Grant No.
12. Sponsoring Agency Name and Address Federal Highway Administration 6300 Georgetown Pike McLean, VA 22101-2296		13. Type of Report and Period Covered Final Report, Nov. 1, 2016 – Dec. 31, 2019 14. Sponsoring Agency Code RP 2017-29
15. Supplementary Notes		

16. Abstract

This report describes the selection and implementation of a shadow project conducted by the North Carolina Department of Transportation (NCDOT) for the Federal Highway Administration's asphalt mixture performance-related specifications (PRS). The overall shadow project process started with the NCDOT selecting a field project to serve as the shadow project. The selected project uses RS9.5C, RI19.0C, RB25.0C mixtures as the surface, intermediate, and base layers, respectively. The North Carolina State University research team acquired 27 mixture samples from the three asphalt layers of the project. The team performance-tested the RS9.5C and RI19.0C mixture samples (using the 'four corners' procedure) for calibration and verification of the performance-volumetric relationships (PVRs) that were developed for the selected mixtures. Once the PVRs were developed, pavement performance was predicted using the mixtures' volumetric properties that were measured in accordance with typical acceptance practices. The verification results revealed that the PVR functions developed for the tested mixtures worked reasonably well to predict pavement performance under the volumetric conditions of the verification samples. The PVRs also were used to evaluate the effects of field construction variability on pavement performance by applying the developed PVRs to measured acceptance quality characteristics. Reasonable trends were found between pavement performance and in-place density. However, the effects of binder content were not captured well by the PVRs due to the narrow range of binder contents in the tested samples that were used to develop the PVRs. Overall, the shadow project's test results were found to predict pavement performance as a function of acceptance quality characteristics in the context of PRS reasonably well.

17. Key Words	18. Distribution Statement
Shadow project, asphalt pavement, performance-related specification, AMPT, performance-volumetric relationship, four corners, FlexMAT^{TM}, FlexPAVE^{TM}, quality assurance	No restrictions. This document is available to the public through the National Technical Information Service, Springfield, VA 22161. http://www.ntis.gov

19. Security Classif. (of this report)	20. Security Classif. (of this page)	21. No. of Pages	22. Price
Unclassified	Unclassified	95	N/A

Form DOT F 1700.7 (8-72) Reproduction of completed page authorized.

DISCLAIMER

The contents of this report reflect the views of the authors and are not necessarily the views of North Carolina State University. The authors are responsible for the facts and the accuracy of the data presented herein. The contents do not necessarily reflect the official views or policies of the North Carolina Department of Transportation at the time of publication. This report does not constitute a standard, specification, or regulation.

ACKNOWLEDGEMENTS

This research was sponsored by the North Carolina Department of Transportation. The Steering and Implementation Committee was comprised of Wiley Jones, III, P.E. (Chair), Todd Wayne Whittington, P.E., Charles R. Colgate, Clark Morrison, Ph.D., P.E., Christopher A. Peoples, P.E., James B. Phillips, P.E., Lamar Sylvester, P.E., Neil Mastin, P.E., and Mustan Kadibhai, P.E. (PM). These advisors have given invaluable direction and support to the research team throughout the project.

EXECUTIVE SUMMARY

This report describes the selection and implementation of a shadow project conducted by the North Carolina Department of Transportation (NCDOT) for the Federal Highway Administration's asphalt mixture performance-related specifications (PRS). The overall shadow project process started with selecting a field project to serve as the shadow project. The NCDOT chose a new full-depth asphalt pavement on Carr Road in Durham, NC for the project. The North Carolina State University (NCSU) research team acquired a total of 27 mixture samples from the surface (RS9.5C mixture), intermediate (RI19.0C mixture), and base (RB25.0C mixture) layers. The research team tested the RS9.5C and RI19.0C mixtures using the suite of Asphalt Mixture Performance Tester (AMPT) performance tests. The AMPT test results then were input to FlexPAVE^{TM} v. 1.1, a three-dimensional finite element program, to predict the fatigue cracking (*% damage*) and rutting performance of standard pavement structures. The research team developed performance-volumetric relationships (PVRs) based on the pavement performance predicted by FlexPAVE^{TM} and the volumetric properties of the so-called 'four corners' samples. The primary benefit of PVRs is that pavement performance can be predicted based on the mixture's volumetric properties that are measured for typical acceptance practice. The verification results revealed that the PVRs developed for the tested mixtures worked reasonably well to predict pavement performance under the volumetric conditions of the verification samples. The average error percentages for *% damage* and rut depth between the FlexPAVE^{TM} simulations and PVR predictions were 8.7% and 21.1% for the RS9.5C mixture and 5.1% and 16.7% for the RI19.0C mixture, respectively. The rut depth results show relatively higher *% error* values than the *% damage* values because the numerical rut depth values are generally lower than the *% damage* values. Although the rut depth predictions show relatively high *% error* values, the numerical differences in rut depth between the FlexPAVE^{TM} predictions and the PVR predictions did not exceed 1 mm, except for one sample. The PVRs also were used to evaluate the effects of field construction variability on pavement performance by applying the measured acceptance quality characteristics to the developed PVRs. Reasonable trends were found between the pavement performance and in-place density values. However, the effects of binder content were not captured well by the PVRs due to the narrow range of binder content in the tested samples that were used to develop the PVRs. Overall, the shadow project's test results were found to predict pavement performance as a function of acceptance quality characteristics in the context of PRS reasonably well.

TABLE OF CONTENTS

LIST OF FIGURES

LIST OF TABLES

LIST OF ABBREVIATIONS

Item	**Definition**
AM-PRS	Asphalt Mixture Performance-Related Specifications
APS	Average Permanent Strain
AMPT	Asphalt Mixture Performance Tester
AQCs	Acceptance quality characteristics
DMR	Dynamic modulus ratio
JMF	Job mix formula
LVDT	Linear variable differential transformer
NCSU	North Carolina State University
NCDOT	North Carolina Department of Transportation
NMAS	Nominal maximum aggregate size
PVR	Performance-volumetric relationship
QA	Quality assurance
RAP	Reclaimed asphalt pavement
RSI	Rutting Strain Index
SSR	Stress sweep rutting
S-VECD	Simplified viscoelastic continuum damage
VFA	Voids filled with asphalt
VMA	Voids in mineral aggregate

CHAPTER 1. INTRODUCTION

An important task for highway agencies is to ensure that pavements are properly constructed so that they will perform well over their intended service life. The process that agencies follow to achieve this task is quality assurance (QA) and, when combined with the contractor's quality control process, a project delivery specification can be used to ensure that appropriate pavement longevity is achieved and that contractors are compensated properly for their work. Today, the acceptance quality characteristics (AQCs) that are used in most quality-related specifications are the volumetric properties of asphalt mixtures because such properties are easily quantifiable, relatively repeatable, and are known to impact pavement longevity. The problem, however, is that the precise relationship between the volumetric properties and pavement performance can vary based on the materials' qualities, and thus, strict volumetric control introduces considerable uncertainty with regard to the pavement performance.

One approach to overcoming this limitation is to use specifications that incorporate material and construction characteristics that are related more closely to performance, i.e., so-called performance-related specifications (PRS). Transportation Research Circular E-C137 defines PRS as "quality assurance specifications that describe the desired levels of key materials and construction quality characteristics that have been found to correlate with fundamental engineering properties that predict performance" (Transportation Research Board 2009). Furthermore, "True PRS … employ the quantified relationships containing the characteristics to predict as-constructed pavement performance. They thus provide the basis for rational acceptance/pay adjustment decisions." So, the key advantages of PRS lie in their focus on AQCs that directly correlate with fundamental engineering properties. The specific correlation can be material-dependent but should be characterizable through supplementary testing and evaluation that may not be part of current agency quality specifications. Other advantages of PRS include that they: (1) motivate contractors to improve pavement construction quality by offering monetary incentives for pavements that perform better than the design pavement, (2) allow and encourage contractors to be innovative and competitive, (3) assign distinct roles and responsibilities for agencies and contractors, and (4) result in better performing pavements.

Due to these benefits of PRS, the Federal Highway Administration (FHWA) has targeted PRS as a "vision for the future" and currently is putting much effort toward developing asphalt mixture PRS (AM-PRS). AM-PRS, hereinafter referred to as PRS for simplicity, are implemented through (1) fundamental material tests that use the Asphalt Mixture Performance Tester (AMPT), (2) analyses that employ mechanistic performance prediction models, (3) development of performance-volumetric relationships (PVRs), and (4) pay tables that are based on pavement life differences between as-designed and as-constructed pavements.

The implementation of PRS by highway agencies requires that the agency first establish a local material database using the AMPT test results. This database can be established by conducting performance-engineered mixture design using typical mixtures found in the agency's individual mixture classifications. Once the local material database becomes available and when a PRS project is identified, the agency can use the material properties stored in the database along with the project-specific pavement structure, climate conditions, and traffic information to develop PVRs that are specific to the project in question. These PVRs can in turn be used to predict the service life of the pavement that has different AQC levels. Pay tables for the different AQC levels then would be developed based on the predicted life and agency-specific cost models, and contractors would be paid according to the pay table. One of the major advantages of such PVR-based PRS is that the current AQC collection process can be employed without needing to make any changes to it.

The primary goal of a FHWA shadow project is to demonstrate to the participating agency the acceptance process of the project and the payment process for the contractor if PRS are used as the contract document. In other words, the shadow project aims to demonstrate the benefits that the shadow agency will gain if PRS are adopted as the agency's QA specifications. The second goal is for the shadow agency to understand the ways that the PRS may impact the agency's general testing and volumetric-based acceptance operations. As most agencies may not be familiar with PRS, an important part of the shadow project is to help the shadow agency understand the general procedures in the PRS by performing each step, one by one. To achieve these goals, several activities, including an AMPT workshop, on-site training, regular conference calls, and proficiency testing, are undertaken as part of the shadow project.

With regard to this shadow project and final report specifically, the shadow agency is the North Carolina Department of Transportation (NCDOT) and the support institution whose researchers aided NCDOT personnel in performing the FHWA PRS procedures is North Carolina State University (NCSU). The structure of the remainder of this report is as follows. Chapter 2 briefly describes the test methods, models, and software programs that are used for the FHWA PRS. Chapter 3 presents the different steps that are involved in a general shadow project. Chapter 4 describes the actual steps taken in the shadow project conducted by the NCDOT and the research team, including the research efforts that were undertaken to develop and verify the PVRs that were developed from the NCDOT's shadow project data. Chapter 5 discusses the application of the developed PVRs to the collected field samples. Finally, conclusions drawn from this NCDOT shadow project are given in Chapter 6.

CHAPTER 2. TEST METHODS, MODELS, AND SOFTWARE PROGRAMS REQUIRED FOR FHWA SHADOW PROJECTS

AMPT Testing

In order to estimate pavement responses under certain conditions, which include the pavement structure, climate, and traffic speed and volume, a basic relationship must be defined between the stress and strain in the various simulated layers in a model, and this relationship should be as similar as possible to the relationship between the *in situ* actual stresses and strains in a real pavement. Because asphalt concrete (AC) is a viscoelastoplastic material, the actual pavement responses have elastic, plastic, and viscous or time- or rate-dependent components and are dependent on a variety of factors, such as temperature, load level, loading time, and stress/strain level. In this sense, mixture-specific properties are essential for accurate response analysis. AMPT testing allows such mixture-specific behavior to be characterized in the lab prior to software simulations and analyses for determination of material properties and eventually pavement performance.

Three AMPT performance tests constitute the basis for PRS: dynamic modulus test, direct tension cyclic fatigue test, and stress sweep rutting (SSR) test. In order to run these tests, shadow project agencies must have facilities for asphalt mixture fabrication, including an oven, gyratory compactor, and miscellaneous tools (pans, scoops, spatulas, etc.), and test specimen preparation equipment, including a coring machine, saw, air void measurement equipment, etc. The three AMPT tests employ cylindrical specimens of two specimen geometries: small (38-mm diameter and 110-mm height) geometry for the dynamic modulus test and the cyclic fatigue test and large (100-mm diameter and 150-mm height) geometry for the SSR test in accordance with AASHTO specifications. For the dynamic modulus and cyclic fatigue tests, the minimum requirement is three small cylindrical test specimens for each test. For the SSR tests, two large cylindrical specimens should be used for each of two temperature tests (high-temperature and low-temperature tests). Therefore, six gyratory-compacted samples are needed to complete one set of AMPT tests. Table 1 provides a summary of the AMPT testing requirements for PRS shadow projects.

Table 1. Shadow Project AMPT Test Requirements

Specimen Geometry	Testing	AASHTO Specifications	Number of Gyratory-Compacted Samples	Number of Test Specimens
Large Cylindrical	Sample Preparation	R 83	-	-
Large Cylindrical	Stress Sweep Rutting	TP 134	4	2 (low temp.) 2 (high temp.)
Small Cylindrical	Sample Preparation	PP 99	-	-
Small Cylindrical	Dynamic Modulus	TP 132	1	3
Small Cylindrical	Cyclic Fatigue	TP 133	1	3

Dynamic Modulus Tests

The dynamic modulus is a performance-related property that can be used for mixture evaluation and for characterizing the stiffness of hot mix asphalt. The dynamic modulus value is the absolute value or the norm of the complex modulus, which is determined by calculating the ratio of stress amplitude to strain amplitude for a material subjected to sinusoidal loading.

Asphalt concrete is a linear viscoelastic material at small strain levels (i.e., between 50 and 75 microstrain) and is also known as being thermorheologically simple, which implies that the effects of loading frequency and temperature can be combined into a single parameter called reduced frequency, which in turn can be used to produce a single curve (or 'mastercurve') that describes the dynamic modulus ($|E^*|$) using time-temperature shift factors, as shown in Figure 1. Once the mastercurve is developed, dynamic modulus values can be predicted for any combination of temperature and loading frequency within the measured parameters and extrapolated for values outside the measured range.

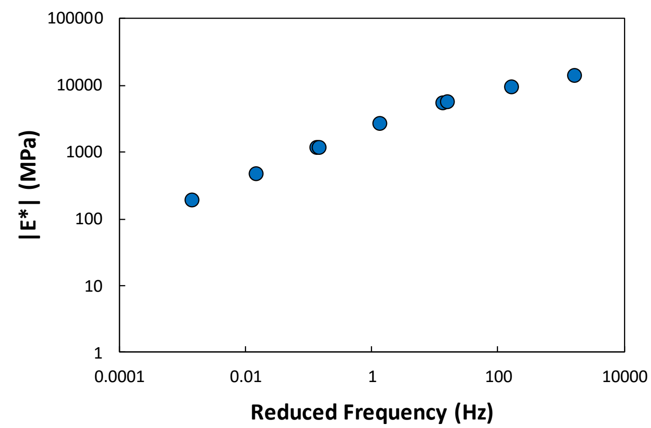

A. Example of dynamic modulus mastercurve.

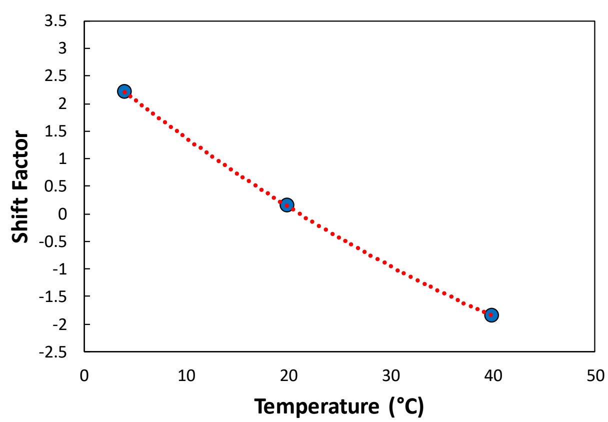

B. Example of time-temperature (t-T) shift factor.

Figure 1. Graph. Example of dynamic modulus mastercurve and time-temperature (t-T) shift factor.

Dynamic modulus tests are conducted at three different loading rates (10 Hz, 1 Hz, and 0.1 Hz) and three temperatures (4°C, 20°C, and 40°C). The AMPT measures the strain, obtained from three LVDTs (linear variable differential transducers), of the sinusoidal load that is applied to the test specimen and automatically calculates the material properties, which include the dynamic modulus, phase angle, and other data quality parameters when the allowable strain range (50 to 75 microstrain) is input during the test, and the test loading frequencies. Then, the test results are imported to FlexMAT™ software to develop the dynamic modulus mastercurve and time-temperature shift factors.

Direct Tension Cyclic Fatigue Tests

The direct tension cyclic fatigue test is an actuator displacement-controlled test that applies repeated cyclic loadings to a test specimen until the specimen fails. The test results include applied stress values, on-specimen axial strain responses, and the number of cycles to failure and are used to calibrate the coefficients in the simplified viscoelastic continuum damage (S-VECD) model. The S-VECD model allows the prediction of the fatigue damage evolution in a mixture under moving traffic loads and realistic climate conditions using FlexPAVE™.

Direct tension cyclic fatigue tests are conducted at 3°C below the temperature at the average performance grade (PG); e.g., 18°C when the mixture contains PG 64-22 binder. The AMPT software asks the user to run the dynamic modulus fingerprint test to estimate the modulus value at the test temperature prior to fatigue testing. Users then input a certain strain level obtained from Table X1 in AASHTO TP 133 based on the fingerprint test results.

The major outputs of this test are the damage characteristic curve, also known as the material integrity (C) versus damage (S) curve, and the pseudo energy-based failure criterion, designated as D^R, as shown in Figure 2. The damage characteristic curve represents the fundamental relationship between C and S for asphalt mixtures in Figure 2-A. D^R is as an average reduction in pseudo stiffness up to failure. D^R is determined as a ratio of the sum of (1-C) to failure to the number of cycles to failure, which is the slope of the linear relationship in Figure 2-B (Wang and Kim 2017). Both the damage characteristic curve and D^R failure criterion are independent of temperature, frequency, and mode of loading. Combined with the linear viscoelastic properties, the damage characteristic curve can be used to predict how fatigue damage grows in asphalt mixtures as fatigue loading continues, and the D^R criterion determines the moment of the failure. These properties also can be used in a pavement structural analysis model to predict the fatigue performance of asphalt pavements. Lastly, the cyclic fatigue test results can be used to determine a fatigue index parameter, S_{app}. The S_{app} parameter represents the effects of a material's modulus and toughness on its fatigue resistance and is a measure of the amount of fatigue damage the material can tolerate under loading (FHWA 2019). Higher S_{app} values indicate better fatigue resistance of the mixture. Figure 3 shows some examples of how different mixture factors affect the S_{app} values.

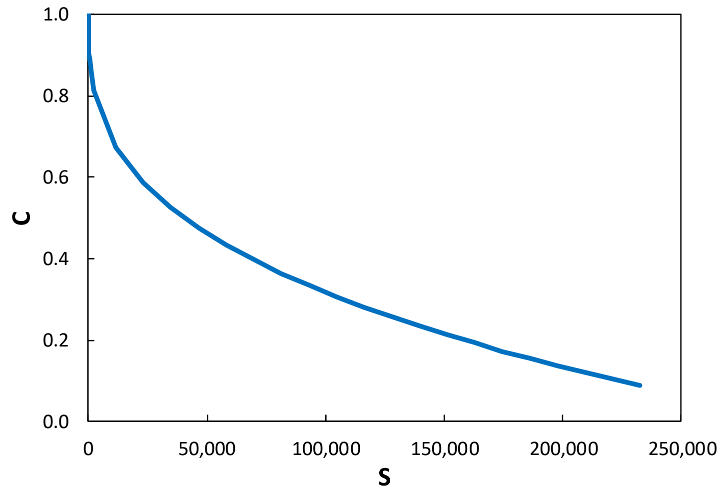

A. Damage characteristic curve.

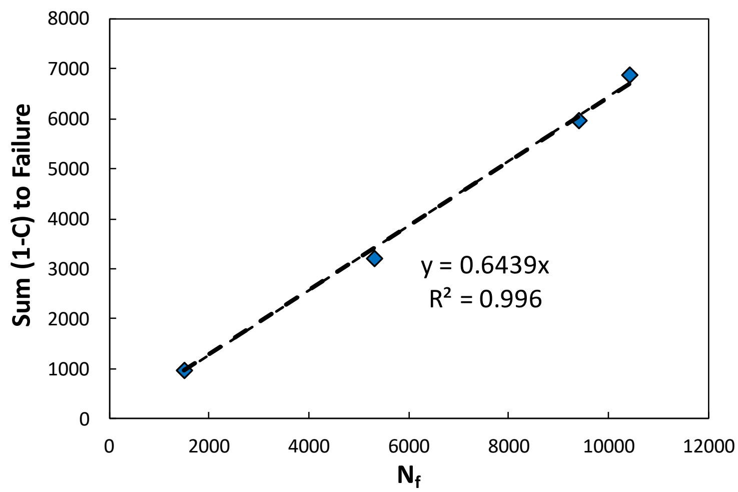

B. Pseudo energy-based failure criterion.

Figure 2. Graph. Major outputs from the direct tension cyclic fatigue test.

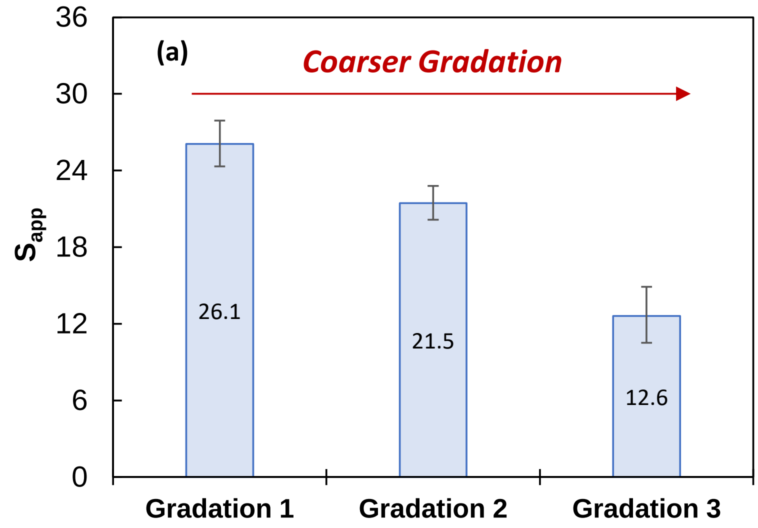

A. Effects of aggregate gradation on S_{app}.

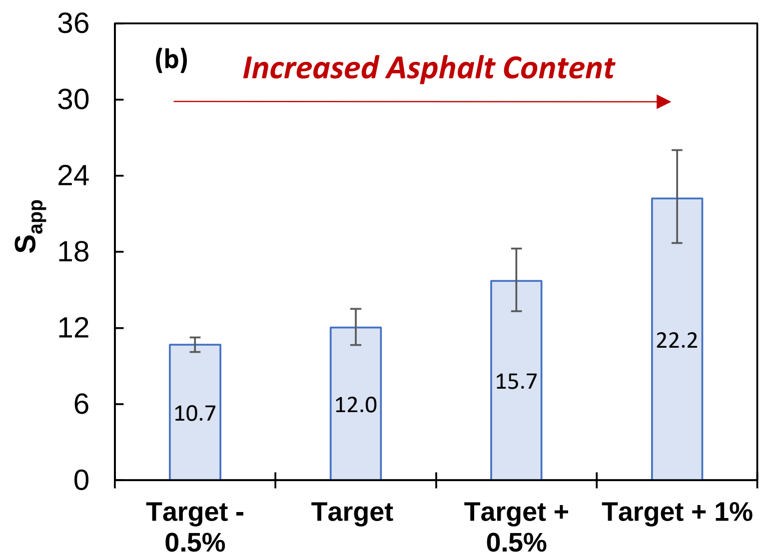

B. Effects of binder content on S_{app}.

Figure 3. Graph. Effects of mixture factors on the fatigue index parameter S_{app}.

Stress Sweep Rutting (SSR) Tests

The SSR test measures the permanent deformation characteristics of an asphalt mixture as a function of deviatoric stress, loading time, and temperature, which all change with pavement depth. The results from four SSR tests, two from each of the high and low temperatures, can be used to develop the shift permanent deformation model. The shift model not only describes the permanent deformation behavior of an asphalt mixture at the material level, but also allows engineers to incorporate the permanent deformation material properties into a pavement structural analysis model to predict the long-term rutting performance of pavements.

SSR tests are conducted at two test temperatures and under the constant confining pressure of 69 kPa (10 psi) with three 200-cycle loading blocks for each of three deviatoric stress levels. The load pulse is 0.4 second for each cycle and the rest period is 1.6 seconds for the low-temperature test and 3.6 seconds for the high-temperature test. The test temperatures are determined according to AASHTO TP 134 and depend on the geographic locations where the mixtures would be used. The AMPT applies confining pressure to the test specimens for an hour prior to SSR testing. The test automatically begins after an hour of confinement.

A rutting index parameter, designated as RSI (Rutting Strain Index), is based on the shift permanent deformation model that is characterized by the SSR test (Ghanbari et al. 2020). The RSI is the average permanent strain and is defined as the ratio of the permanent deformation in an asphalt layer to the thickness of that layer at the end of a 20-year pavement service life with 30 million 18-kip standard axle load repetitions for a standard structure. The RSI is presented in percent. A mixture with a lower RSI value has greater resistance to rutting. Effects of mixture factors on the RSI values is presented in Figure 4.

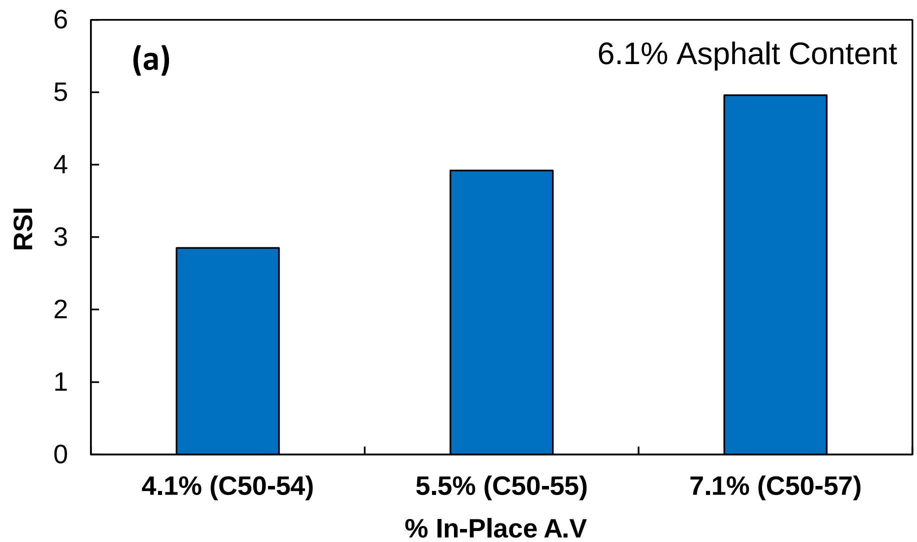

A. Effects of in-place density on RSI.

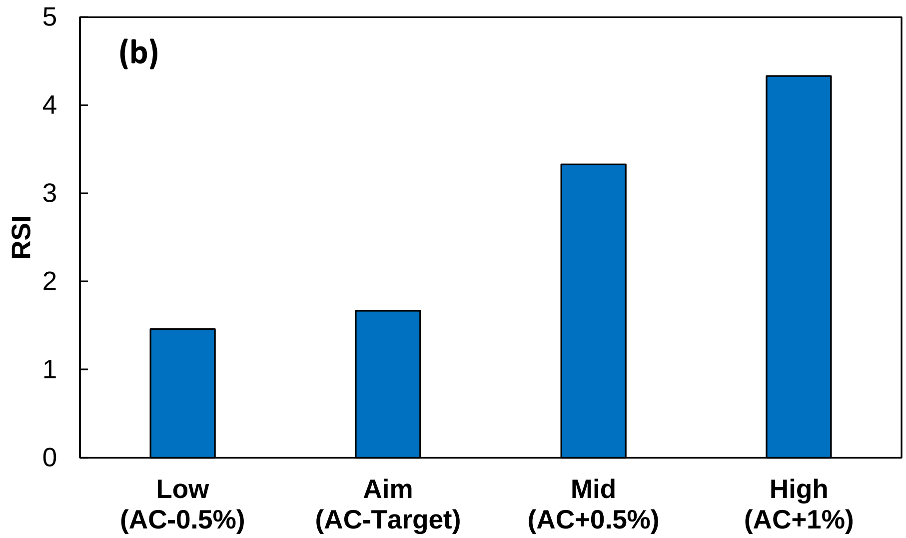

B. Effects of binder content on RSI.

Figure 4. Graph. Effects of mixture factors on RSI.

Mixture-Level Data Analysis Using FlexMAT™

The AMPT test results are input to FlexMAT™ for mixture-level analysis. The research team developed two different Excel-based data analysis software packages, FlexMAT™ Cracking and FlexMAT™ Rutting, to characterize performance models using data files generated by the AMPT. FlexMAT™ Cracking analyzes the dynamic modulus test results and the cyclic fatigue test results. From the dynamic modulus data, FlexMAT™ Cracking determines the time-temperature shift factor and Prony series model coefficients. The dynamic modulus analysis results are integrated with the direct tension cyclic fatigue test results to determine the damage characteristic curve, the D^R failure criterion, and the S_{app} index parameter. In addition, this template can be used to predict fatigue life at any strain amplitude, temperature, and loading frequency of interest. The FlexMAT™ Rutting template calculates the shift permanent deformation model parameters as well as the RSI parameter.

Using simple clicks, FlexMAT™ also generates output files, which then can be used in the pavement performance analysis software, FlexPAVE™.

Pavement Performance Simulations Using FlexPAVE™

FlexPAVE™ is software that also was developed by the research team. This software employs VECD theory to account for the effects of loading rate and temperature on pavement responses and distress mechanisms. FlexPAVE™ allows the simulation of pavement structures that consist of AC and unbound materials. Each AC layer can be assigned various material properties by inputting the output files that are generated from FlexMAT™. Lastly, project location, traffic conditions, and design vehicle configurations can be assigned for the given project. Climatic conditions are determined using the Enhanced Integrated Climatic Model based on the project location.

The major output from FlexPAVE^{TM} simulations is pavement performance predictions, which are provided in the form of damage percentage (*% damage*) and rut depth (cm) over the design life of the pavement. Note that, at the time of this writing, fully verified transfer functions are not available for FlexPAVE^{TM}.

CHAPTER 3. GENERAL SHADOW PROJECT PROTOCOL

Although the focus of this report is the NCDOT shadow project, this chapter provides the overall protocol for any FHWA shadow project that is aided by the research team. The primary events that take place during a complete shadow project are as follows: a two-day AMPT hands-on training workshop held at, on-site training at the shadow agency's facility, proficiency testing by both the shadow agency and the research team for comparative purposes, performance-engineered mix design, development of PVRs for the project-specific conditions, development of service life tables using PVRs, the collection of construction mixture samples, acceptance testing of the mixture samples, AMPT testing of the samples by both the shadow agency and the research team, verification of the PVRs using the performance data from the AMPT tests, and application of the life tables by the shadow project agency. The following terms are defined for this shadow project to avoid confusion.

- Mixture: A mixture that is employed for the shadow project.
- Sample: A sample is obtained from mixtures that are produced based on the same job mix formula (JMF) but obtained from different truck loads.
- Specimen: A specimen is cored and cut from a gyratory-compacted mixture sample and used for performance tests.

AMPT Hands-on Training Workshop and On-site Training

The research team provides two types of AMPT training for agency personnel prior to beginning a shadow project: a two-day AMPT workshop held at NCSU and an on-site training session held at the agency's laboratory.

For the AMPT workshop, the research team provides hands-on training for laboratory test procedures and analysis protocol. All the participants of the workshop go through a half-day session introducing the PRS concept, AMPT test methods, models, and software programs. Then the participants are grouped into the technician team and engineer team. The technician team learns about test specimen preparation, AMPT operations, and test procedures, and the data analysis team learns to analyze the test results using FlexMAT™ and FlexPAVE™.

The primary aim of the on-site training is to train the agency personnel to conduct AMPT tests in the agency's lab. A member of the research team visits the shadow project agency and reviews all the shadow project test procedures with agency personnel. The on-site training also serves to provide a comprehensive check on the current conditions of the agency's lab and to ensure that the items needed to run the AMPT tests are available and operational. An NCSU trainer checks and records the current condition of the agency's lab to determine whether any modifications or improvements are necessary. The on-site training, like the AMPT workshop, typically takes two days.

In addition to these face-to-face training sessions, various resources are available in Google Drive to shadow agencies (https://drive.google.com/drive/folders/1A3ia3BWRyF_drErXYOce26UeQbhbaIJl). These resources include AMPT hands-on training workshop notes, FlexMAT™ and FlexPAVE™ software programs, manual and video clips on sample fabrication and AMPT testing, and shadow project guidelines.

Proficiency Testing

The proficiency tests are conducted after the AMPT on-site training has been completed. The shadow project agency and the research team each conduct AMPT performance tests using the same mixture. Then, the research team compares the two sets of test results. This process constitutes proficiency testing and consists of the following steps:

a. The shadow project agency fabricates 12 gyratory-compacted samples using a mixture that is commonly used by that agency and targets 5% ± 0.5% air void content for the cored and cut test specimens.
b. The shadow project agency ships six randomly selected gyratory-compacted samples to the research team.
c. Using the six retained specimens, the agency cores and cuts two gyratory-compacted samples to make eight small specimens for the dynamic modulus and cyclic fatigue tests and cores and cuts the remaining four gyratory-compacted samples for the SSR tests.
d. The research team performs the same coring and cutting procedure using the six specimens that the agency shipped to the University.
e. Both the shadow project agency and the research team run the three AMPT tests.
f. The agency sends its AMPT test results to NCSU. The research team analyzes the data, compares the agency's results to the NCSU reference test results, and holds a debriefing call with agency personnel to discuss the results and any associated protocol concerns.

The two main purposes of the proficiency tests are to (1) familiarize the shadow agency's personnel with the test equipment and processes prior to testing during the actual shadow project and (2) check whether the performance test results generated by the agency are repeatable compared to the results generated by the research team. Once the test results are considered reasonable, the agency is considered to be proficient with regard to conducting AMPT tests. Then, the PRS shadow project can begin.

Shadow Project Selection

Once the proficiency testing is completed, the agency selects an actual construction project to serve as the shadow project. The selection guidelines for the shadow project include that the project must use a mixture that is part of a mainline pavement structure (e.g., not used in ramps, shoulders, aprons, intersections, or turning lanes). Second, the project should be large enough that the mixture must be placed over multiple days to simulate the variability that naturally occurs over the course of large projects. The agency is asked to obtain samples from ten different truck loads for the shadow project (to assess variability). For projects that involve multiple mixture types (e.g., surface and intermediate layers), the agency has the option to sample from each of the mixture types. In these cases, the agency is required to sample ten times for each mixture type that is included in the study.

Mixture Sampling

As the next step, the agency acquires the asphalt mixture to be used for the AMPT tests from the selected project following the AASHTO T 168 method. As mentioned, the agency is asked to obtain ten samples from ten different truck loads, which allows the research team to investigate meaningful variations among the ten samples. Approximately 400 lb of asphalt mixture samples must be acquired from each truck, and the acquired samples should be stored in a sealed container and kept in temperature-controlled storage before they are shipped to the research team. In addition, the agency should track the field locations where the ten samples were obtained, referring to station and truck numbers, in order to measure field densities.

Quality Assurance Test Results for Field Samples

The agency should conduct volumetric tests using its own method and the acquired samples to measure the AQCs, i.e., design air void contents, voids in mineral aggregate (VMA) and voids filled with asphalt (VFA) at the compaction design level (N_{des}), maximum specific gravity, and binder content. The in-place densities (or in-place air voids) at the places where the ten samples were paved should be provided to the research team along with the AQCs. The in-place density measuring method and the number of replicates can vary for the shadow agency's project-specific conditions. The shadow agency should use its current method to evaluate the in-place densities for the shadow project.

Table 2 shows an example of general shadow project AQC results and in-place densities of field samples. Note that the AQCs and in-place densities are used to calculate the samples' volumetric characteristics. The calculated volumetric characteristics are then used to calibrate and build the mixture's PVRs. Prior to the PVR calibration process, the samples are assigned to be used either for PVR calibration or for PVR verification. The agency keeps the calibration samples to run the AMPT tests and sends the rest of the samples, i.e., the verification samples, the AQC data, and the in-place density data to the research team. (This testing plan varies for different agencies, depending on their proficiency of the AMPT testing and availability of resources.)

Table 2. Example of Acceptance Test Results of Field Samples

Sample ID	Sampling Date	G_{sb}	G_{mm}	Air Void (%) at N_{des}	Binder Content (%)	VMA (%) at N_{des}	VFA (%) at N_{des}	In-place Density (%)
Sample 1	3/18/2019	2.680	2.427	3.9	5.8	15.5	83	93.2
Sample 4	3/22/2019	2.680	2.429	4.3	5.6	14.3	88	94.1
Sample 10	3/28/2019	2.680	2.432	3.1	5.5	14.0	89	94.5

Note: G_{sb} is aggregate bulk specific gravity, G_{mm} is maximum specific gravity, N_{des} is the design compaction level, VMA is voids in mineral aggregate, VFA is voids filled with asphalt.

AMPT Tests of Field Samples

The protocols for the three AMPT tests conducted during shadow projects are identical to those used for the proficiency tests (see CHAPTER 2). The shadow project agency and the research team each conduct AMPT tests using target air void contents that were determined during the

PVR calibration phase. For the data analyses, FlexMAT™ and FlexPAVE™ utilize the AMPT test results to simulate pavement performance.

Performance-Volumetric Relationship Calibration

The underlying concept of the PVR is that the performance of an asphalt mixture under any volumetric conditions can be predicted by testing the asphalt mixture at a few selected volumetric conditions; then, the relationship between the mixture's performance and the volumetric conditions can be developed. A previous study by the research team (Wang et al. 2019) suggests that four volumetric conditions are sufficient to develop the PVR for a given mixture. These four volumetric conditions (hereinafter called 'four corners' due to their furthest distance from each other within the quadrangular range of the volumetric conditions) should be selected at the widest points within the range of volumetric conditions in order to capture the performance of the mixture at any given volumetric condition. For shadow projects, the four corners are defined by first selecting three to four construction samples and compacting them to the lowest and highest air void contents the agency's specifications allow. CHAPTER 4 provides details regarding selection of the samples for PVR calibration using data obtained from an actual shadow project.

In order to make PVRs simple equations, the samples' volumetric characteristics need to be simplified. The in-place VMA (VMA_{IP}) and in-place VFA (VFA_{IP}) are used to represent the samples' volumetric characteristics. The *% damage* and permanent deformation (rut depths) of the asphalt mixture are obtained from the FlexPAVE™ simulations. A linear function is employed for the PVR development and is based on findings from the previous study by the research team (Wang et al. 2019). Two PVR equations are used for *% damage* and rut depth, as shown in equations (1) and (2), respectively.

$$\% \, damage = a_f \times VMA_{IP} + b_f \times VFA_{IP} + d_f \qquad (1)$$

$$Rut\,Depth\,(mm) = a_r \times VMA_{IP} + b_r \times VFA_{IP} + d_r \qquad (2)$$

where

VMA_{IP} = the in-place VMA,

VFA_{IP} = the in-place VFA,

a_f, b_f, and d_f = the fitting coefficients for *% damage*, and

a_r, b_r, and d_r = the fitting coefficients for rut depth.

Equations (3) and (5) are taken from Superpave mix design, Superpave Series No. 2 (Asphalt Institution 1996), to estimate the changes in the VMA_{IP} and VFA_{IP} as functions of changes in in-place density and binder content. Note that equation (3) is divided by 100 because P_s is the aggregate content percentage by total mass, which is considered to be 100 percent. Also, P_s and G_{mm} change when the binder content changes.

$$VMA_{IP} = 100 - \frac{\%G_{mm} \times G_{mm} \times P_s}{100 \times G_{sb}} \qquad (3)$$

$$G_{mm} = \frac{P_{mm}}{\frac{P_s}{G_{se}} + \frac{P_b}{G_b}} \qquad (4)$$

where

$\%G_{mm}$ = the as-constructed compaction level (95% indicates 5% of the in-place air void content),

G_{mm} = the theoretical maximum density of the asphalt mixture,

P_s = the aggregate content (percent by total mass of mixture),

G_{sb} = the bulk specific gravity of the aggregate,

P_{mm} = the percent by mass of total loose mixture, which is 100,

P_b = the asphalt content (percent by total mass of mixture), and

G_b = the specific gravity of asphalt.

$$VFA_{IP} = 100 \times \left(\frac{VMA_{IP} - V_{a,IP}}{VMA_{IP}}\right) \qquad (5)$$

where

$V_{a,IP}$ = the in-place air void content.

In order to express equations (3) and (5) in terms of the volumetric properties that are commonly used, equations (6) and (7) are introduced for G_{mm} and VMA, respectively.

$$G_{mm} = \frac{100 \times G_{mb}}{100 - V_a} \qquad (6)$$

where

G_{mb} = the bulk specific gravity of compacted mixtures, and

V_a = the air void percentage of the specimen at the design compaction level (N_{des}).

$$VMA = 100 - \frac{G_{mb} \times P_s}{G_{sb}} \qquad (7)$$

where

VMA = the voids in mineral aggregate at the design compaction level (N_{des}).

Rearranging equations (3) and (5) and using the relationships in equations (6) and (7) yield:

$$VMA_{IP} = 100 - \frac{\%G_{mm}}{100 - V_a} \times (100 - VMA) \qquad (8)$$

$$VFA_{IP} = 100 - \frac{100 - \%G_{mm}}{VMA_{IP}} \times 100 \qquad (9)$$

Equations (8) and (9) can be used to develop the shadow mixture specification range for the VMA_{IP} and VFA_{IP}. The $\%G_{mm}$, V_a, and VMA values are the specified minimum and maximum values in the agency's specifications and will differ for each shadow project.

Based on a previous study conducted by the research team, the changes in the VMA_{IP} and VFA_{IP} values show patterns when the in-place density, binder content, and aggregate gradation change, as observed in Figure 5.

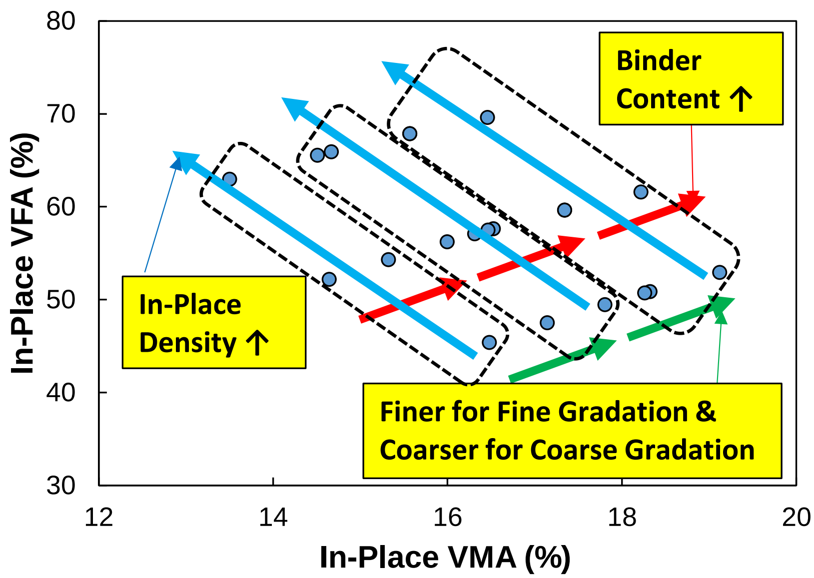

Figure 5. Graph. Changes in in-place VMA and in-place VFA as a function of mixture properties.

CHAPTER 4. THE NORTH CAROLINA DEPARTMENT OF TRANSPORTATION SHADOW PROJECT

This chapter provides a chronological overview of the events that took place to complete the NCDOT's PRS shadow project, including analysis of the AMPT test results and PVR development and verification. The research team's role was to provide help to the agency (NCDOT) in terms of selection of the paving project, collection of construction samples, AMPT performance testing, data analysis, and other activities required for the shadow project.

The primary events that have taken place for the NCDOT's shadow project are listed chronologically as follows. The main contact person at the NCDOT was Dr. Wiley Jones at wwjones1@ncdot.gov and Maira Ibarra at mibarra@ncdot.gov.

- Material sampling: February to March 2019
- Proficiency testing (NCDOT): N/A
- Proficiency testing (NCSU): N/A
- AMPT workshop: August 2019
- On-site training: N/A
- PRS shadow project testing (NCDOT): N/A
- PRS shadow project testing (NCSU): July 2019 – February 2020
- PVR development: March 2020

Training Resources

The NCDOT team attended the two-day AMPT hands-on workshop in August 2019 that was led by the research team to learn about laboratory test procedures, including specimen fabrication, dynamic modulus tests, direct tension cyclic fatigue tests, and stress sweep rutting (SSR) tests. Also, the NCDOT team attended a hands-on training session to learn about AMPT test analysis protocols that use FlexMAT™ and FlexPAVE™. However, the on-site training session could not be held because the NCDOT lab was not yet ready to run the AMPT performance tests. The following notes were made during the investigation of the NCDOT lab conditions and during the AMPT workshop.

- The NCDOT has an AMPT that was manufactured by the IPC Global Controls Group.
- The NCDOT lab does not have a gyratory compactor that is able to fabricate specimens at 180-mm height.
- The NCDOT lab has a target gluing device, but it needed a height adjustment item to accommodate small specimens.

Communication Log

Table 3 provides a summary of the communications between the research team and NCDOT personnel.

Table 3. Communication Log

Date	Type	Log
Feb. 8, 2019	Meeting	The protocol for the shadow project plan was introduced. The field project (full-depth asphalt) was selected.
Feb. 13, 2019	E-mail	Job mix formulas for the field project mixtures (RS9.5C, RI19.0C, and RB25.0C) were provided by the NCDOT and sent to NCSU.
Feb. 14, 2019	E-mail	The selected section did not pass the density criterion. Paving was postponed.

Proficiency Testing

In this project, proficiency testing was not conducted because the NCDOT lab was not fully ready to run the AMPT performance tests.

Pavement Information and Material Acquisition for Shadow Project

The NCDOT chose a new full-depth asphalt project to serve as the shadow project. The location of the project is Carr Road in Durham, NC 27703 (Durham's East End Connector Project). This project's pavement was composed of 1.675 in. (4.3 cm) thick AC surface (RS9.5C mixture), 4 in. (10 cm) thick intermediate (RI19.0C mixture), and 4.4 in. (11 cm) thick base (RB25.0C mixture) layers. The original plan was to acquire ten mixture samples from each layer. However, for the intermediate layer samples, the plant operations stopped mixture production in the middle of the sampling period, and only seven samples could be obtained. Therefore, 27 mixture samples (ten AC surface, seven AC intermediate, and ten AC base layer samples) from 27 different truck loads were acquired.

Table 4 provides a summary of the general pavement information for the NCDOT shadow project that includes the material properties. Note that the pavement thicknesses presented in Table 4 are the averaged values of the measured thicknesses of each of the three AC layers after QA procedures had been carried out. The research team acquired the shadow project mixtures with the assistance of NCDOT personnel from February to March 2019. The sampled mixtures were stored in five-gallon plastic buckets using cotton bags. Around 400 lb of materials for each sample were obtained.

Table 4. General Pavement Information

Pavement Structure	1.675 in. (4.3 cm) of Surface Course 4 in. (10 cm) of Intermediate Course 4.4 in. (11 cm) of Base Course
Mixture	RS9.5C (AC Surface)
NMAS (mm)	9.5
Virgin Binder Type	PG 64-22
RAP Content (%)	40
Total Binder Content (%)	5.8
Mixture	RI19.0C (AC Intermediate)
NMAS (mm)	19
Virgin Binder Type	PG 64-22
RAP Content (%)	30
Total Binder Content (%)	4.6
Mixture	RB25.0C (AC Base)
NMAS (mm)	25
Virgin Binder Type	PG 64-22
RAP Content (%)	30
Total Binder Content (%)	4.2

Note: NMAS is nominal maximum aggregate size, and RAP is reclaimed asphalt pavement.

NCDOT's Acceptance Test Results for Obtained Samples

The NCDOT conducted acceptance tests of the 27 acquired samples to obtain the AQCs and then provided the resultant data to the research team. Table 5, Table 6, and Table 7 present summaries of the measured AQCs for the three mixtures, respectively. The volumetric characteristics of these samples, which were needed later to develop the PVRs, were calculated using NCSU-measured specific gravity values.

Table 5. Acceptance Quality Characteristics Obtained from the NCDOT (RS9.5C)

Sample ID	G_{sb}	G_{mb}	G_{mm}	Air Voids at N_{des} (%)	Asphalt Binder (%)	VMA at N_{des} (%)	VFA at N_{des} (%)	Core Density (%)
RS9.5C-1	2.680	2.364	2.427	2.6	5.8	15.5	83	93.2
RS9.5C-2	2.680	2.388	2.429	1.7	5.6	14.3	88	91.5
RS9.5C-3	2.680	2.364	2.420	2.3	6.1	15.9	86	93.5
RS9.5C-4	2.680	2.365	2.423	2.4	5.9	15.5	85	94.2
RS9.5C-5	2.680	2.361	2.427	2.7	6.0	16.1	83	94.3
RS9.5C-6	2.680	2.373	2.426	2.2	5.9	15.4	86	92.5
RS9.5C-7	2.680	2.361	2.431	2.9	5.8	15.8	82	91.2
RS9.5C-8	2.680	2.368	2.426	2.4	6.2	16.2	85	93.5
RS9.5C-9	2.680	2.358	2.421	2.6	6.0	15.9	84	95.1
RS9.5C-10	2.680	2.361	2.422	2.5	6.1	16.1	84	94.8

Note: G_{sb} is aggregate bulk specific gravity, G_{mb} is mixture bulk specific gravity, G_{mm} is maximum specific gravity, VMA is voids in mineral aggregate, VFA is voids filled with asphalt, and N_{des} is the design compaction level.

Table 6. Acceptance Quality Characteristics Obtained from the NCDOT (RI19.0C)

Sample ID	G_{sb}	G_{mb}	G_{mm}	Air Voids at N_{des} (%)	Asphalt Binder (%)	VMA at N_{des} (%)	VFA at N_{des} (%)	Core Density (%)
RI19.0C-1	2.688	2.388	2.485	3.9	4.6	13.9	72	96.2
RI19.0C-2	2.688	2.398	2.475	3.1	4.8	13.6	77	95.1
RI19.0C-3	2.688	2.402	2.469	2.7	4.7	13.0	79	95.7
RI19.0C-4	2.688	2.386	2.480	3.8	4.6	13.7	72	93.7
RI19.0C-5	2.688	2.393	2.480	3.5	4.5	13.2	73	94.3
RI19.0C-6	2.688	2.372	2.489	4.7	4.1	13.5	65	94.3
RI19.0C-7	2.688	2.390	2.474	3.4	4.6	13.3	74	92.3

Note: Gsb is aggregate bulk specific gravity, Gmb is mixture bulk specific gravity, Gmm is maximum specific gravity, VMA is voids in mineral aggregate, VFA is voids filled with asphalt, and Ndes is the design compaction level.

Table 7. Acceptance Quality Characteristics Obtained from the NCDOT (RB25.0C)

Sample ID	G_{sb}	G_{mb}	G_{mm}	Air Voids at N_{des} (%)	Asphalt Binder (%)	VMA at N_{des} (%)	VFA at N_{des} (%)	Core Density (%)
RB25.0C-1	2.709	2.406	2.509	4.1	4.1	13.3	69	93.8
RB25.0C-2	2.709	2.414	2.499	3.4	4.3	13.2	74	93.6
RB25.0C-3	2.709	2.411	2.488	3.1	4.7	13.8	78	93.8
RB25.0C-4	2.709	2.406	2.496	3.6	4.2	13.0	72	95.0
RB25.0C-5	2.709	2.422	2.492	2.8	4.3	12.6	78	95.5
RB25.0C-6	2.709	2.415	2.508	3.7	4.1	13.0	72	95.5
RB25.0C-7	2.709	2.415	2.495	3.2	4.4	13.2	76	95.3
RB25.0C-8	2.709	2.415	2.487	2.9	4.3	12.6	77	94.6
RB25.0C-9	2.709	2.407	2.499	3.7	4.2	13.2	72	94.7
RB25.0C-10	2.709	2.415	2.510	3.8	4.0	12.8	70	94.1

Note: G_{sb} is aggregate bulk specific gravity, G_{mb} is mixture bulk specific gravity, G_{mm} is maximum specific gravity, VMA is voids in mineral aggregate, VFA is voids filled with asphalt, and N_{des} is the design compaction level.

Selection of Performance-Volumetric Relationship Calibration Conditions

Based on the AQCs measured by the NCDOT, the research team created three plots for the acquired samples with regard to volumetric conditions. The volumetric properties are the in-place voids in mineral aggregate (VMA_{IP}) and in-place voids filled with asphalt (VFA_{IP}). Figure 6, Figure 7, and Figure 8 show the plots for the three mixtures and Table 8 presents the individual control limits and density requirements obtained from the NCDOT Asphalt Quality Management System (QMS) Manual 2018 that were converted to the volumetric conditions used for the plots. Note that 98% of the maximum in-place density was assumed because the maximum limit was not specified in the QMS manual.

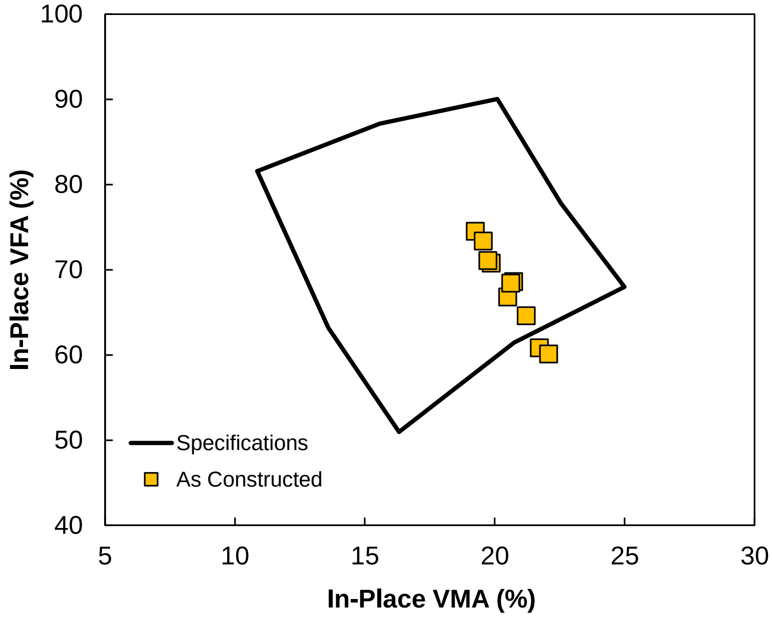

Figure 6. Graph. Calculated in-place VMA and in-place VFA for ten samples within specification limits for RS9.5C.

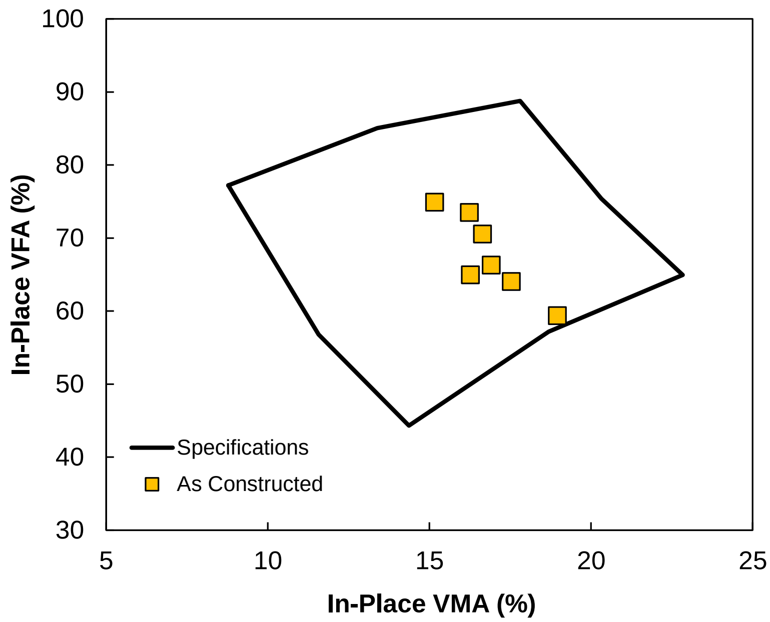

Figure 7. Graph. Calculated in-place VMA and in-place VFA for seven samples within specification limits for RI19.0C.

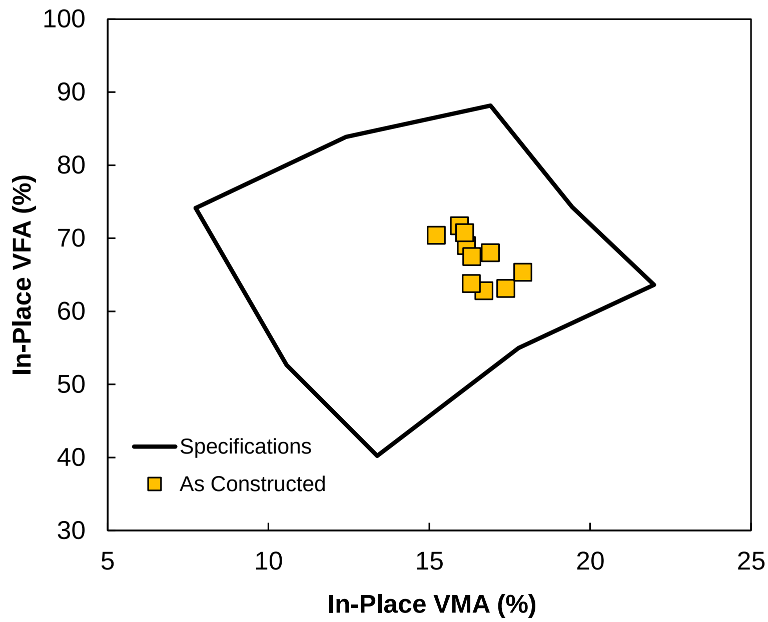

Figure 8. Graph. Calculated in-place VMA and in-place VFA for ten samples within specification limits for RB25.0C.

Table 8. Specification Limits (NCDOT QMS Manual 2018) for the Three Mixtures

Property	Criteria and Limits	Criteria and Limits	Criteria and Limits
Mixture	RS9.5C	RI19.0C	RB25.0C
VMA	Min 14.5%	Min 12.5%	Min 11.5%
VFA	65 - 78%	65 – 78%	65 – 78%
Binder Content	± 0.7%	± 0.7%	± 0.7%
Air Void Content	± 2.0%	± 2.0%	± 2.0%
In-Place Density	92% – 98%	92% – 98%	92% – 98%

Note: VMA is voids in mineral aggregate. VFA is voids filled with asphalt binder.

Equations (4), (8), and (9) were used to convert the specification limits to the volumetric conditions. The minimum and maximum values in Table 8 were input into the equations to create the ranges in the volumetric domain. Note that the gradations and the binder contents for the samples cannot be changed. Therefore, one way to change the VMA_{IP} and VFA_{IP} of the samples to make four corners is to change the target air void contents of the test specimens.

For the RS9.5C mixture, as an example, the research team selected four samples (Samples 1, 3, 7, and 10) to calibrate the PVR because these four samples were located at the outer boundary of the ten samples in the volumetric domain, as shown in Figure 9.

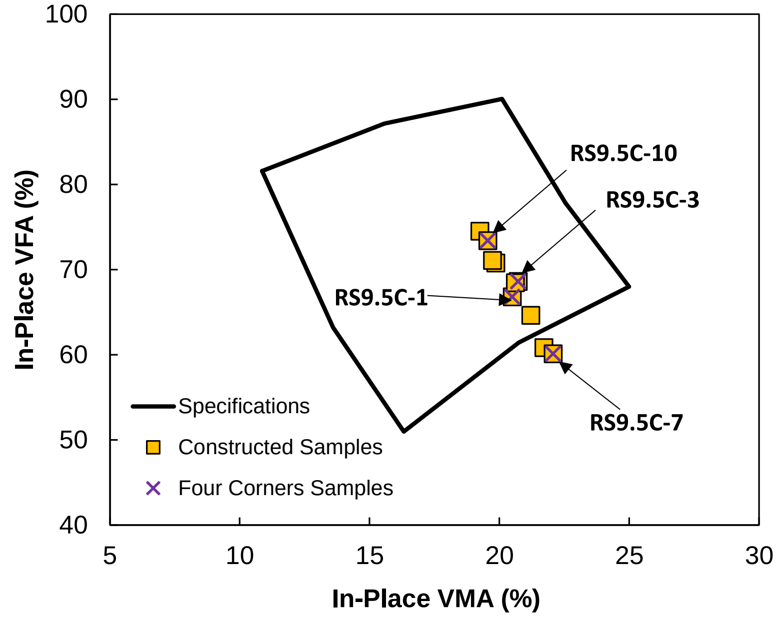

Figure 9. Graph. Selected four samples to calibrate four corners (RS9.5C).

The target air void contents of the four samples were set as 2.5% for Sample 1, 4% for Sample 10, and 7.5% for Samples 3 and 7, as shown in Figure 10. The reason that one of the four samples was targeted at 4.0% air void content was to determine the pavement performance at the target air void of the design compaction level (N_{des}). Using the same method, the four corners were calibrated also for RI19.0C and RB25.0C, represented in Figure 11 and Figure 12, respectively. Table 9 presents a summary of the test plan.

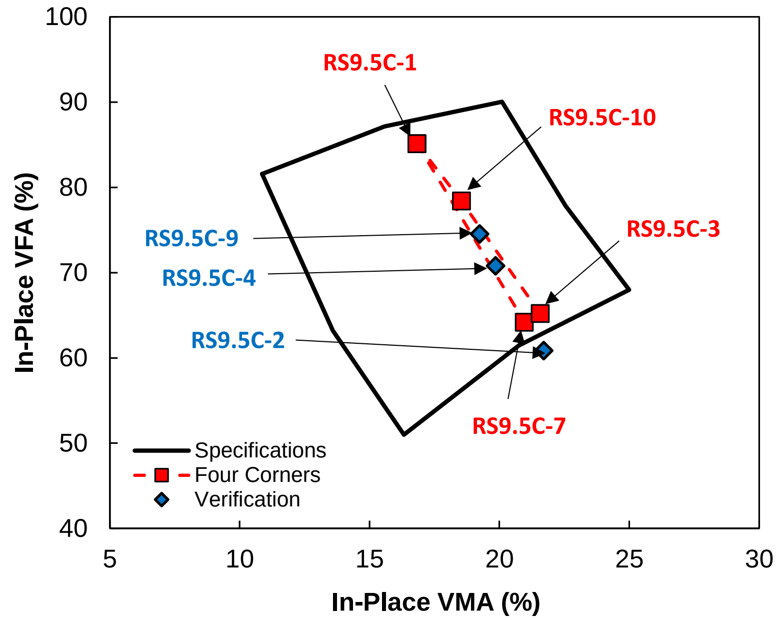

Figure 10. Graph. Volumetric conditions of the four samples used to calibrate the performance-volumetric relationship for RS9.5C.

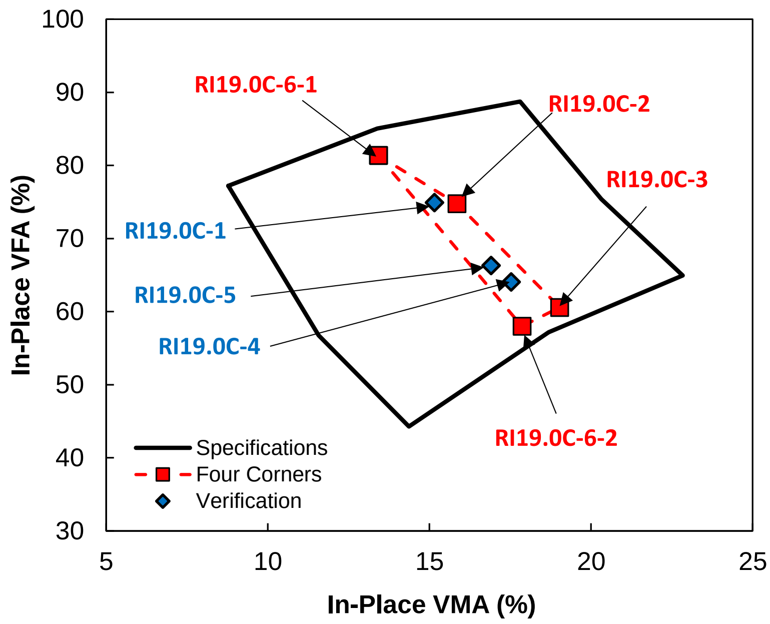

Figure 11. Graph. Volumetric conditions of the four samples used to calibrate the performance-volumetric relationship for RI19.0C.

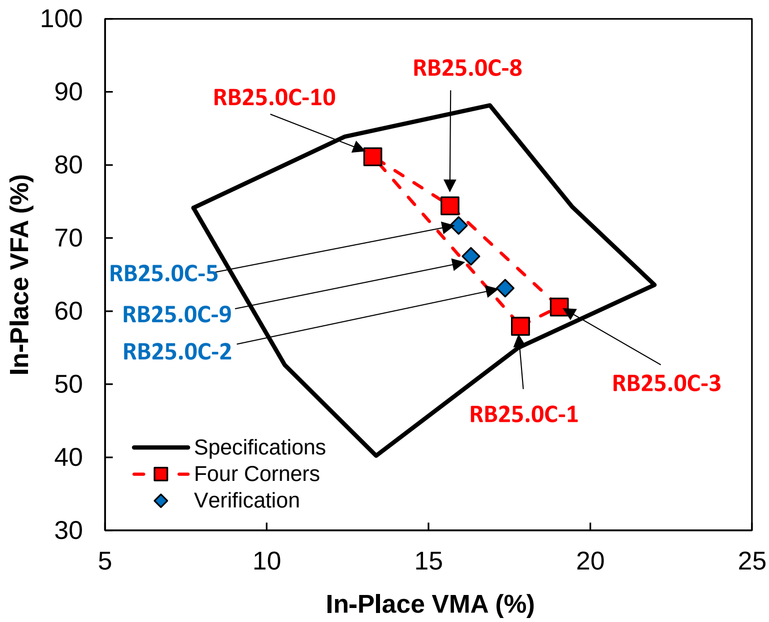

Figure 12. Graph. Volumetric conditions of the four samples used to calibrate the performance-volumetric relationship for RB25.0C.

Table 9. Test Plan to Calibrate the Performance-Volumetric Relationships of the Three Mixtures

Sample ID	Test Purpose	Target Test Specimen Air Void Content (%)
RS9.5C-1	4 Corners	2.5
RS9.5C-3	4 Corners	7.5
RS9.5C-7	4 Corners	7.5
RS9.5C-10	4 Corners	4.0
RS9.5C-2	PVR Verification	8.5
RS9.5C-4	PVR Verification	5.8
RS9.5C-9	PVR Verification	4.9
RI19.0C-2	4 Corners	4.0
RI19.0C-3	4 Corners	7.5
RI19.0C-6-1	4 Corners	2.5
RI19.0C-6-2	4 Corners	7.5
RI19.0C-1	PVR Verification	3.8
RI19.0C-4	PVR Verification	6.3
RI19.0C-5	PVR Verification	5.7
RB25.0C-1	4 Corners	7.5
RB25.0C-3	4 Corners	7.5
RB25.0C-8	4 Corners	4
RB25.0C-10	4 Corners	2.5
RB25.0C-2	PVR Verification	6.4
RB25.0C-5	PVR Verification	4.5
RB25.0C-9	PVR Verification	5.3

Test Specimen Fabrication

Air Void Study

The research team conducted an air void study prior to test specimen fabrication for the shadow project to determine the mass of a mixture that would be needed to prepare a test specimen to the target air void content. A randomly chosen sample (RS9.5C, Sample 7) was used for the air void study. Three gyratory-compacted samples were fabricated to target the three air void contents for the test specimens: 1.5%, 3.5%, and 5.5%, respectively. The research team employed the saturated surface-dry method (AASHTO T 166) to measure the air void contents, which was the same air void measurement method that the NCDOT uses. The air void study utilized 100-mm diameter and 150-mm height specimens. Equation (10) was used to calculate the targeted mass of each target air void content in accordance with AASHTO R 83.

$$Mass = \left[\frac{100-(V_{at}+F)}{100}\right] \times G_{mm} \times 176.7147 \times H \qquad (10)$$

where

Mass = the estimated mass of the mixture that is needed to prepare a test specimen to the target air void content,

V_{at} = the target air void content for the test specimen,

G_{mm} = the maximum specific gravity of the mixture,

H = the height of the gyratory sample (cm), and

F = the air void adjustment factor: 1.0 for fine-graded and 1.5 for coarse-graded mixtures.

Figure 13 presents the air void study results and indicates that the measured test specimen air void contents and total mass values for Sample RS9.5C-7 have a linear relationship. Table 10 presents a summary of the measurements.

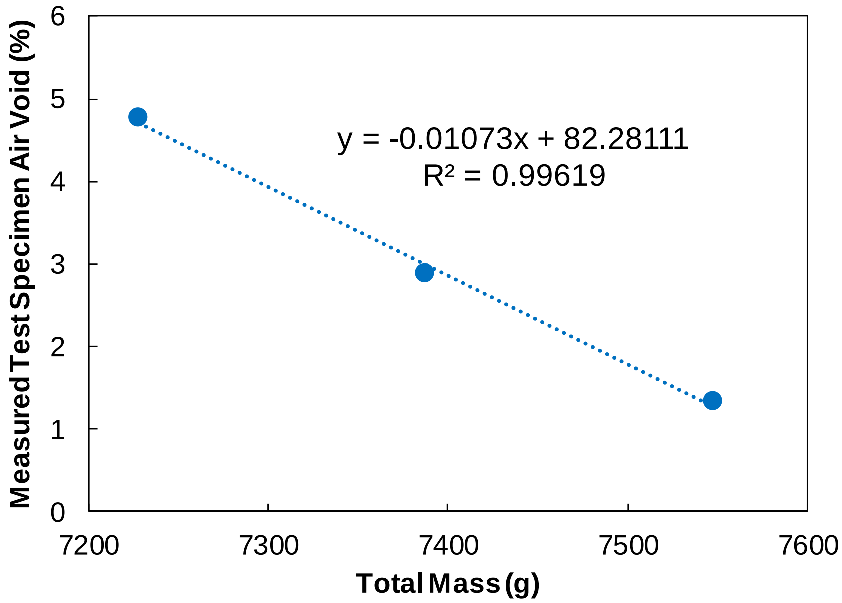

Figure 13. Graph. Air void study results for Sample RS9.5C-7.

Table 10. Measured Target Mass and Air Void Contents for Air Void Study

Target Mass (g)	Bulk Specimen Air Void Content (%)	Test Specimen Air Void Content (%)
7230.0	5.5	4.8
7384.7	3.5	2.9
7539.4	1.7	1.3

Based on the results of a previous study conducted by the research team, the air void study results for the large geometry specimens (D 100-mm x H 150-mm) could be applied to achieve the target air void contents for the small geometry specimens (D 38-mm x H 110-mm). Therefore, the developed relationship was applied to the rest of the samples for specimen fabrication. The same air void study method was used for RI19.0C. Note that the base layer mixture, RB25.0C, was not tested because of the limited time in the project.

Shadow Project Specimen Fabrication

The test specimens used for the four corners and verification purposes were fabricated based on the PVR calibration plans. The gyratory-compacted specimens obtained from samples of the two mixtures, RS9.5C and RI19.0C, were fabricated at the compaction temperature of 138°C. Then, the compacted specimens were cored and cut to the appropriate geometry. The air void contents were measured using the saturated surface-dry method (AASHTO T 166). Table 11 through Table 13 present the averaged measured air void contents of the test specimens for the three AMPT tests (dynamic modulus, direct tension cyclic fatigue, and SSR tests), respectively, and the calculated VMA_{IP} and VFA_{IP} for each performance test (Table 12 and Table 13). Note that RI19.0C Sample 6 was used to create two different air void contents, which resulted in Samples 6-1 and 6-2.

Table 11. Averaged Measured Air Void Contents of Dynamic Modulus Test Specimens

Sample ID	Target Air Void Content (%)	Actual Air Void Content (%)
RS9.5C-1	2.5	2.4
RS9.5C-2	8.5	8.4
RS9.5C-3	7.5	7.5
RS9.5C-4	5.8	5.6
RS9.5C-7	7.5	7.9
RS9.5C-9	4.9	4.7
RS9.5C-10	4.0	3.5
RI19.0C-1	3.8	3.9
RI19.0C-2	4.0	4.5
RI19.0C-3	7.5	7.6
RI19.0C-4	6.3	6.7
RI19.0C-5	5.7	5.6
RI19.0C-6-1	2.5	2.4
RI19.0C-6-2	7.5	7.2

Table 12. Averaged Measured Air Void Contents and Volumetric Information for Direct Tension Cyclic Fatigue Test Specimens

Sample ID	Target Air Void Content (%)	Actual Air Void Content (%)	In-Place VMA (%)	In-Place VFA (%)
RS9.5C-1	2.5	2.4	16.7	85.7
RS9.5C-2	8.5	8.6	21.8	60.6
RS9.5C-3	7.5	7.3	21.4	65.8
RS9.5C-4	5.8	5.6	19.7	71.7
RS9.5C-7	7.5	7.4	20.8	64.7
RS9.5C-9	4.9	5.0	19.3	74.2
RS9.5C-10	4.0	3.7	18.3	79.7
RI19.0C-1	3.8	3.6	15.0	76.0
RI19.0C-2	4.0	4.0	15.8	74.9
RI19.0C-3	7.5	7.5	19.0	60.7
RI19.0C-4	6.3	6.4	17.6	63.5
RI19.0C-5	5.7	6.1	17.2	64.8
RI19.0C-6-1	2.5	2.5	13.5	81.1
RI19.0C-6-2	7.5	7.2	17.6	59.0

Table 13. Averaged Measured Air Void Contents and Volumetric Information for Stress Sweep Rutting Test Specimens

Sample ID	Target Air Void Content (%)	Actual Air Void Content (%)	In-Place VMA (%)	In-Place VFA (%)
RS9.5C-1	2.5	2.3	16.7	86.2
RS9.5C-2	8.5	8.4	21.6	61.1
RS9.5C-3	7.5	7.9	21.9	64.1
RS9.5C-4	5.8	5.5	19.6	71.9
RS9.5C-7	7.5	7.6	21.1	63.7
RS9.5C-9	4.9	4.8	19.1	75.0
RS9.5C-10	4.0	3.5	18.1	80.5
RI19.0C-1	3.8	3.8	15.2	74.8
RI19.0C-2	4.0	4.4	16.2	72.7
RI19.0C-3	7.5	7.9	19.3	59.4
RI19.0C-4	6.3	6.7	17.9	62.4
RI19.0C-5	5.7	5.8	17.0	65.9
RI19.0C-6-1	2.5	2.1	13.1	83.7
RI19.0C-6-2	7.5	7.4	17.8	58.3

AMPT Tests, Analysis, and Results

The research team conducted the AMPT tests, as described in Table 1. Table 14 provides a summary of the test temperatures used for each of the three AMPT tests of the two mixtures, RS9.5C and RI19.0C.

Table 14. Test Temperatures Used for AMPT Performance Tests

Performance Test	Test Temperature	Test Temperature
Mixture	RS9.5C	RI19.0C
Dynamic Modulus	4°C, 20°C, and 40°C	4°C, 20°C, and 40°C
Cyclic Fatigue	18°C	18°C
Stress Sweep Rutting	Low temperature: 29°C High temperature: 50°C	Low temperature: 26°C High temperature: 46°C

The test results generated from the AMPT were input to FlexMAT™ Cracking and Rutting v. 1.1.2; this software can be found at the FHWA's website (https://www.fhwa.dot.gov/pavement/asphalt/analysis/). Table 15 presents a summary of the major outputs generated from FlexMAT™. The analyzed output data (files) from FlexMAT™ were later input to FlexPAVE™ to simulate pavement performance. Appendix presents all of the numerical AMPT test results for each sample.

Table 15. Major Outputs of AMPT Tests

Sample	Alpha	D^R	S_{app}	RSI
RS9.5C-1	3.54	0.63	27.55	1.6
RS9.5C-2	3.17	0.65	20.73	10.4
RS9.5C-3	3.26	0.68	25.75	6.0
RS9.5C-4	3.30	0.68	29.37	3.7
RS9.5C-7	3.24	0.66	22.42	6.4
RS9.5C-9	3.29	0.67	27.03	3.1
RS9.5C-10	3.41	0.67	29.19	3.3
RI19.0C-1	3.28	0.44	10.15	1.2
RI19.0C-2	3.13	0.50	11.39	1.7
RI19.0C-3	3.10	0.44	7.35	3.0
RI19.0C-4	3.24	0.42	7.79	2.1
RI19.0C-5	3.16	0.45	10.58	2.0
RI19.0C-6-1	3.63	0.55	15.1	0.9
RI19.0C-6-2	3.35	0.57	10.12	2.0

Note: D^R is a failure criterion defined as the average reduction in pseudo stiffness up to failure. S_{app} is a fatigue index parameter and is a measure of the amount of fatigue damage the material can tolerate under loading. RSI is rutting stress index.

FlexPAVE™ Simulation Results

The AMPT data processed by FlexMAT™ were used for the FlexPAVE™ v. 1.1 simulations. Hereafter, FlexPAVE™ v. 1.1 is referred to simply as FlexPAVE™. The averaged measured thicknesses of each of the three AC layers were used for the pavement structures. The properties of the AC surface and AC intermediate layer mixtures were obtained from the AMPT test results, and the properties of the AC base layer mixture were obtained from the properties of an RB25.0B mixture that was tested in a previous research project (test air void 4.0%) to simulate the field pavement performance. The unbound layers, i.e., the aggregate base layer and subgrade layer, were 'placed' under the RB25.0B layer. Note that the thickness of the aggregate base is taken from the project structural design. The material properties of the unbound layers include the modulus values and Poisson's ratios that were default values in FlexPAVE™. Raleigh, North Carolina was selected as the climatic data source. The daily equivalent single-axle load (ESAL) was input as 4,167, which is the maximum design ESAL (30,000,000) divided by 20 years. The traffic growth rate was assumed as 0 percent. As mentioned in CHAPTER 2, the major output from FlexPAVE™ simulations is pavement performance, which is provided in the form of the damage percentage (*% damage*) and rut depth over the design life of the pavement. Table 16 presents all of the input sources used for the FlexPAVE™ simulations.

Table 16. Input Sources Used for FlexPAVE™ Simulations

FlexPAVE™ Inputs	Input
Pavement Type	New Pavement
Analysis Options	Pavement Performance Analysis
Pavement Design Life (Years)	20
Asphalt Concrete Surface	Material Properties: Imported from AMPT Test Results, Thickness: 1.675 in. (4.3 cm)
Asphalt Concrete Intermediate	Material Properties: Imported from AMPT Test Results, Thickness: 4 in. (10 cm)
Asphalt Concrete Base	Material Properties: Imported from Single RB25.0B Test Results (Test Air Void 4%), Thickness: 4.4 in. (11 cm)
Aggregate Base	Elastic Modulus: 275,790 kPa Thickness: 10 in. (25 cm) Poisson's Ratio: 0.35
Subgrade	Elastic Modulus: 68,948 kPa Poisson's Ratio: 0.4
Climate	Raleigh, NC
Traffic	Daily ESAL: 4,167 with no traffic growth

Three cases of FlexPAVE™ simulations were run to develop reasonable PVRs for the RS9.5C and RI19.0C mixtures. The first simulation case uses a three-layer pavement structure where all three AC layers were modeled to determine the pavement performance and to develop the PVRs for the AC surface and AC intermediate layers. The second simulation case uses a two-layer pavement structure where two AC layers (AC surface and AC intermediate) instead of three AC layers were modeled to determine the pavement performance and to develop the PVRs for the AC surface and AC intermediate layers. The third simulation case uses a single-layer pavement structure where a single AC layer (the AC surface layer and AC intermediate layer individually) was modeled to determine the pavement performance and to develop the PVRs for each of the surface and intermediate layers.

FlexPAVE™ Simulation Results for Three-Layer Pavement Structure: Case 1

In order to determine the simulated performance of the three-layer pavement structure, three different AC layers were input with the unbound layers to FlexPAVE™. Table 17 presents the input values used for the FlexPAVE™ simulations for this case.

Table 17. Inputs for FlexPAVE™ Simulations of Three-Layer Pavement Structure

FlexPAVE™ Inputs	Input
Pavement Type	New Pavement
Analysis Options	Pavement Performance Analysis
Pavement Design Life (Years)	20
Asphalt Concrete Surface	Material Properties: Imported from AMPT Test Results, Thickness: 1.675 in. (4.3 cm)
Asphalt Concrete Intermediate	Material Properties: Imported from AMPT Test Results, Thickness: 4 in. (10 cm)
Asphalt Concrete Base	Material Properties: Imported from Single RB25.0B Test Results (Test Air Void 4%), Thickness: 4.4 in. (11 cm)
Aggregate Base	Elastic Modulus: 275,790 kPa Thickness: 10 in. (25 cm) Poisson's Ratio: 0.35
Subgrade	Elastic Modulus: 68,948 kPa Poisson's Ratio: 0.4
Climate	Raleigh, NC
Traffic	Daily ESAL: 4,167 with no traffic growth

For any shadow project, a PVR should be developed for each AC layer (mixture) of a pavement structure that has multiple AC layers. Therefore, in this project, two PVRs were developed for each of the AMPT-tested mixtures (i.e., the AC surface and AC intermediate layer mixtures). In order to develop a PVR for each mixture, the different performance results that correspond to the varied volumetric conditions of the mixture must be captured. In other words, the pavement properties of the AC layer of interest are changed while the properties of the other AC layers remain the same. In order to capture the AC surface layer performance with the varied volumetric conditions for a three-layer pavement structure, for example, the test results of the AC surface layer samples (RS9.5C) are input to FlexPAVE™, while the inputs for the AC intermediate and AC base layers are kept the same as the reference layers.

This method was applied to all three cases of the FlexPAVE™ simulations. Samples RS9.5C-7 and RI19.0C-4 were selected for the reference layers of the AC surface and intermediate layers, respectively, because the air void contents at N_{des} of these samples were close to the target air void content at N_{des}, which is 4.0 percent. Therefore, for the AC surface layer analysis, Samples RI19.0C-4 and RB25.0B were used for the reference layers. For the intermediate layer analysis, Samples RS9.5C-7 and RB25.0B were used for the reference layers. Figure 14 shows the analysis method schematically. Table 18 and Table 19 present the simulation results for the AC surface and AC intermediate layers, respectively, using the reference layers.

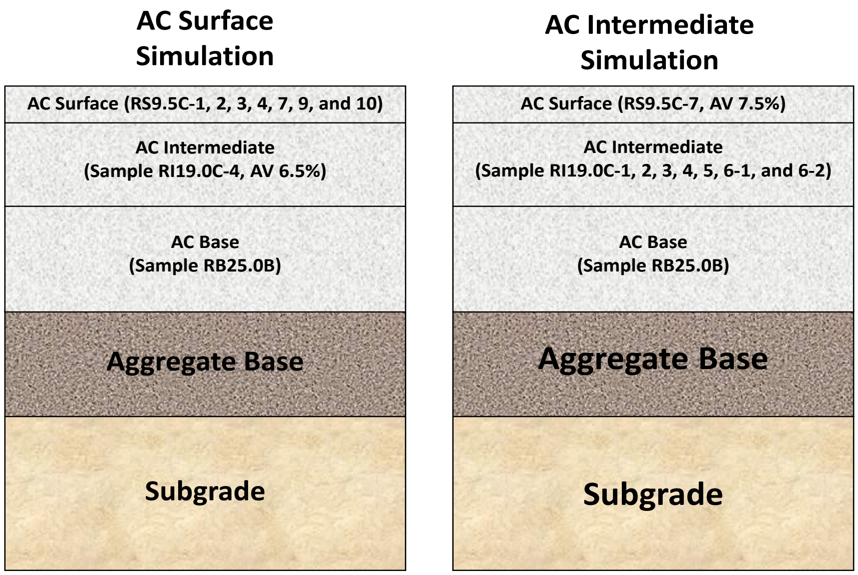

Figure 14. Illustration. AC Surface and AC intermediate FlexPAVE™ analysis method: example of three AC layers.

Table 18. FlexPAVE™ Simulation Results for AC Surface Layer Using Three-Layer Pavement Structure

Sample	AC Surface *% damage*	AC Surface Rut Depth (mm)
RS9.5C-1	0.03	0.8
RS9.5C-2	0.46	6.4
RS9.5C-3	0.20	4.0
RS9.5C-4	0.12	2.2
RS9.5C-7	0.33	4.4
RS9.5C-9	0.12	1.8
RS9.5C-10	0.07	2.0

Table 19. FlexPAVE™ Simulation Results for AC Intermediate Layer Using Three-Layer Pavement Structure

Sample	AC Intermediate *% damage*	AC Intermediate Rut Depth (mm)
RI19.0C-1	0.05	1.5
RI19.0C-2	0.12	1.9
RI19.0C-3	0.18	4.4
RI19.0C-4	0.08	2.7
RI19.0C-5	0.06	2.5
RI19.0C-6-1	0.01	1.5
RI19.0C-6-2	0.14	3.3

Because FlexPAVE™ simulations provide a single *% damage* value for all asphalt layers together at a certain time, the *% damage* values for the AC surface and AC intermediate layers presented in Table 18 and Table 19, respectively, are the recalculated values based on the reference area of each layer, as illustrated in Figure 15. According to the FlexPAVE™ *% damage* calculation procedure, FlexPAVE™ uses two overlapping triangles to form a reference area within which the damage evolution can be considered. The top inverted triangle has a 170-cm wide base that is located at the top of the surface layer and a vertex that is located at the bottom of the bottom asphalt layer. The 120-cm wide base of the second triangle is located at the bottom of the bottom asphalt layer and its vertex is positioned at the surface layer.

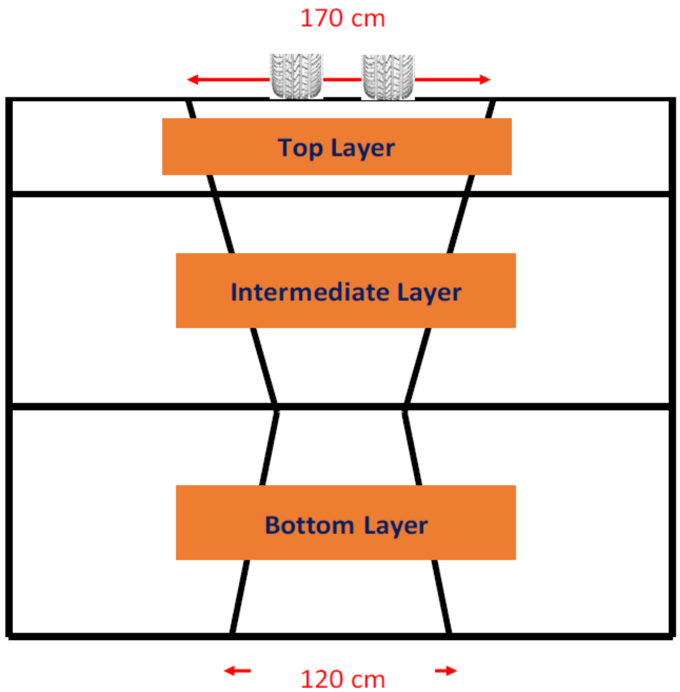

Source: FHWA

Figure 15. Illustration. Reference areas used for percentage of damage (*% damage*) calculations.

Based on the simulated pavement performance of the three-layer structure, the simulated *% damage* values for all the samples of both the AC surface and AC intermediate layers were significantly too low to develop the PVRs. This outcome does not mean that the simulation results were not usable to develop the PVRs, but they would not have been reasonable. Figure 16 shows one of the results of the damage distribution at 20 years for the three AC layers (the RS9.5C-3, RI19.0C-4, and RB25.0B mixtures). Figure 16 indicates that no visible damage occurred in the AC surface and AC intermediate layers. Numerically, 0.9% and 0.5% of the damage occurred in the AC surface and intermediate layers, respectively, and 98.6% of the damage occurred in the AC base layer. These results are due to the fact that FlexPAVE™ v. 1.1 does not have an asphalt pavement aging model that can be applied to pavement simulations, so most damage occurs at the bottom of asphalt layers together.

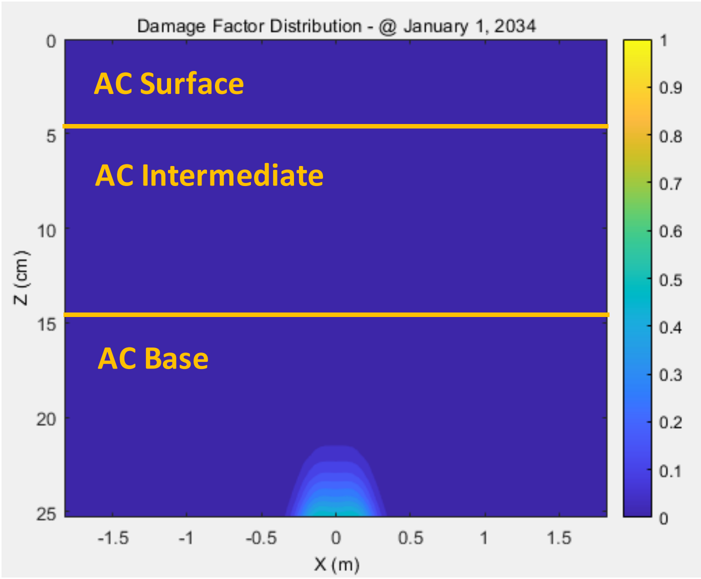

Figure 16. Illustration. Example of simulated damage distribution for three asphalt concrete layers at 20 years.

FlexPAVE™ Simulation Results for Two-Layer Pavement Structure: Case 2

For this case simulation, two AC layers, i.e., the AC surface and AC intermediate layers, an aggregate base layer, and a subgrade layer were used. Table 20 presents the inputs used for the FlexPAVE™ simulations for this case.

Table 20. Inputs for FlexPAVE™ Simulations of Two-Layer Pavement Structure

FlexPAVE™ Inputs	Input
Pavement Type	New Pavement
Analysis Options	Pavement Performance Analysis
Pavement Design Life (Years)	20
Asphalt Concrete Surface	Material Properties: Imported from AMPT Test Results, Thickness: 1.675 in. (4.3 cm)
Asphalt Concrete Intermediate	Material Properties: Imported from AMPT Test Results, Thickness: 4 in. (10 cm)
Aggregate Base	Elastic Modulus: 275,790 kPa Thickness: 10 in. (25 cm) Poisson’s Ratio: 0.35
Subgrade	Elastic Modulus: 68,948 kPa Poisson’s Ratio: 0.4
Climate	Raleigh, NC
Traffic	Daily ESAL: 4,167 with no traffic growth

This second simulation case used the same method for both the simulation and *% damage* calculation for each AC layer as was used for the three AC layers case. Samples RS9.5C-7 and

RI19.0C-4 were used as the reference layers. Table 21 and Table 22 show the simulation results for the AC surface and AC intermediate layers, respectively, using each reference layer.

Table 21. FlexPAVE^{TM} Simulation Results for Asphalt Concrete Surface Layer Using Two-Layer Pavement Structure

Sample	AC Surface *% damage*	AC Surface Rut Depth (mm)
RS9.5C-1	0.5	0.8
RS9.5C-2	4.9	6.3
RS9.5C-3	3.0	4.0
RS9.5C-4	1.9	2.2
RS9.5C-7	4.0	4.3
RS9.5C-9	1.9	1.8
RS9.5C-10	1.0	1.9

Table 22. FlexPAVE^{TM} Simulation Results for Asphalt Concrete Intermediate Layer Using Two-Layer Pavement Structure

Sample	AC Intermediate *% damage*	AC Intermediate Rut Depth (mm)
RI19.0C-1	25.8	1.3
RI19.0C-2	28.4	1.7
RI19.0C-3	33.9	3.6
RI19.0C-4	30.2	2.3
RI19.0C-5	26.9	2.2
RI19.0C-6-1	19.5	1.2
RI19.0C-6-2	31.3	2.6

Unlike the simulation results for the three AC layers, the simulation results for two AC layers show more reasonable amounts of damage in the AC surface and AC intermediate layers that can be used for PVR development. The thinner pavement structure (two AC layers compared to three AC layers) allows more damage to be generated in both the AC surface and AC intermediate layers, as shown in Figure 17.

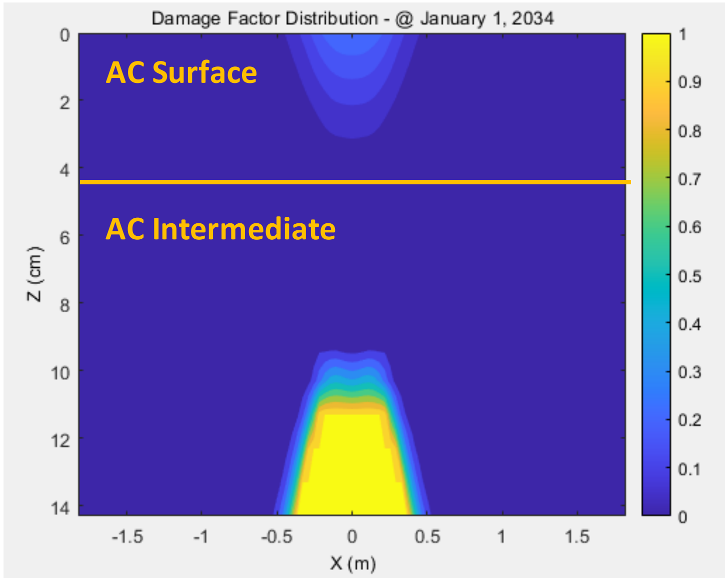

Figure 17. Illustration. Example of simulated damage distribution for two AC layers at 20 years.

FlexPAVE™ Simulation Results Using a Single-Layer Pavement Structure: Case 3

For this simulation case, a single AC surface layer and a single AC intermediate layer were used with an aggregate base and subgrade. Table 23 and Table 24 present the inputs used for the FlexPAVE™ simulations for the AC surface and AC intermediate layers, respectively.

Table 23. Inputs for FlexPAVE™ Simulations of Single-Layer Pavement Structure for AC Surface Layer

FlexPAVE™ Inputs	Input
Pavement Design Life (Years)	20
Asphalt Concrete Surface	Material Properties: Imported from AMPT Test Results, Thickness: 1.675 in. (4.3 cm)
Aggregate Base	Elastic Modulus: 275,790 kPa Thickness: 10 in. (25 cm) Poisson's Ratio: 0.35
Subgrade	Elastic Modulus: 68,948 kPa Poisson's Ratio: 0.4
Climate	Raleigh, NC
Traffic	Daily ESAL: 4,167 with no traffic growth

Table 24. Inputs for FlexPAVE^{TM} Simulations of Single-Layer Pavement Structure for AC Intermediate Layer

FlexPAVE^{TM} Inputs	Input
Pavement Design Life (Years)	20
Asphalt Concrete Intermediate	Material Properties: Imported from AMPT Test Results, Thickness: 4 in. (10 cm)
Aggregate Base	Elastic Modulus: 275,790 kPa Thickness: 10 in. (25 cm) Poisson's Ratio: 0.35
Subgrade	Elastic Modulus: 68,948 kPa Poisson's Ratio: 0.4
Climate	Raleigh, NC
Traffic	Daily ESAL: 4,167 with no traffic growth

Table 25 and Table 26 show the simulation results for the AC surface and AC intermediate layers, respectively. Note that the *% damage* recalculation using the reference area concept is not used for this case.

Table 25. FlexPAVE^{TM} Simulation Results for Single-Layer Pavement Structure for AC Surface Layer

Sample	AC Surface *% damage*	AC Surface Rut Depth (mm)
RS9.5C-1	23.8	0.7
RS9.5C-2	32.4	5.3
RS9.5C-3	28.8	3.3
RS9.5C-4	26.5	1.8
RS9.5C-7	30.9	3.5
RS9.5C-9	28.0	1.5
RS9.5C-10	25.6	1.6

Table 26. FlexPAVE^{TM} Simulation Results for Single-Layer Pavement Structure for AC Intermediate Layer

Sample	AC Intermediate *% damage*	AC Intermediate Rut Depth (mm)
RI19.0C-1	26.2	1.5
RI19.0C-2	29.9	2.0
RI19.0C-3	37.5	4.7
RI19.0C-4	32.7	2.8
RI19.0C-5	28.0	2.6
RI19.0C-6-1	19.3	1.5
RI19.0C-6-2	32.1	3.6

The simulation results show that the largest amount of distress for all three cases was generated for each individual AC layer (Case 3) because the pavement had the thinnest AC layer thickness compared to pavement structures with multiple AC layers. The single AC layer case and multiple AC layer cases were compared in terms of damage to investigate the performance trends of each sample in the different simulation cases, as shown in Figure 18 to Figure 21.

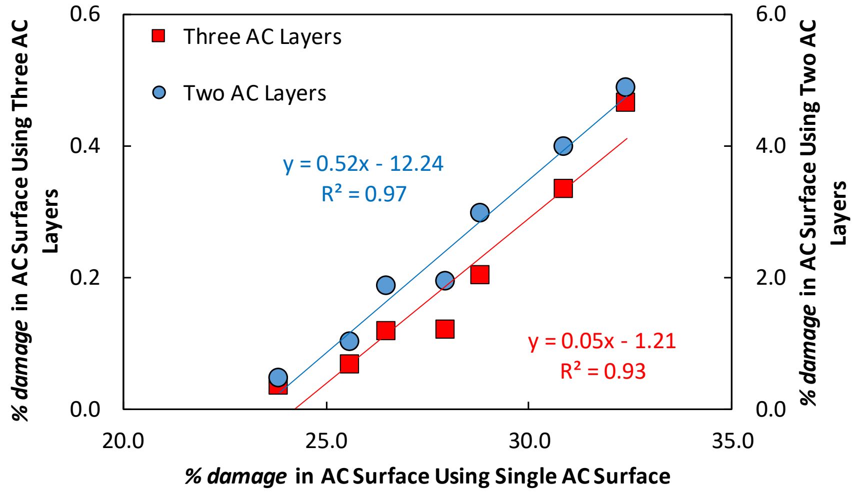

Figure 18. Graph. Comparison of simulated *% damage* in case of single AC surface layer and cases of two and three AC layers.

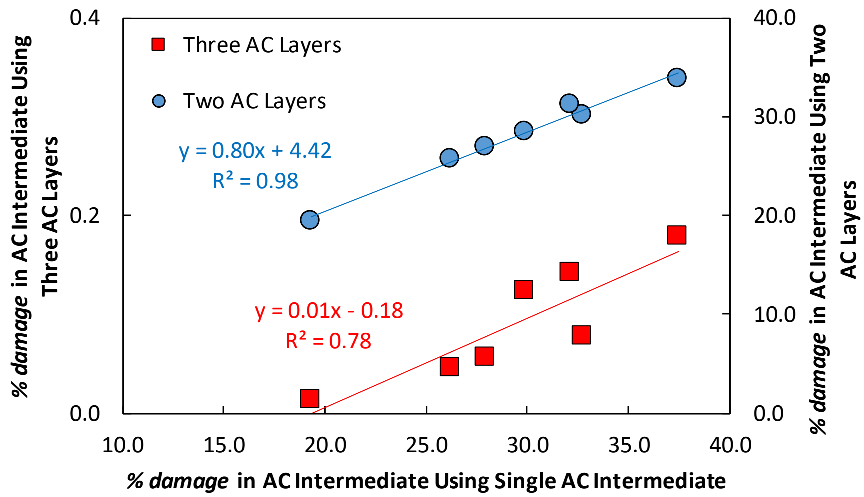

Figure 19. Graph. Comparison of simulated *% damage* in case of single AC intermediate layer and cases of two and three AC layers.

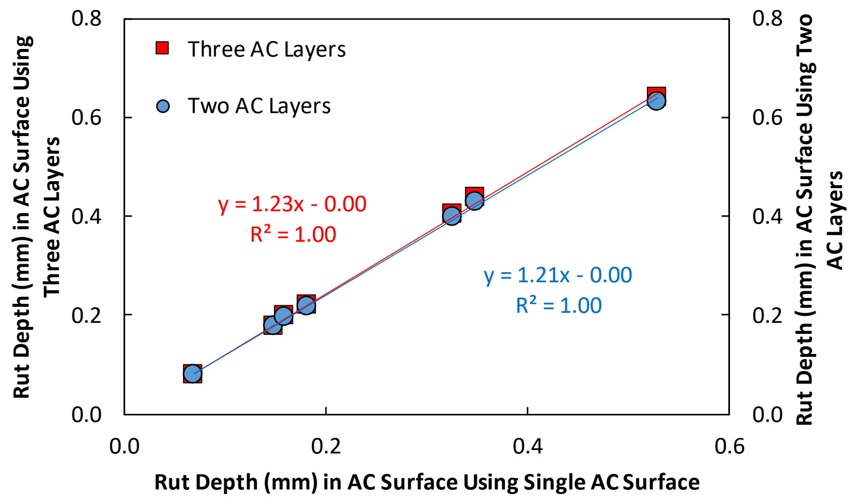

Figure 20. Graph. Comparison of simulated rut depth in case of single AC surface layer and cases of two and three AC layers.

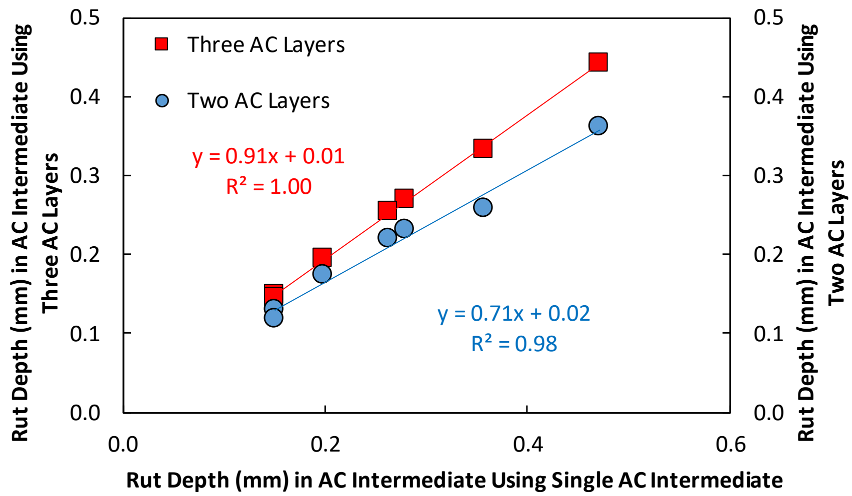

Figure 21. Graph. Comparison of simulated rut depth in case of single AC intermediate layer and cases of two and three AC layers.

The comparisons show that the simulated performance of all the tested samples have similar trends for the three cases. Although the numerical simulated distress values differ, they have the same trends with a minimum R^2 value of 0.78 for the *% damage* of the AC intermediate layer in the three-layer case compared to the single AC intermediate layer shown in Figure 19. The other cases show R^2 values higher than 0.9, which indicates that the FlexPAVE™ simulations for the three cases can be used to develop the PVRs. Note that the simulated rut depths of the two- and three-layer cases shown in Figure 20 are similar.

In order to obtain the most reasonable PVR, the case of the two AC layer simulation (Case 2) was chosen for two reasons. First, the case of three AC layers resulted in significantly low *%*

damage values for the AC surface layer and AC intermediate layer because of their combined thickness. Second, although the case of the single AC surface layer and single AC intermediate layer generated enough *% damage* to develop reasonable PVRs, it was not similar enough to actual pavement structures. Therefore, the case of the two-layer structure was chosen as the best option in terms of the amount of *% damage* and simulating real field conditions. Table 27 and Table 28 provide summaries of the FlexPAVE™ simulation results, i.e., *% damage* and rut depths, respectively, along with the volumetric properties for each sample and mixture of the selected case for PVR development.

Table 27. Simulated *% damage* from FlexPAVE™ and Volumetric Properties Used to Develop and Verify Performance-Volumetric Relationship

Sample	Purpose	In-Place VMA (%)	In-Place VFA (%)	*% damage*
RS9.5C-1	4 Corners	16.7	85.7	0.5
RS9.5C-2	Verification	21.8	60.6	4.9
RS9.5C-3	4 Corners	21.4	65.8	3.0
RS9.5C-4	Verification	19.7	71.7	1.9
RS9.5C-7	4 Corners	20.8	64.7	4.0
RS9.5C-9	Verification	19.3	74.2	1.9
RS9.5C-10	4 Corners	18.3	79.7	1.0
RI19.0C-1	Verification	15.0	76.0	25.8
RI19.0C-2	4 Corners	15.8	74.9	28.4
RI19.0C-3	4 Corners	19.0	60.7	33.9
RI19.0C-4	Verification	17.6	63.5	30.2
RI19.0C-5	Verification	17.2	64.8	26.9
RI19.0C-6-1	4 Corners	13.5	81.1	19.5
RI19.0C-6-2	4 Corners	17.6	59.0	31.3

Table 28. Simulated Rut Depths from FlexPAVE™ and Volumetric Properties Used to Develop and Verify Performance-Volumetric Relationship

Sample	Purpose	In-Place VMA (%)	In-Place VFA (%)	Rut Depth (mm)
RS9.5C-1	4 Corners	16.7	86.2	0.8
RS9.5C-2	Verification	21.6	61.1	6.3
RS9.5C-3	4 Corners	21.9	64.1	4.0
RS9.5C-4	Verification	19.6	71.9	2.2
RS9.5C-7	4 Corners	21.1	63.7	4.3
RS9.5C-9	Verification	19.1	75.0	1.8
RS9.5C-10	4 Corners	18.1	80.5	1.9
RI19.0C-1	Verification	15.2	74.8	1.3
RI19.0C-2	4 Corners	16.2	72.7	1.7
RI19.0C-3	4 Corners	19.3	59.4	3.6
RI19.0C-4	Verification	17.9	62.4	2.3
RI19.0C-5	Verification	17.0	65.9	2.2
RI19.0C-6-1	4 Corners	13.1	83.7	1.2
RI19.0C-6-2	4 Corners	17.8	58.3	2.6

The Performance-Volumetric Relationship

As mentioned in CHAPTER 3, the PVR is a tool that can be used to predict pavement performance from volumetric properties. The PVR represents the relationship between the volumetric properties (VMA_{IP} and VFA_{IP}) and FlexPAVE™ simulation results (*% damage* and rut depth) using linear regression. Four PVR equations, equation (11) to (12) for *% damage* and rut depth for RS9.5C, and equation (13) to (14) for *% damage* and rut depth for RI19.0C, respectively, were developed from the shadow project test results to predict the cracking and rutting performance of the two mixtures. Table 29 and Table 30 present the coefficients and intercepts used for equation (11) through (14). The PVR fitting was conducted using Microsoft Excel and the Data Analysis tool.

Table 29. Coefficients for Performance-Volumetric Relationship for Shadow Project Mixture (RS9.5C)

Performance	a	b	d	R^2
% Damage	-1.071	-0.378	50.746	0.99
AC Rut Depth	-0.165	-0.180	19.207	0.99

Table 30. Coefficient for Performance-Volumetric Relationship for Shadow Project Mixture (RI19.0C)

Performance	a	b	d	R^2
% Damage	2.915	0.085	-25.67	0.96
AC Rut Depth	0.440	0.014	-6.00	0.91

$$\%\,Damage = -1.071VMA_{IP} - 0.378VFA_{IP} + 50.746 \qquad (11)$$

$$Rut\ Depth\,(mm) = -0.165VMA_{IP} - 0.18VFA_{IP} + 19.207 \qquad (12)$$

$$\%\,Damage = 2.915VMA_{IP} + 0.085VFA_{IP} - 25.67 \qquad (13)$$

$$Rut\ Depth\,(mm) = 0.440VMA_{IP} + 0.014VFA_{IP} - 6 \qquad (14)$$

Performance-Volumetric Relationship Verification

The information for the samples that were slated for verification purposes was used to verify the developed PVRs. The volumetric properties of the verification samples were input to the developed PVR equations. The developed PVRs are verified by comparing the results predicted from the PVR and the FlexPAVE™ simulation results, as shown in Figure 22 through Figure 25 for the *% damage* and rut depths of the two mixtures, respectively. Figure 22 to Figure 25 indicate that the verification samples are located close to the line of equality (LOE) for both cases of the two mixtures.

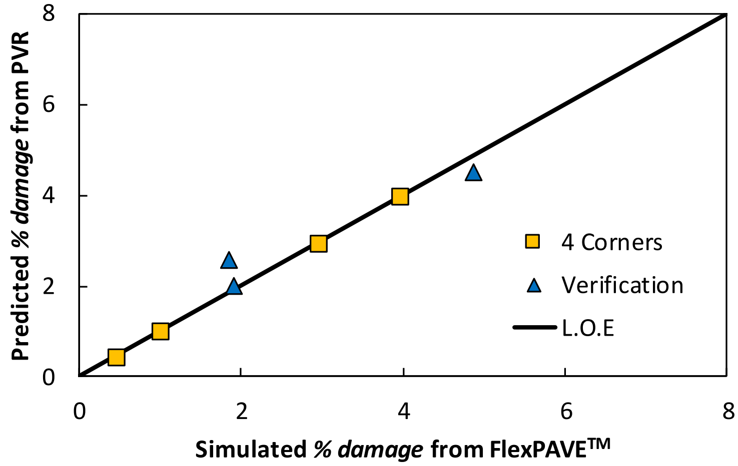

Figure 22. Graph. Comparison of *% damage* predicted from PVR and FlexPAVE™ simulations (RS9.5C).

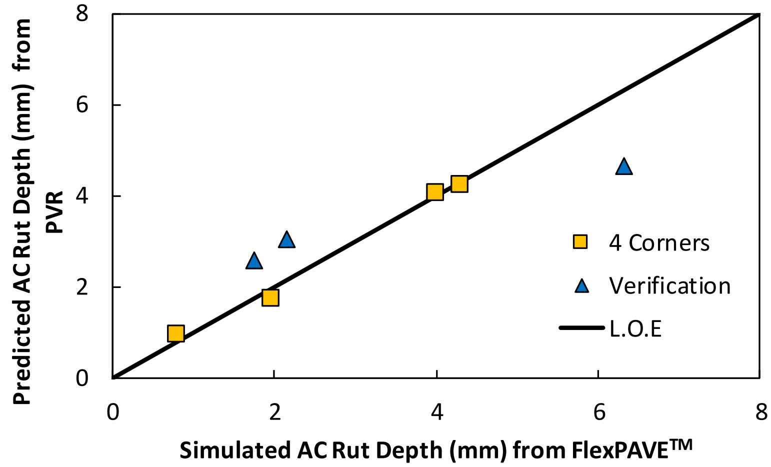

Figure 23. Graph. Comparison of rut depths predicted from PVR and FlexPAVE™ simulations (RS9.5C).

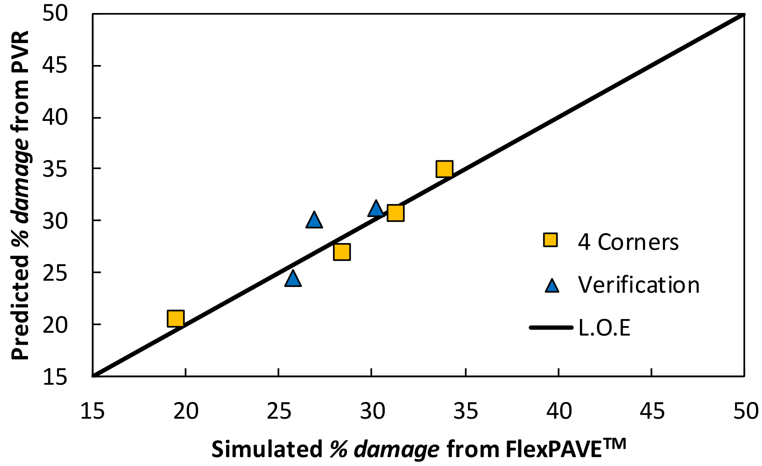

Figure 24. Graph. Comparison of *% damage* predicted from PVR and FlexPAVE™ simulations (RI19.0C).

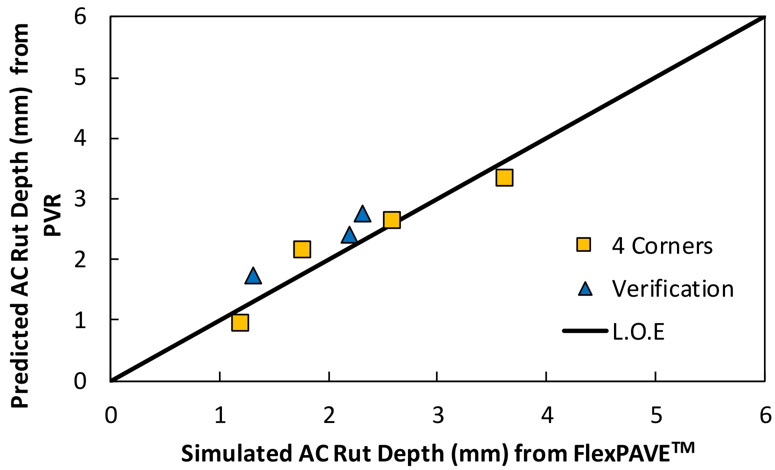

Figure 25. Graph. Comparison of rut depths predicted from PVR and FlexPAVE™ simulations (RI19.0C).

Table 31 and Table 32 provide a summary of the numerical results and the percentage of error (*% error*) between the PVR predictions and the FlexPAVE™ simulations for the *% damage* and rut depths of the two mixtures, respectively. As shown in Table 31, the *% error* of the *% damage* between the predictions and simulations for RS9.5C and RI19.0C averaged 8.7% and 5.1%, respectively. Table 32 shows that the rut depth averages are 21.1% for RS9.5C and 16.7% for RI19.0C. Moreover, the *% error* for each sample did not exceed 10% in the *% damage* predictions, except for one case of each mixture. The rut depth results show relatively higher *% error* values than the *% damage* values because the numerical rut depth values are generally lower than the *% damage* values. The numerical differences in rut depth between the FlexPAVE™ prediction and the PVR prediction did not exceed 1 mm, except for RS9.5C-2. Thus, these results prove that the developed PVRs work well for predicting performance without the need for performance tests.

Table 31. Summary of Numerical Performance Results Obtained from Performance-Volumetric Relationship and FlexPAVE^{TM} Simulation Predictions (*% damage*)

Purpose	Sample	*% damage* from FlexPAVE^{TM}	*% damage* from PVR	*% Error*
4 Corners	RS9.5C-1	0.5	0.4	4.3
4 Corners	RS9.5C-3	3.0	2.9	0.5
4 Corners	RS9.5C-7	4.0	4.0	0.1
4 Corners	RS9.5C-10	1.0	1.0	2.9
Verification	RS9.5C-2	4.9	4.5	7.3
Verification	RS9.5C-7	1.9	2.6	40.4
Verification	RS9.5C-9	1.9	2.0	5.4
Average	RS9.5C	-	-	8.7
4 Corners	RI19.0C-2	28.4	26.9	5.3
4 Corners	RI19.0C-3	33.9	34.9	3.1
4 Corners	RI19.0C-6-1	19.5	20.5	5.2
4 Corners	RI19.0C-6-2	31.3	30.7	1.8
Verification	RI19.0C-1	25.8	24.5	5.0
Verification	RI19.0C-4	30.2	31.2	3.3
Verification	RI19.0C-5	26.9	30.1	11.9
Average	RI19.0C	-	-	5.1

Table 32. Summary of Numerical Performance Results Obtained from Performance-Volumetric Relationship and FlexPAVE™ Simulation Predictions (Rut Depth)

Purpose	Sample	Rut depth (mm) from FlexPAVE™	Rut depth (mm) from PVR	*% Error*
4 Corners	RS9.5C-1	0.8	1.0	21.0
4 Corners	RS9.5C-3	4.0	4.1	2.4
4 Corners	RS9.5C-7	4.3	4.3	0.9
4 Corners	RS9.5C-10	1.9	1.7	11.4
Verification	RS9.5C-2	6.3	4.6	26.6
Verification	RS9.5C-7	2.2	3.0	40.7
Verification	RS9.5C-9	1.8	2.5	45.0
Average	RS9.5C	-	-	21.1
4 Corners	RI19.0C-2	1.7	2.2	24.3
4 Corners	RI19.0C-3	3.6	3.3	7.4
4 Corners	RI19.0C-6-1	1.2	0.9	19.5
4 Corners	RI19.0C-6-2	2.6	2.6	2.7
Verification	RI19.0C-1	1.3	1.7	33.2
Verification	RI19.0C-4	2.3	2.8	19.7
Verification	RI19.0C-5	2.2	2.4	9.8
Average	RI19.0C	-	-	16.7

CHAPTER 5. EVALUATION OF FIELD CONSTRUCTION USING PERFORMANCE-VOLUMETRIC RELATIONSHIPS

Because the PVRs were proven to be able to predict pavement performance using the volumetric conditions, the effects of mixture variability and construction variability on pavement performance were evaluated using the developed PVRs for the RS9.5C and RI19.0C mixtures.

Sample and Field Construction Variability

The variability of the measured AQCs was investigated at both the mixture level and the construction level. Because four variables, i.e., maximum specific gravity (G_{mm}), binder content, in-place density, and aggregate bulk specific gravity (G_{sb}), were used to calculate the two volumetric conditions (VMA_{IP} and VFA_{IP}) for the PVRs, these four variables needed to be evaluated by comparing them to individual control limits and density requirements obtained from the NCDOT QMS manual (2018). Of these four variables, the binder content and in-place density values of the two mixtures were compared, schematically and numerically, to the control limits shown in Figure 26 through Figure 41 and Table 33 and Table 34, respectively. The other two variables were not compared to the control limits because the NCDOT shadow project used the same G_{sb} value from the JMF for each mixture and because the G_{mm} control limit is not specified in the NCDOT QMS manual specifications.

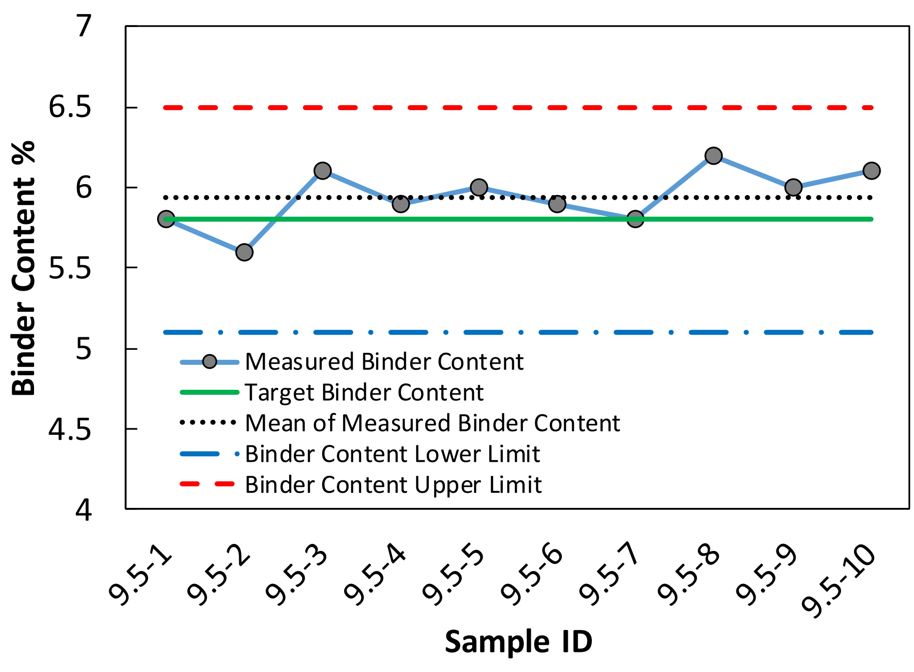

Figure 26. Graph. Measured variability of binder content of ten samples (RS9.5C).

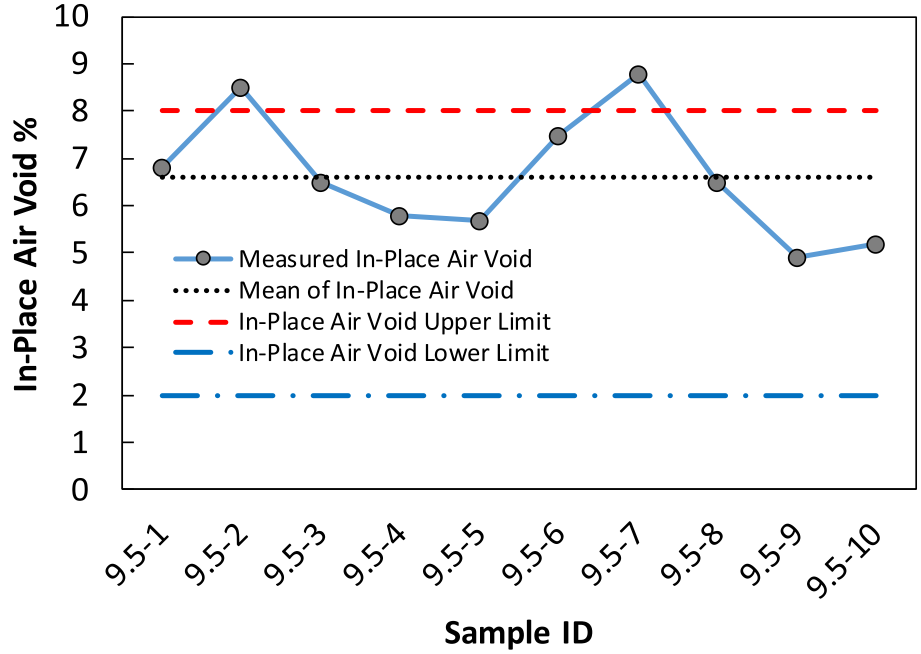

Figure 27. Graph. Measured in-place air void content of ten samples (RS9.5C).

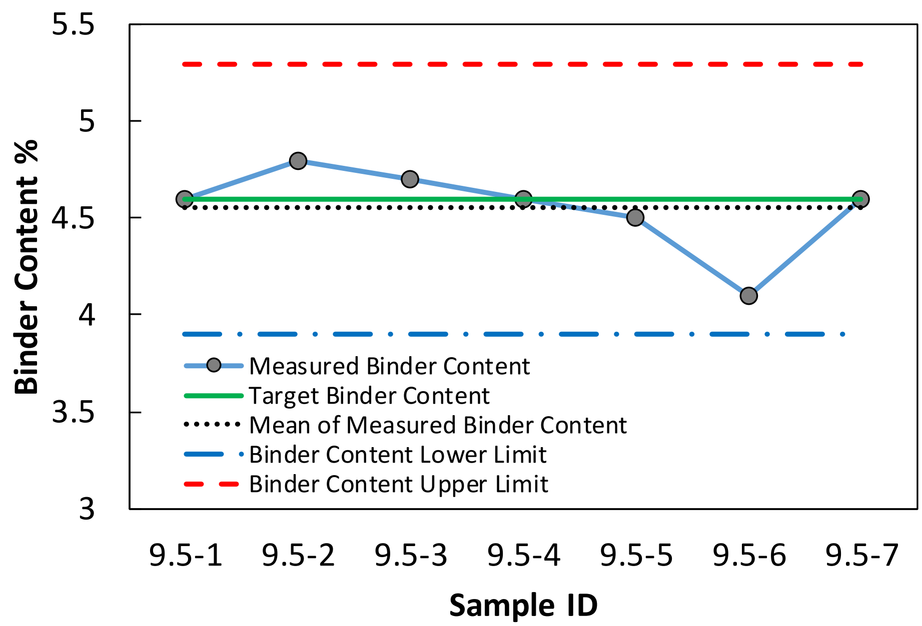

Figure 28. Graph. Measured variability of binder content of seven samples (RI19.0C).

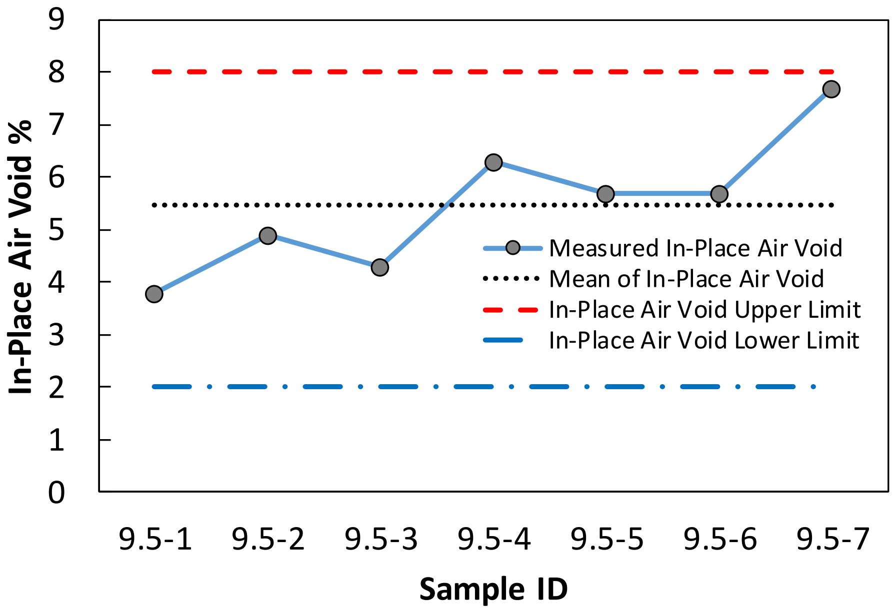

Figure 29. Graph. Measured variability of in-place air void content of seven samples (RI19.0C).

Table 33. Comparison of Mixture and Construction Variability to Control Limits (RS9.5C)

Sample	Asphalt Binder (%)	In-Place Air Void Content (%)	G_{mm}
9.5-1	5.8	6.8	2.427
9.5-2	5.6	8.5	2.429
9.5-3	6.1	6.5	2.420
9.5-4	5.9	5.8	2.423
9.5-5	6.0	5.7	2.427
9.5-6	5.9	7.5	2.426
9.5-7	5.8	8.8	2.431
9.5-8	6.2	6.5	2.426
9.5-9	6	4.9	2.421
9.5-10	6.1	5.2	2.422
Individual Limit	5.1 – 6.5	2 – 8	-
Average	5.6	6.6	2.425
COV%	3.0	19.9	0.1

Table 34. Comparison of Mixture and Construction Variability to Control Limits (RI19.0C)

Sample	Asphalt Binder (%)	In-Place Air Void Content (%)	G_{mm}
19-1	4.6	3.8	2.485
19-2	4.8	4.9	2.475
19-3	4.7	4.3	2.469
19-4	4.6	6.3	2.480
19-5	4.5	5.7	2.480
19-6	4.1	5.7	2.489
19-7	4.6	7.7	2.474
Individual Limit	3.9 – 5.3	2 – 8	-
Average	4.6	5.5	2.479
COV%	4.9	23.8	0.3

The variability of the binder contents (mixture quality) and in-place air void contents (construction quality) is expressed as the coefficient of variation (COV); for the shadow project, these values were 3.0% and 19.9% for RS9.5C, and 4.9% and 23.8% for RI19.0C, respectively. The variability of the in-place air void contents was significantly greater (higher values) than for the binder contents. The difference between the maximum and minimum values of the ten RS 9.5C samples was 0.6% for the binder content (between Samples 9.5-2 and 9.5-8) and 3.9% for the in-place air void content (between Samples 9.5-9 and 9.5-7). For RI19.0C, the difference between the maximum and minimum values of the seven samples was 0.7% for the binder content (between Samples 19-6 and 19-2) and 3.9% for the in-place air void content (between Samples 19-1 and 19-7). The in-place air void contents of Samples 9.5-2 and 9.5-7 exceeded the maximum field density requirement range. This analysis shows that more variability occurred at the construction level than at the mixture level.

Evaluation of Constructed Pavement Performance Using Performance-Volumetric Relationships

Pavement performance was predicted using the PVRs for the two-layer pavement structure. Table 35 and Table 36 show the variables that were used for the calculation of the volumetric properties, the calculated volumetric properties, and the predicted results of the pavement performance using PVRs for the obtained samples of the two mixtures. Figure 30 and Figure 31 present graphs of the performance predictions for the two mixtures, respectively. The performance of the ten RS9.5C samples was predicted as 3.1% for *% damage* and 3.6-mm for AC rut depth, on average. For the seven RI19.0C samples, 29.1% for *% damage* and 2.4-mm for AC rut depth were predicted, on average. The maximum percentages of difference among the ten RS9.5C samples for both *% damage* and rut depth were calculated as 78.3% and 57.8%, respectively, and, for the seven RI19.0C samples, were 32.7% and 59.2%, respectively. Note that these predicted performance results are based on the simulations where the mixture properties of the layer in question are changed and the reference mixture properties are used for the other layer. That is, to evaluate the effects of the variability in the RS9.5C mixture, the results were predicted under conditions of an 11-cm AC intermediate layer (Sample RI19.0C-4) at 6.6% in-place air void content underneath the surface layer. For RI19.0C, the results were predicted under conditions of a 4.3-cm AC surface layer (Sample RS9.5C-7) at 7.5% in-place air void content above the intermediate layer.

Table 35. Mixture and Construction Variables for Ten Samples (RS9.5C)

Sample	G_{sb}	G_{mm}	Binder Content (%)	In-Place Air Void Content (%)	In-Place VMA (%)	In-Place VFA (%)	*% damage*	AC Rut Depth (mm)
9.5-1	2.680	2.427	5.8	6.8	20.5	66.8	3.5	3.8
9.5-2	2.680	2.429	5.6	8.5	21.7	60.9	4.5	4.7
9.5-3	2.680	2.420	6.1	6.5	20.7	68.6	2.6	3.4
9.5-4	2.680	2.423	5.9	58	19.9	70.8	2.7	3.2
9.5-5	2.680	2.427	6.0	5.7	19.7	71.1	2.7	3.2
9.5-6	2.680	2.426	5.9	7.5	21.2	64.6	3.6	4.1
9.5-7	2.680	2.431	5.8	8.8	22.1	60.1	4.4	4.7
9.5-8	2.680	2.426	6.2	6.5	20.6	68.5	2.8	3.5
9.5-9	2.680	2.421	6.0	4.9	19.2	74.5	2.0	2.6
9.5-10	2.680	2.422	6.1	5.2	19.6	73.4	2.1	2.8
Average	2.680	2.425	6.0	6.6	-	-	3.1	3.6

Note: Gsb is aggregate bulk specific gravity, Gmm is maximum specific gravity, In-Place VMA is in-place voids in mineral aggregate, and In-Place VFA is in-place voids filled with asphalt binder.

Table 36. Mixture and Construction Variables for Seven Samples (RI19.0C)

Sample	G_{sb}	G_{mm}	Binder Content (%)	In-Place Air Void Content (%)	In-Place VMA (%)	In-Place VFA (%)	*% damage*	AC Rut Depth (mm)
19-1	2.688	2.485	4.6	3.8	15.2	74.9	24.9	1.7
19-2	2.688	2.475	4.8	4.9	16.6	70.6	28.9	2.3
19-3	2.688	2.469	4.7	4.3	16.2	73.5	27.9	2.2
19-4	2.688	2.480	4.6	6.3	17.5	64.1	30.9	2.6
19-5	2.688	2.480	4.5	5.7	16.9	66.3	29.3	2.4
19-6	2.688	2.489	4.1	5.7	16.3	64.9	27.3	2.1
19-7	2.688	2.474	4.6	7.7	19.0	59.4	34.7	3.2
Average	2.688	2.479	4.6	5.5	-	-	29.1	2.4

Note: G_{sb} is aggregate bulk specific gravity, G_{mm} is maximum specific gravity, In-Place VMA is in-place voids in mineral aggregate, and In-Place VFA is in-place voids filled with asphalt binder.

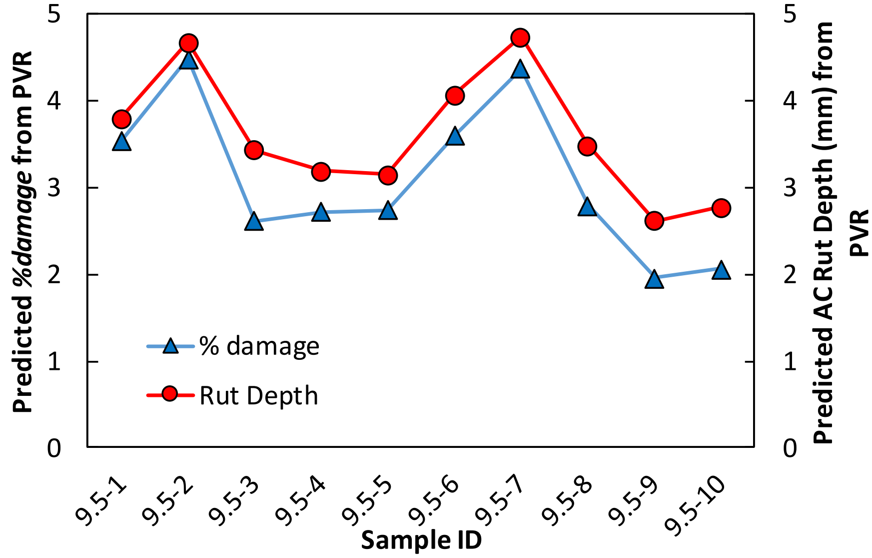

Figure 30. Graph. Predicted performance of ten samples (RS9.5C).

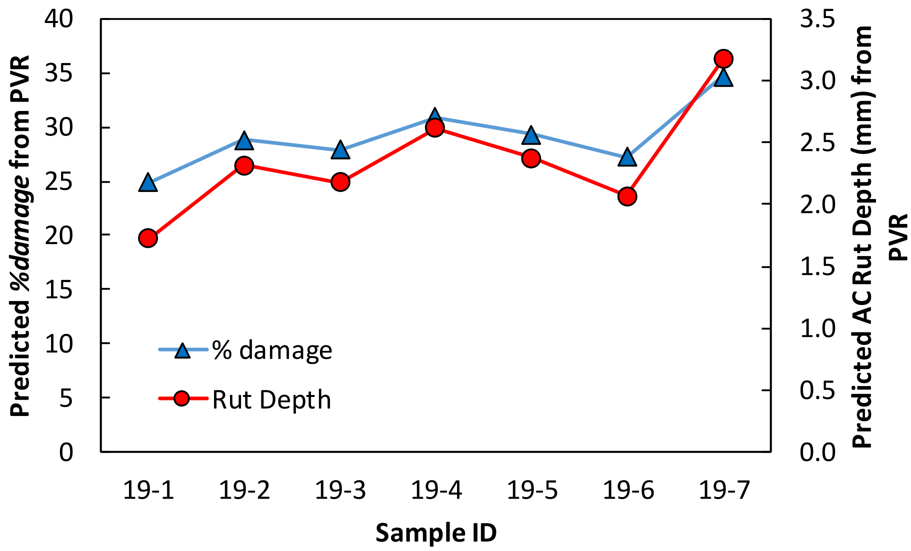

Figure 31. Graph. Predicted performance of seven samples (RI19.0C).

In order to understand the PVR concept fully, the factors that affect pavement performance must be understood as well. This analysis was implemented based on the information described in the previous section. First, the predicted performance of the obtained samples was plotted in terms of in-place density (in-place air void content) and binder content, as shown in Figure 32 through Figure 35. Based on these figures, the in-place air void content clearly plays a larger role in terms of pavement performance compared to binder content for both mixtures. In Figure 32 and Figure 34, the pavement seems to become increasingly susceptible to cracking and rutting as the in-place air void content is increased, which is a reasonable trend. However, the performance trends for the binder contents are not as clear as for the in-place air void contents. For RS9.5C in Figure 33, the pavement generally has a decreasing trend of cracking as the binder content is increased, which is a reasonable trend. However, the rutting trend with regard to binder content is difficult to accept because a soft mixture with a high binder content should be more susceptible to rutting. For RI19.0C, no clear trend was found between pavement performance and binder content.

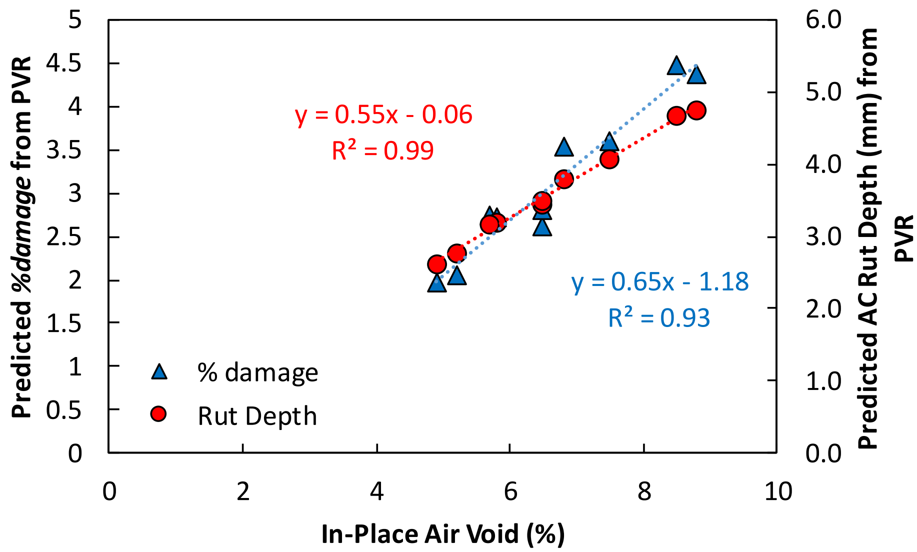

Figure 32. Graph. Comparison of predicted performance and measured in-place air void content for ten samples (RS9.5C).

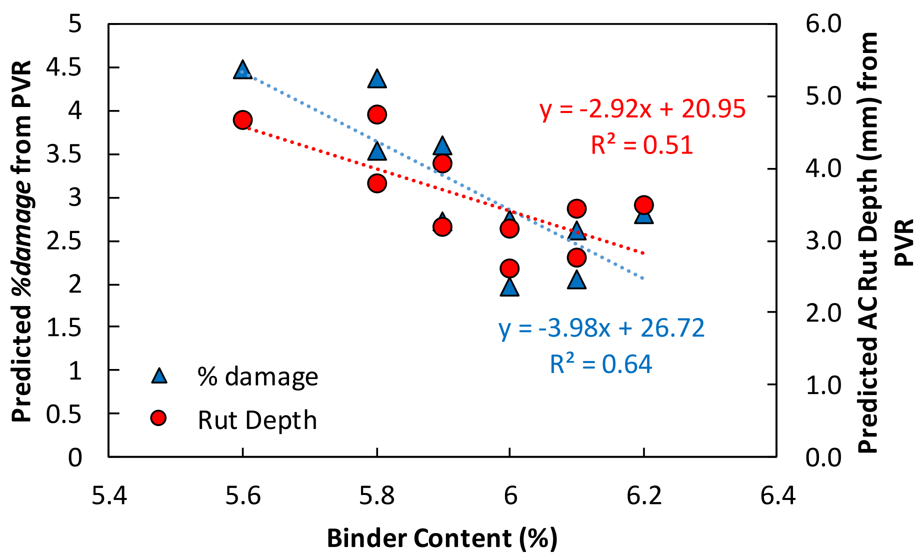

Figure 33. Graph. Comparison of predicted performance and measured binder content for ten samples (RS9.5C).

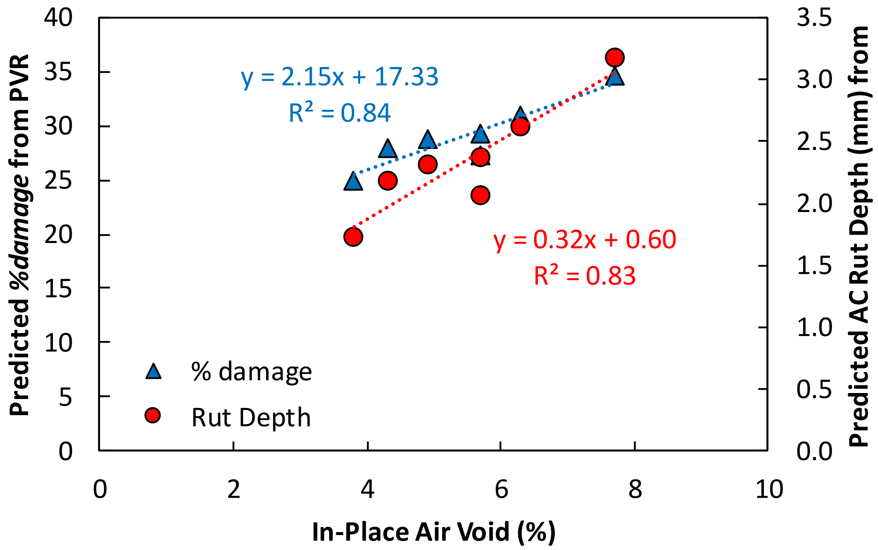

Figure 34. Graph. Comparison of predicted performance and measured in-place air void content for seven samples (RI19.0C).

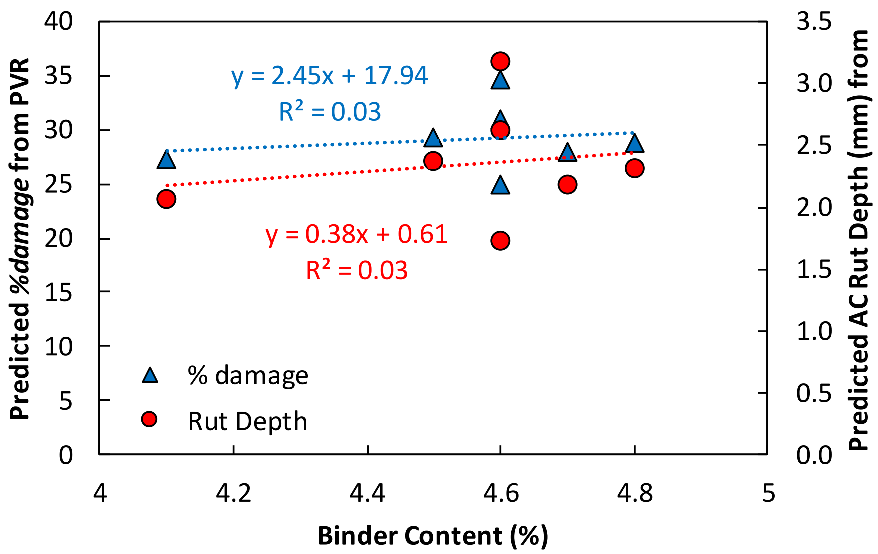

Figure 35. Graph. Comparison of predicted performance and measured binder content for seven samples (RI19.0C).

In order to investigate the impacts of the air void content and binder content on pavement performance, a sample from each mixture that had an air void content at the design compaction level (N_{des}) that was the most similar to that of the JMF was chosen as the reference sample. Based on Table 6, the air void contents at the N_{des} for RS9.5C-7 and RI19.0C-1 were measured as 2.9% and 3.9%, respectively, and the JMF target was 4.0% for both mixtures. Therefore, these two samples were chosen for the sensitivity analysis of the PVRs. In order to conduct sensitivity analysis, one variable is changed while the other variables remain fixed. Here, the binder content and in-place air void content were changed from 3% to 8%, respectively, while the other three factors remained the same to calculate the volumetric conditions. Figure 36 through Figure 39 show the sensitivity of the performance predicted from the PVR when only the in-place air void content and binder content were changed for both mixtures. For Figure 37 and Figure 39, the change in G_{mm} values with the binder contents was estimated using the G_{se} equation presented in equation (4). The G_{se} value for equation (4) was calculated using equation (15) based on the information for RS9.5C-7 and RI19.0C-1 presented in Table 6, respectively. For the G_b value, 1.034 was used because it is the same value the NCDOT uses for both mixtures.

$$G_{se} = \frac{P_{mm} - P_b}{\frac{P_{mm}}{G_{mm}} - \frac{P_b}{G_b}} \qquad (15)$$

where

G_{se} = the effective specific gravity of aggregate,

P_{mm} = the percentage by mass of the total loose mixture, which is 100,

P_b = the asphalt content (percentage by total mass of the mixture),

G_{mm} = the maximum specific gravity, and

G_b = the specific gravity of asphalt.

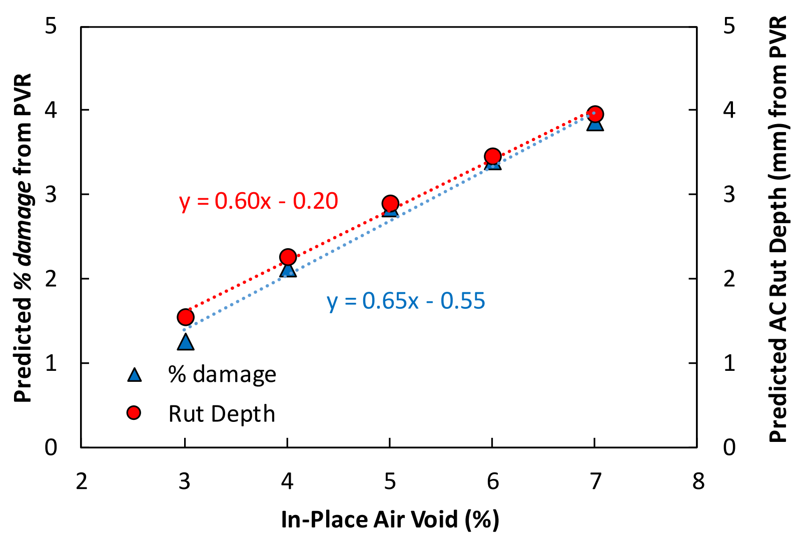

Figure 36. Graph. Sensitivity of predicted performance to in-place air void content (RS9.5C-7).

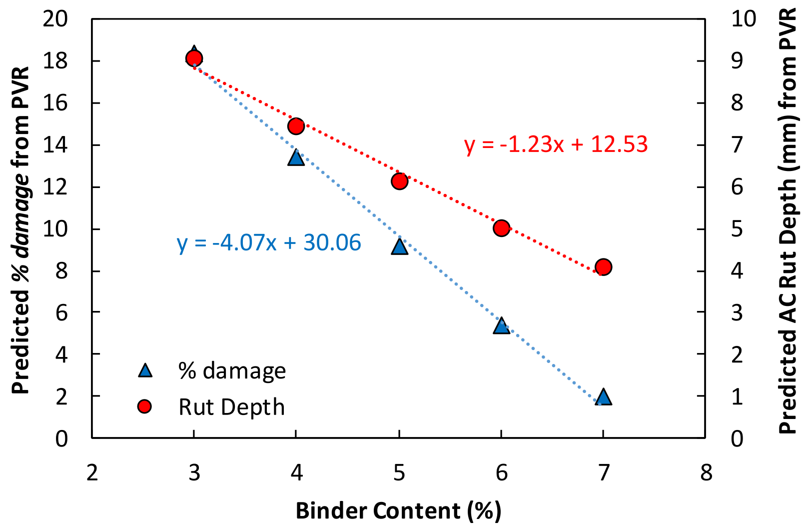

Figure 37. Graph. Sensitivity of predicted performance to binder content (RS9.5C-7).

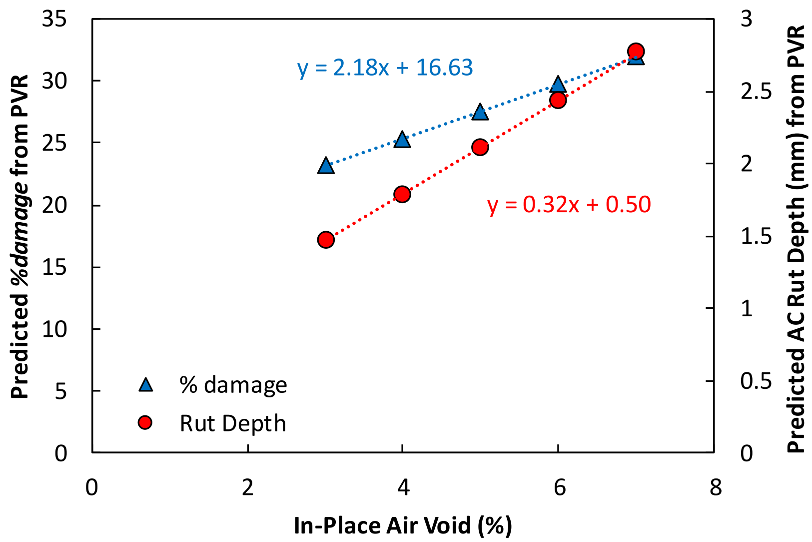

Figure 38. Graph. Sensitivity of predicted performance to in-place air void content (RI19.0C-1).

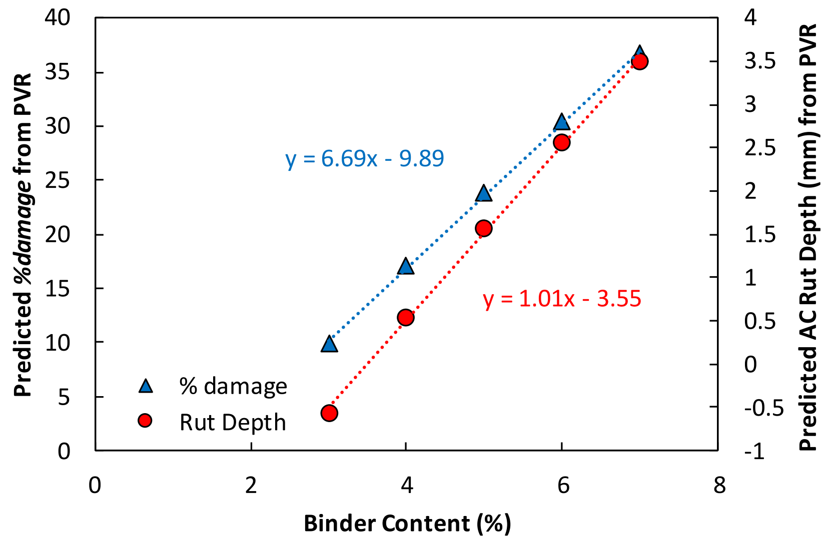

Figure 39. Graph. Sensitivity of predicted performance to binder content (RI19.0C-1).

Figure 36 and Figure 38 show that a 1% change in in-place air voids generates 0.65% and 2.18% of the change in *% damage* and 0.6-mm and 0.32-mm of the change in rut depth for RS9.5C-7 and RI19.0C-1, respectively. Also, Figure 37 and Figure 39 show that a 1% change in binder content generates 4.07% and 6.69% of the change in *% damage* and 1.23-mm and 1.01-mm of the rut depth for RS9.5C-7 and RI19.0C-1, respectively. The relationship between performance and in-place density makes sense because a higher air void content allows more room for cracks or ruts caused by traffic loads. Also, the relationships between *% damage* and the binder content of RS9.5C-7 and between rut depth and the binder content of RI19.0C-1 are reasonable because the higher binder content makes the mixture softer so that the pavement can dissipate the stress energy that causes fatigue damage compared to a stiffer pavement, but the pavement easily deforms under the traffic load.

However, the relationships between the rut depth and binder content of RS9.5C-7 and between *% damage* and the binder content of RI19.0C-1 are difficult to accept. The reason is thought to be the narrow range of the binder content in the collected samples, as shown in Figure 40 and Figure 41. The maximum differences between the binder contents at the four corners are 0.3% for RS9.5C and 0.7% for RI19.0C, which did not significantly affect the VMA_{IP} and VFA_{IP} calculations. Making the binder content effect side wider was not possible for this shadow project unless the measured AQC binder contents exhibited substantial variability among the collected samples. Thus, the developed PVRs were not able to capture the binder effect well due to the narrow range of the binder content, which affected the VMA_{IP} and VFA_{IP} used for PVR calibration. Note, however, that the PVR concept developed for performance-engineered mix design has proven that the PVR is able to capture the binder effect well. Therefore, this discrepancy can be considered to be a limitation of this shadow project's PVR specifically.

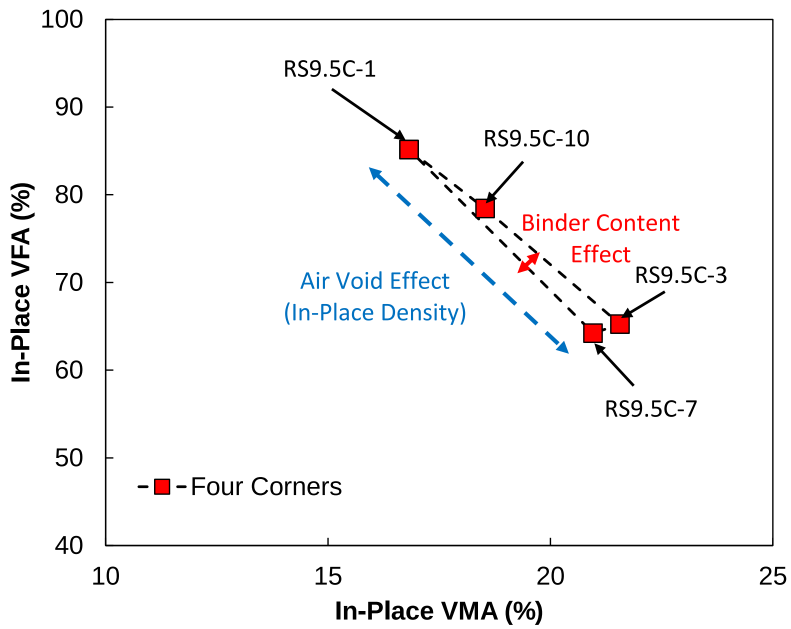

Figure 40. Graph. Effects of binder content and air void content on PVR calibration (RS9.5C).

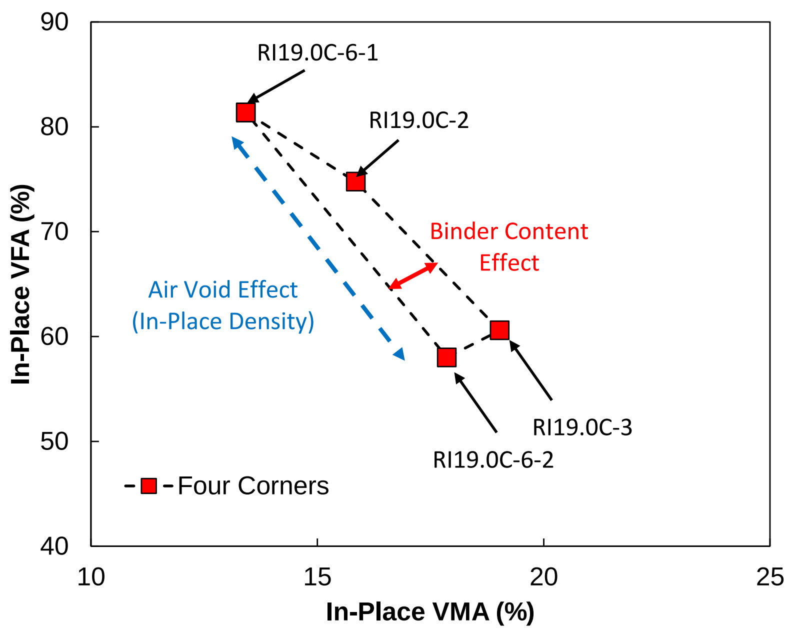

Figure 41. Graph. Effects of binder content and air void content on PVR calibration (RI19.0C).

Evaluation of Constructed Pavement Thickness Variability Using Performance-Volumetric Relationship

Although pavement performance has been predicted and evaluated for the constructed pavements, the impact of the difference between the as-designed and as-constructed layer thickness on pavement performance also should be evaluated. The NCDOT measured the layer thicknesses at the locations where the 27 samples were paved; Table 37 presents a comparison of the measured thicknesses and the pavement structural design thicknesses.

Table 37. Measured and Design Thicknesses for Pavement Structure

Sample	Measured Thickness	Sample	Measured Thickness	Sample	Measured Thickness
RS9.5-1	1.625 in. (4.1 cm)	RI19-1	4 in. (10.2 cm)	RB25-1	4.5 in. (11.4 cm)
RS9.5-2	1.5 in. (3.8 cm)	RI19-2	4 in. (10.2 cm)	RB25-2	5 in. (12.7 cm)
RS9.5-3	1.5 in. (3.8 cm)	RI19-3	3.875 in. (9.8 cm)	RB25-3	4.5 in. (11.4 cm)
RS9.5-4	1.75 in. (4.4 cm)	RI19-4	4.125 in. (10.5 cm)	RB25-4	4 in. (10.2 cm)
RS9.5-5	1.875 in. (4.8 cm)	RI19-5	4 in. (10.2 cm)	RB25-5	4.5 in. (11.4 cm)
RS9.5-6	1.5 in. (3.8 cm)	RI19-6	4 in. (10.2 cm)	RB25-6	4.5 in. (11.4 cm)
RS9.5-7	1.75 in. (4.4 cm)	RI19-7	4 in. (10.2 cm)	RB25-7	4.5 in. (11.4 cm)
RS9.5-8	1.75in. (4.4 cm)	-	-	RB25-8	4 in. (10.2 cm)
RS9.5-9	1.5 in. (3.8 cm)	-	-	RB25-9	4 in. (10.2 cm)
RS9.5-10	2 in. (5.1 cm)	-	-	RB25-10	-
Average	1.675 in. (4.3 cm)	Average	4 in. (10 cm)	Average	(11.1 cm)
Design	3 in. (7.6 cm)	Design	4 in. (10 cm)	Design	(11.4 cm)

Table 37 shows that the AC surface layer was constructed to be approximately 3.3-cm (1.3 in.) thinner than the designed thickness whereas the AC intermediate and AC base layers were constructed to thicknesses similar to the design targets. Therefore, the impact of these differences in AC surface layer thickness on pavement performance should be investigated. In order to perform this analysis, the two-layer case (Case 2) that was employed for the PVR development was selected for the FlexPAVE™ simulations, but the surface layer thickness was changed from 4.3-cm to 7.6-cm. Table 38 presents the inputs used for this case simulation.

Table 38. Inputs for FlexPAVE^{TM} Simulations of Two-Layer Pavement Structure

FlexPAVE^{TM} Inputs	Input
Pavement Design Life (Years)	20
Asphalt Concrete Surface	Material Properties: Imported from AMPT Test Results, Thickness: 3 in. (7.6 cm)
Asphalt Concrete Intermediate	Material Properties: Imported from AMPT Test Results, Thickness: 4 in. (10 cm)
Aggregate Base	Elastic Modulus: 275,790 kPa Thickness: 10 in. (25 cm) Poisson's Ratio: 0.35
Subgrade	Elastic Modulus: 68,948 kPa Poisson's Ratio: 0.4
Climate	Raleigh, NC
Traffic	Daily ESAL: 4,167 with no traffic growth

The same method that was used for the two-layer simulation case was used also for the simulation and *% damage* calculation for the individual AC surface layer and AC intermediate layer by inputting the data for the RS9.5C-7 and RI19.0C-4 samples for the reference layers. Table 39 and Table 40 show the simulation results for the AC surface layer and AC intermediate layer, respectively.

Table 39. FlexPAVE^{TM} Simulation Results for AC Surface Layer with Design AC Surface Thickness Using the Two-Layer Structure

Sample	AC Surface *% damage*	AC Surface Rut Depth (mm)
RS9.5C-1	0.2	1.3
RS9.5C-2	2.6	10.1
RS9.5C-3	1.5	6.3
RS9.5C-4	0.8	3.5
RS9.5C-7	2.1	6.8
RS9.5C-9	0.8	2.8
RS9.5C-10	0.4	3.1

Table 40. FlexPAVE^{TM} Simulation Results for AC Intermediate Layer with Design AC Surface Thickness Using the Two-Layer Structure

Sample	AC Intermediate *% damage*	AC Intermediate Rut Depth (mm)
RI19.0C-1	24.5	1.2
RI19.0C-2	27.7	1.6
RI19.0C-3	35.2	3.0
RI19.0C-4	30.3	2.0
RI19.0C-5	26.1	1.9
RI19.0C-6-1	17.2	1.0
RI19.0C-6-2	32.1	2.0

Table 41 through Table 44 compare the simulated *% damage* and rut depth values for the AC surface layer and AC intermediate layer, respectively, under AC surface layers with 4.3-cm and 7.6-cm thicknesses.

Table 41. Comparison of Simulated *% damage* in AC Surface Layer under Two AC Surface Layer Thickness Conditions

Sample	**Average Sample Air Void (%)**	***% damage* in AC Surface (4.3 cm)**	***% damage* in AC Surface (7.6 cm)**	**Increase/Decrease (From 4.3 cm to 7.6 cm)**
RS9.5C-1	2.4	0.5	0.2	-64.9%
RS9.5C-2	8.6	4.9	2.6	-46.0%
RS9.5C-3	7.3	3.0	1.5	-49.8%
RS9.5C-4	5.6	1.9	0.8	-54.7%
RS9.5C-7	7.4	4.0	2.1	-47.5%
RS9.5C-9	5.0	1.9	0.8	-56.3%
RS9.5C-10	3.7	1.0	0.4	-61.6%
Average	-	-	-	-54.4%

Table 42. Comparison of Simulated *% damage* in AC Intermediate Layer under Two AC Surface Layer Thickness Conditions

Sample	**Average Sample Air Void (%)**	***% damage* in AC Intermediate (4.3 cm)**	***% damage* in AC Intermediate (7.6 cm)**	**Increase/Decrease (From 4.3 cm to 7.6 cm)**
RI19.0C-1	3.6	25.8	24.5	-5.0%
RI19.0C-2	4.0	28.4	27.7	-2.6%
RI19.0C-3	7.5	33.9	35.2	+4.0%
RI19.0C-4	6.4	30.2	30.3	+0.5%
RI19.0C-5	6.1	26.9	26.1	-3.2%
RI19.0C-6-1	2.5	19.5	17.2	-11.7%
RI19.0C-6-2	7.2	31.3	32.1	+2.8%
Average	-	-	-	-2.2%

Table 43. Comparison of Simulated Rut Depth in AC Surface Layer under Two AC Surface Layer Thickness Conditions

Sample	Average Sample Air Void (%)	Rut Depth (mm) in Surface (4.3 cm)	Rut Depth (mm) in Surface (7.6 cm)	% Change (from 4.3 cm to 7.6 cm)
RS9.5C-1	2.3	0.8	1.3	+65.4%
RS9.5C-2	8.4	6.3	0.1	+60.1%
RS9.5C-3	7.9	4.0	6.3	+57.8%
RS9.5C-4	5.5	2.2	3.5	+61.3%
RS9.5C-7	7.6	4.3	6.8	+57.7%
RS9.5C-9	4.8	1.8	2.8	+62.1%
RS9.5C-10	3.5	1.9	3.1	+59.9%
Average	-	-	-	+60.6%

Table 44. Comparison of Simulated Rut Depth in AC Intermediate Layer under Two AC Surface Layer Thickness Conditions

Sample	Average Sample Air Void (%)	Rut Depth (mm) in Intermediate (4.3 cm)	Rut Depth (mm) in Intermediate (7.6 cm)	% Change (from 4.3 cm to 7.6 cm)
RI19.0C-1	3.8	1.3	1.2	-9.4%
RI19.0C-2	4.0	1.7	1.6	-7.6%
RI19.0C-3	7.5	3.6	3.0	-17.4%
RI19.0C-4	6.3	2.3	2.0	-11.8%
RI19.0C-5	5.7	2.2	1.9	-11.3%
RI19.0C-6-1	2.5	1.2	1.0	-18.3%
RI19.0C-6-2	7.5	2.6	2.0	-21.7%
Average	-	-	-	-13.9%

The simulated performance under the two-layer scenario shows average decreases in *% damage* of 54.4% and 2.2% for the AC surface and AC intermediate layers, respectively, as the AC surface thickness was changed from 4.3-cm to 7.6-cm. For rut depth, the simulated performance shows a 60.6% average increase in the AC surface layer and 13.9% average decrease in the AC intermediate layer.

Because the thickness of the unbound layers underneath the AC pavement surface remains the same, a 3.3-cm thicker AC surface layer can possibly generate higher total rut depth values. This outcome is because FlexPAVE™ uses the average permanent strain (APS), which is the RSI value divided by 100 and is obtained from the SSR test results of each sample, and then multiplies the AC layer thickness by the APS value to calculate the rut depth. Therefore, the APS is considered a mixture or sample property. If the APS value of a certain mixture is 0.04, for example, and the layer thicknesses using this mixture are 10-cm and 20-cm, then FlexPAVE™ calculates the AC layer thicknesses as 0.40-cm and 0.80-cm, respectively. Note that this calculation is only applicable to AC layers. Furthermore, RS9.5C samples 2, 3, 4, and 7 and RI19.0C samples 3, 4, 5, and 6-2 were tested at very high air void contents, so they have high APS values for the simulations. For these reasons, a thicker AC surface layer can possibly lead to higher rut depth values that in turn affect the total rut depth.

The PVRs for the design AC surface layer thickness were developed using the same volumetric conditions and linear regression method as described in CHAPTER 4. Table 45 and Table 46 present summaries of the calibrated PVR coefficients and intercepts for RS9.5C and RI19.0C, respectively. The developed PVRs also were verified using the same method by comparing the performance simulated by FlexPAVE™ with the predictions from the PVRs, as shown in Figure 42 through Figure 45. Figure 42 to Figure 45 indicate that the verification samples are located close to the LOE for both cases of the two mixtures.

Table 45. PVR Coefficients for RS9.5C in the Two-Layer Structure with Design AC Surface Layer Thickness

Performance	a	b	d	R^2
% Damage	-0.665	-0.223	30.415	0.99
AC Rut Depth	-0.257	-0.280	30.03	0.99

Table 46. PVR Coefficients for RI19.0C in the Two-Layer Structure with Design AC Surface Layer Thickness

Performance	a	b	d	R^2
% Damage	3.382	0.033	-29.967	0.97
AC Rut Depth	0.464	0.037	-8.352	0.95

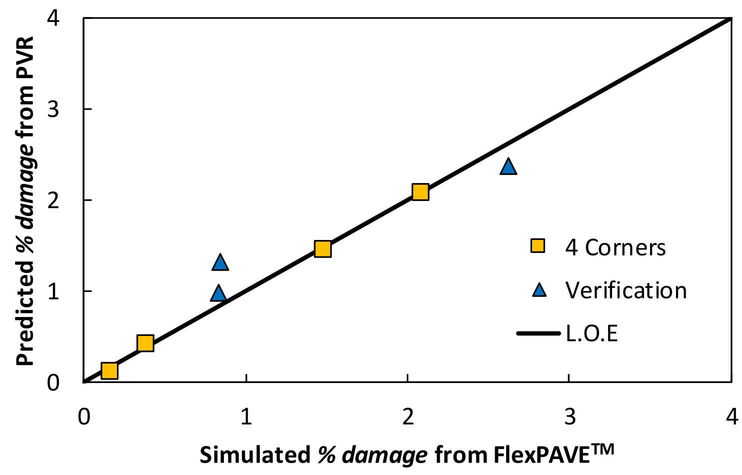

Figure 42. Graph. Comparison of *% damage* of RS9.5C predicted from PVR and simulated by FlexPAVE™ in the two-layer structure with design AC surface layer thickness.

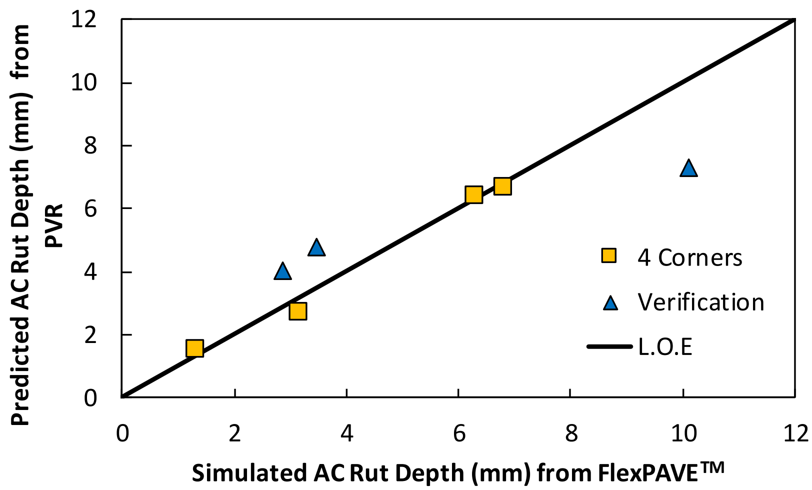

Figure 43. Graph. Comparison of rut depth of RS9.5C predicted from PVR and simulated by FlexPAVE™ in the two-layer structure with design AC surface layer thickness.

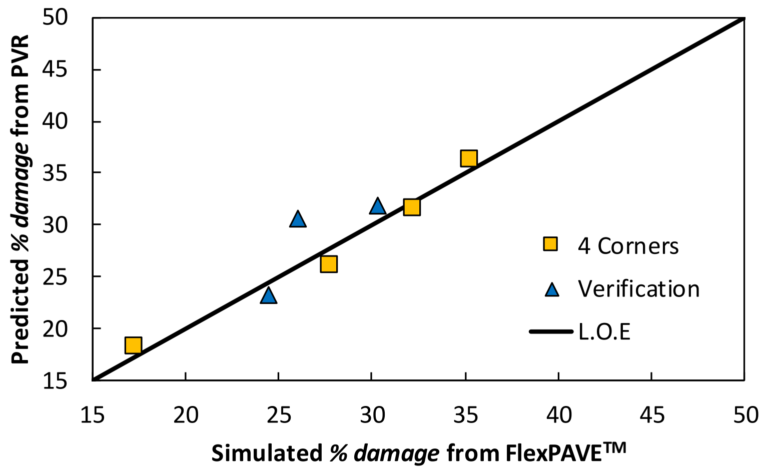

Figure 44. Graph. Comparison of *% damage* of RI19.0C predicted from PVR and simulated by FlexPAVE™ in the two-layer structure with design AC surface layer thickness.

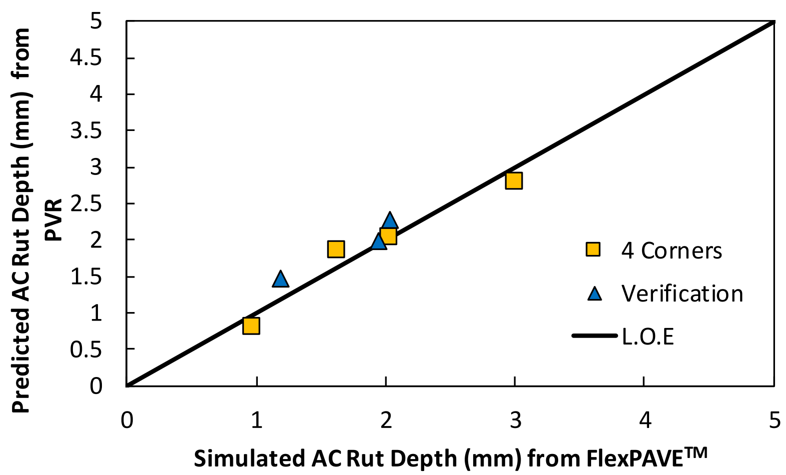

Figure 45. Graph. Comparison of rut depth of RI19.0C predicted from PVR and simulated by FlexPAVE™ in the two-layer structure with design AC surface layer thickness.

As a last step, the field pavement performance was evaluated using the developed PVRs for the as-designed AC surface layer thickness (7.6-cm) and was compared to the pavement performance using the PVRs for the as-constructed AC surface layer thickness (average 4.3-cm), as shown in Figure 46 and Figure 47 for RS9.5C and RI19.0C, respectively. Table 47 and Table 48 present the numerical comparisons of the predicted performance for RS9.5C and RI19.0C, respectively. Note that the same volumetric conditions for each sample shown in Table 35 and were applied to predict the pavement performance.

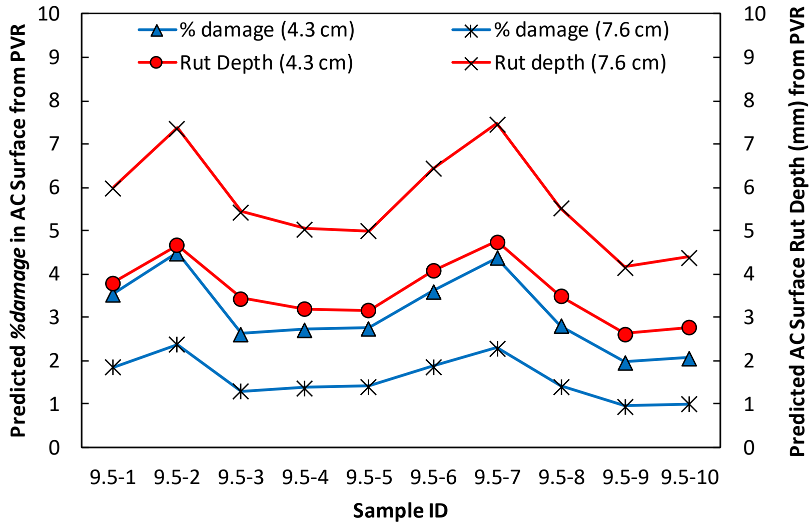

Figure 46. Graph. Comparison of predicted values of ten RS9.5C samples at two AC surface layer thicknesses.

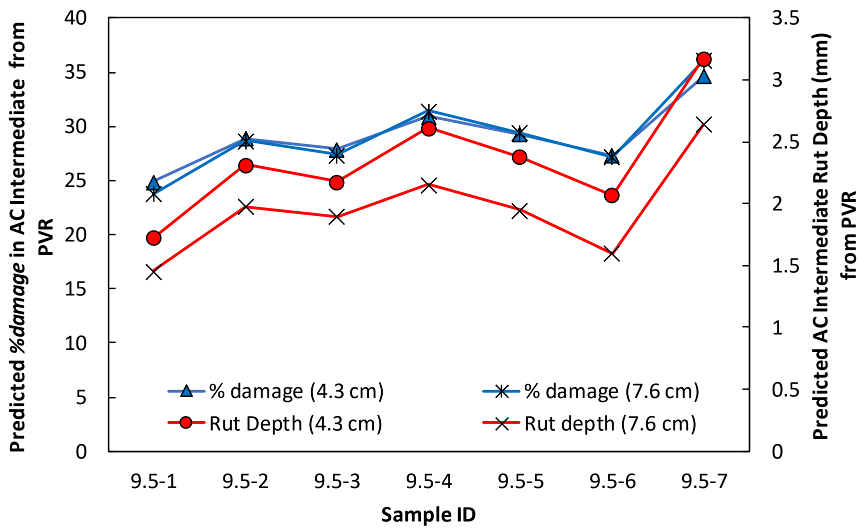

Figure 47. Graph. Comparison of predicted values of seven RI19.0C samples at two AC surface layer thicknesses.

Table 47. Predicted Performance Comparison of Ten RS9.5C Samples at Two AC Surface Layer Thicknesses

Sample	% damage (AC Surface 4.3 cm)	% damage (AC Surface 7.6 cm)	Rut Depth (AC Surface 4.3 cm)	Rut Depth (AC Surface 7.6 cm)
9.5-1	3.5	1.8	3.8	6.0
9.5-2	4.5	2.4	4.7	7.4
9.5-3	2.6	1.3	3.4	5.4
9.5-4	2.7	1.4	3.2	5.0
9.5-5	2.7	1.4	3.2	5.0
9.5-6	3.6	1.9	4.1	6.4
9.5-7	4.4	2.3	4.7	7.5
9.5-8	2.8	1.4	3.5	5.5
9.5-9	2.0	1.0	2.6	4.2
9.5-10	2.1	1.0	2.8	4.4
Average	3.1	1.6	3.6	5.7
Inc/Decrease (4.3 to 7.6 cm)	-	-48.9%	-	+58.0%

Table 48. Predicted Performance Comparison of Seven RI19.0C Samples at Two AC Surface Layer Thicknesses

Sample	% damage (AC Surface 4.3 cm)	% damage (AC Surface 7.6 cm)	Rut Depth (AC Surface 4.3 cm)	Rut Depth (AC Surface 7.6 cm)
19-1	24.9	23.8	1.7	1.5
19-2	28.9	28.7	2.3	2.0
19-3	27.9	27.4	2.2	1.9
19-4	30.9	31.4	2.6	2.2
19-5	29.3	29.4	2.4	1.9
19-6	27.3	27.2	2.1	1.6
19-7	34.7	36.1	3.2	2.6
Average	29.1	29.2	2.4	2.0
In/Decrease (4.3 to 7.6 cm)	-	+0.1%	-	-17.0%

The performance predictions for the ten RS9.5C samples with the 7.6-cm AC surface layer thickness were 1.6% for *% damage* and 5.7-mm for AC rut depth, on average. These results represent a 48.9% decrease for *% damage* and 58% increase for rut depth compared to the performance predictions at the 4.3-cm AC surface layer thickness. For the seven RI19.0C samples, the performance predictions were on average 29.2% for *% damage* and 2-mm for rut depth for the 7.6-cm AC surface layer thickness. The average *% damage* of the RI19.0C samples was not affected by the change in AC surface thickness, but the average rut depth showed a 17% decrease. Therefore, the predictions indicate that a 3.3-cm thicker AC surface layer can reduce cracking in AC surface layers and rutting in AC intermediate layers. However, a thicker surface layer also can possibly increase rutting in the AC surface layer.

CHAPTER 6. CONCLUSIONS

The conclusions that can be drawn from the work presented in this report are as follows.

- Three FlexPAVE^{TM} simulation cases were implemented: a three-layer case, a two-layer case, and a single-layer case. All layers were AC layers. The three-layer case was the closest to the field conditions, but the simulated performance results for the AC surface and AC intermediate layers were not reasonable to use for the development of PVRs for the mixtures used in the surface and intermediate layers. This limitation is mostly due to the lack of aging model in FlexPAVE^{TM} v. 1.1.

- The PVRs were developed using the AMPT test results and FlexPAVE^{TM} simulation results for the two-layer case. The average *% error* values for *% damage* and rut depth between the FlexPAVE^{TM} simulations and the PVR predictions were 8.7% and 21.1% for RS9.5C and 5.1% and 16.7% for RI19.0C, respectively. Although the rut depth predictions show relatively high *% error* values, the numerical differences in rut depth between the FlexPAVE^{TM} predictions and the PVR predictions did not exceed 1 mm, except for one sample.

- Based on the measured AQCs for the RS9.5C mixture, the binder contents of the ten RS9.5C samples were in the acceptable range, but the in-place air void contents of two of the samples were higher than the acceptable range. The COVs of the binder contents and in-place air void contents for the ten samples were 3.0% and 19.9%, respectively.

- Based on the measured AQCs for the RI19.0C mixture, the binder contents and in-place air void contents of the seven RI19.0C samples were in the acceptable range. The COVs of the binder contents and in-place air void contents for the seven samples were 4.9% and 23.8%, respectively.

- The predicted pavement performance of the ten RS9.5C samples was on average 3.1% for *% damage* and 3.6 mm for AC rut depth. The maximum percentage differences within the ten samples were calculated as 78.3% for *% damage* and 57.8% for rut depth.

- The predicted pavement performance of the seven RI19.0C samples was on average 29.1% for *% damage* and 2.4 mm for AC rut depth. The maximum percentage differences within the seven samples were calculated as 32.7% for *% damage* and 59.2% for rut depth.

- The fatigue damage and rutting performance predicted from the developed PVRs showed reasonable trends with regard to changes in in-place air void contents. However, the rut depth trends for RS9.5C and *% damage* trends for RI19.0C with regard to the binder contents were not acceptable. The reason for these outcomes appears to be that the range of the binder contents in the PVR calibration samples was significantly narrower than the range of the in-place air void contents. This discrepancy can be considered as a limitation of this shadow project's PVRs in their ability to capture the effects of binder content on pavement performance.

- The impact of construction variability in terms of layer thickness differences between the as-designed (7.6 cm) and as-constructed (4.3 cm) pavements was investigated in two AC layers structures. A difference of around 3.3 cm between the design and constructed layer thicknesses led to a 48.9% decrease in *% damage* in the AC surface layer and a 17% decrease in rut depth in the AC intermediate layer, on average. However, the difference in AC layer thickness can also cause a 58% increase in rut depth in the AC surface layer.

REFERENCES

1. Wang, Y. and Y. R. Kim. (2017). Development of a Pseudo Strain Energy-Based Fatigue Failure Criterion for Asphalt Mixtures. *International Journal of Pavement Engineering*, DOI: 10.1080/10298436.2017.1394100.

2. Federal Highway Administration (2019). Cyclic Fatigue Index Parameter, S_{app}, for Asphalt Performance Engineered Mixture Design. FHWA-HIF-19-091.

3. Ghanbari, A., B. S. Underwood, and Y. R. Kim. (2020). Development of a Rutting Index Parameter Based on the Stress Sweep Rutting Test and Permanent Deformation Shift Model. *International Journal of Pavement Engineering*. DOI: 10.1080/10298436.2020.1748190.

4. Wang, Y., A. Ghanbari, B. S. Underwood, and Y. R. Kim. (2019). Development of a Performance-Volumetric Relationship for Asphalt Mixtures. *Transportation Research Record: Journal of the Transportation Research Board*, DOT: 10.1177/0361198119845364.

5. Superpave Mix Design: Superpave Series No. 2 (SP-2). (1996). *Asphalt Institution*, Lexington, KY.

6. Jeong, J. et al. (2020). Pavement Performance Predictions Using Performance-Volumetric Relationship and Evaluation of Construction Variability: Example of MaineDOT Shadow Project for the Development of Performance-Related Specifications. *Construction and Building Materials*. (Under Review)

APPENDIX. RESULTS OF AMPT PERFORMANCE TESTS

This appendix summarizes the NCDOT shadow project AMPT performance test results for the ten RS9.5C mixture samples and seven RI19.0C mixture samples. The three subsections, Dynamic Modulus Test Results, Direct Tension Cyclic Fatigue Test Results, and Stress Sweep Rutting Test Results, present the test data and results of these three AMPT performance tests, respectively.

Dynamic Modulus Test Results

Table 49 and Table 50 present summaries of the dynamic modulus test results for the tested RS9.5C samples and tested RI19.0C samples, respectively.

Table 49. Dynamic Modulus Test Results (RS9.5C)

Sample	Temperature (°C)	Specimen Number	Frequency (Hz)	Dynamic Modulus (MPa)	Phase Angle (Degrees)
RS9.5C-1	4	1	10	15713	8.87
RS9.5C-1	4	1	1	12305	10.98
RS9.5C-1	4	1	0.1	9217	13.77
RS9.5C-1	20	1	10	8222	17.05
RS9.5C-1	20	1	1	5191	21.74
RS9.5C-1	20	1	0.1	2980	26.66
RS9.5C-1	40	1	10	2405	31.13
RS9.5C-1	40	1	1	1099	34.52
RS9.5C-1	40	1	0.1	474	34.79
RS9.5C-1	4	2	10	15603	9.4
RS9.5C-1	4	2	1	12186	11.36
RS9.5C-1	4	2	0.1	9095	14.04
RS9.5C-1	20	2	10	7952	17.71
RS9.5C-1	20	2	1	4916	22.65
RS9.5C-1	20	2	0.1	2764	27.77
RS9.5C-1	40	2	10	2091	32.67
RS9.5C-1	40	2	1	899	35.98
RS9.5C-1	40	2	0.1	353	36.75
RS9.5C-1	4	3	10	15399	9.2
RS9.5C-1	4	3	1	12035	11.02
RS9.5C-1	4	3	0.1	9025	13.56
RS9.5C-1	20	3	10	7581	17.92
RS9.5C-1	20	3	1	4693	22.95
RS9.5C-1	20	3	0.1	2625	28.15
RS9.5C-1	40	3	10	1997	32.61
RS9.5C-1	40	3	1	868	35.43
RS9.5C-1	40	3	0.1	360	35.17

RS9.5C-2	4	1	10	10487	10.84
RS9.5C-2	4	1	1	7851	13.25
RS9.5C-2	4	1	0.1	5531	16.53
RS9.5C-2	20	1	10	5082	19.43
RS9.5C-2	20	1	1	3003	24.52
RS9.5C-2	20	1	0.1	1603	29.25
RS9.5C-2	40	1	10	1123	33.28
RS9.5C-2	40	1	1	449	35.19
RS9.5C-2	40	1	0.1	182	34.15
RS9.5C-2	4	2	10	10447	10.59
RS9.5C-2	4	2	1	7812	12.94
RS9.5C-2	4	2	0.1	5524	16.28
RS9.5C-2	20	2	10	4867	19.97
RS9.5C-2	20	2	1	2835	24.92
RS9.5C-2	20	2	0.1	1516	29.6
RS9.5C-2	40	2	10	1138	33.29
RS9.5C-2	40	2	1	448	35.51
RS9.5C-2	40	2	0.1	174	35.5
RS9.5C-2	4	3	10	10231	10.81
RS9.5C-2	4	3	1	7638	13.17
RS9.5C-2	4	3	0.1	5394	16.49
RS9.5C-2	20	3	10	4603	20.51
RS9.5C-2	20	3	1	2652	25.55
RS9.5C-2	20	3	0.1	1389	30.15
RS9.5C-2	40	3	10	1056	33.25
RS9.5C-2	40	3	1	412	35.94
RS9.5C-2	40	3	0.1	165	35.37
RS9.5C-3	4	1	10	10820	9.97
RS9.5C-3	4	1	1	8181	12.1
RS9.5C-3	4	1	0.1	5847	15.28
RS9.5C-3	20	1	10	4789	20.19
RS9.5C-3	20	1	1	2794	25
RS9.5C-3	20	1	0.1	1482	29.49
RS9.5C-3	40	1	10	1183	33.08
RS9.5C-3	40	1	1	459	35.99
RS9.5C-3	40	1	0.1	179	35.75
RS9.5C-3	4	2	10	10384	10.87
RS9.5C-3	4	2	1	7783	13.04
RS9.5C-3	4	2	0.1	5528	16.13
RS9.5C-3	20	2	10	4797	19.96
RS9.5C-3	20	2	1	2779	25.17

RS9.5C-3	20	2	0.1	1464	30.13
RS9.5C-3	40	2	10	1144	33.07
RS9.5C-3	40	2	1	443	35.65
RS9.5C-3	40	2	0.1	170	35.7
RS9.5C-3	4	3	10	10756	10.37
RS9.5C-3	4	3	1	8124	12.58
RS9.5C-3	4	3	0.1	5793	15.8
RS9.5C-3	20	3	10	1200	33.16
RS9.5C-3	20	3	1	482	35.62
RS9.5C-3	20	3	0.1	203	34.83
RS9.5C-4	40	1	10	11965	10.17
RS9.5C-4	40	1	1	9026	12.56
RS9.5C-4	40	1	0.1	6486	15.82
RS9.5C-4	20	1	10	5642	20.15
RS9.5C-4	20	1	1	3320	24.88
RS9.5C-4	20	1	0.1	1787	29.47
RS9.5C-4	40	1	10	1612	32.86
RS9.5C-4	40	1	1	686	35.93
RS9.5C-4	40	1	0.1	276	36.15
RS9.5C-4	4	2	10	11790	10.39
RS9.5C-4	4	2	1	8937	12.57
RS9.5C-4	4	2	0.1	6453	15.65
RS9.5C-4	20	2	10	5455	19.82
RS9.5C-4	20	2	1	3192	24.95
RS9.5C-4	20	2	0.1	1703	29.88
RS9.5C-4	40	2	10	1422	33.58
RS9.5C-4	40	2	1	576	36.4
RS9.5C-4	40	2	0.1	223	36.73
RS9.5C-4	4	3	10	11555	10.41
RS9.5C-4	4	3	1	8706	12.69
RS9.5C-4	4	3	0.1	6294	15.76
RS9.5C-4	20	3	10	5383	19.78
RS9.5C-4	20	3	1	3156	24.88
RS9.5C-4	20	3	0.1	1690	29.82
RS9.5C-4	40	3	10	1337	33.03
RS9.5C-4	40	3	1	543	35.72
RS9.5C-4	40	3	0.1	218	35.69
RS9.5C-7	4	1	10	10814	10.67
RS9.5C-7	4	1	1	8161	13.06
RS9.5C-7	4	1	0.1	5825	16.13
RS9.5C-7	20	1	10	4942	19.93

RS9.5C-7	20	1	1	2931	23.61
RS9.5C-7	20	1	0.1	1576	26.87
RS9.5C-7	40	1	10	1254	31.61
RS9.5C-7	40	1	1	519	33.49
RS9.5C-7	40	1	0.1	212	33.24
RS9.5C-7	4	2	10	10945	10.49
RS9.5C-7	4	2	1	8175	12.98
RS9.5C-7	4	2	0.1	5760	16.35
RS9.5C-7	20	2	10	4698	21.15
RS9.5C-7	20	2	1	2693	26.21
RS9.5C-7	20	2	0.1	1429	30.31
RS9.5C-7	40	2	10	1155	32.39
RS9.5C-7	40	2	1	449	34.76
RS9.5C-7	40	2	0.1	172	35.22
RS9.5C-7	4	3	10	10492	10.8
RS9.5C-7	4	3	1	7863	13.22
RS9.5C-7	4	3	0.1	5525	16.49
RS9.5C-7	20	3	10	4614	20.99
RS9.5C-7	20	3	1	2636	26.06
RS9.5C-7	20	3	0.1	1379	30.51
RS9.5C-7	40	3	10	1151	32.37
RS9.5C-7	40	3	1	457	34.99
RS9.5C-7	40	3	0.1	175	35.53
RS9.5C-9	4	1	10	12613	10.23
RS9.5C-9	4	1	1	9552	12.61
RS9.5C-9	4	1	0.1	6880	15.73
RS9.5C-9	20	1	10	5951	19.42
RS9.5C-9	20	1	1	3480	24.81
RS9.5C-9	20	1	0.1	1851	29.91
RS9.5C-9	40	1	10	1441	33.5
RS9.5C-9	40	1	1	574	36.26
RS9.5C-9	40	1	0.1	220	36.37
RS9.5C-9	4	2	10	12413	10.34
RS9.5C-9	4	2	1	9360	12.64
RS9.5C-9	4	2	0.1	6694	15.88
RS9.5C-9	20	2	10	5873	19.67
RS9.5C-9	20	2	1	3429	25.16
RS9.5C-9	20	2	0.1	1809	30.41
RS9.5C-9	40	2	10	1463	33.31
RS9.5C-9	40	2	1	595	35.61
RS9.5C-9	40	2	0.1	240	34.56

RS9.5C-9	4	3	10	12504	10.31
RS9.5C-9	4	3	1	9499	12.52
RS9.5C-9	4	3	0.1	6908	15.61
RS9.5C-9	20	3	10	6036	19.24
RS9.5C-9	20	3	1	3574	24.48
RS9.5C-9	20	3	0.1	1908	29.62
RS9.5C-9	40	3	10	1464	34.1
RS9.5C-9	40	3	1	581	37.13
RS9.5C-9	40	3	0.1	220	37.15
RS9.5C-10	4	1	10	14530	9.68
RS9.5C-10	4	1	1	11117	11.72
RS9.5C-10	4	1	0.1	8142	14.31
RS9.5C-10	20	1	10	7357	17.67
RS9.5C-10	20	1	1	4488	22.8
RS9.5C-10	20	1	0.1	2500	28.12
RS9.5C-10	40	1	10	2106	31.88
RS9.5C-10	40	1	1	925	35.32
RS9.5C-10	40	1	0.1	361	36.36
RS9.5C-10	4	2	10	14264	9.82
RS9.5C-10	4	2	1	10997	11.83
RS9.5C-10	4	2	0.1	8148	14.65
RS9.5C-10	20	2	10	7155	18.25
RS9.5C-10	20	2	1	4353	23.36
RS9.5C-10	20	2	0.1	2423	28.46
RS9.5C-10	40	2	10	1947	32.28
RS9.5C-10	40	2	1	839	35.47
RS9.5C-10	40	2	0.1	338	35.56
RS9.5C-10	4	3	10	14302	9.44
RS9.5C-10	4	3	1	10997	11.58
RS9.5C-10	4	3	0.1	8127	14.4
RS9.5C-10	20	3	10	7059	18.06
RS9.5C-10	20	3	1	4276	23.43
RS9.5C-10	20	3	0.1	2353	28.7
RS9.5C-10	40	3	10	1869	32.55
RS9.5C-10	40	3	1	795.3	35.44
RS9.5C-10	40	3	0.1	316	35.06

Table 50. Dynamic Modulus Test Results (RI19.0C)

Sample	Temperature (°C)	Specimen Number	Frequency (Hz)	Dynamic Modulus (MPa)	Phase Angle (Degrees)
RI19.0C-1	4	1	10	18260	8.36
RI19.0C-1	4	1	1	14489	10.92
RI19.0C-1	4	1	0.1	10799	14.68
RI19.0C-1	20	1	10	9989	16.68
RI19.0C-1	20	1	1	6267	22.95
RI19.0C-1	20	1	0.1	3425	29.59
RI19.0C-1	40	1	10	2827	33.25
RI19.0C-1	40	1	1	1167	36.65
RI19.0C-1	40	1	0.1	436	35.45
RI19.0C-1	4	2	10	18562	7.83
RI19.0C-1	4	2	1	14886	10.23
RI19.0C-1	4	2	0.1	11247	13.86
RI19.0C-1	20	2	10	10208	16.56
RI19.0C-1	20	2	1	6393	22.82
RI19.0C-1	20	2	0.1	3475	30.04
RI19.0C-1	40	2	10	2926	32.4
RI19.0C-1	40	2	1	1202	35.37
RI19.0C-1	40	2	0.1	424	34.89
RI19.0C-1	4	3	10	19231	7.93
RI19.0C-1	4	3	1	15415	10.32
RI19.0C-1	4	3	0.1	11628	13.99
RI19.0C-1	20	3	10	10467	16.64
RI19.0C-1	20	3	1	6582	22.94
RI19.0C-1	20	3	0.1	3591	29.82
RI19.0C-1	40	3	10	2834	33.39
RI19.0C-1	40	3	1	1145	36.44
RI19.0C-1	40	3	0.1	400	35.73
RI19.0C-2	4	1	10	16224	8.7
RI19.0C-2	4	1	1	12796	11.18
RI19.0C-2	4	1	0.1	9526	14.91
RI19.0C-2	20	1	10	8735	17.42
RI19.0C-2	20	1	1	5425	23.12
RI19.0C-2	20	1	0.1	2900	29.22
RI19.0C-2	40	1	10	2348	32.65
RI19.0C-2	40	1	1	929	35.21
RI19.0C-2	40	1	0.1	318	35.04
RI19.0C-2	4	2	10	16503	8.8
RI19.0C-2	4	2	1	12987	11.42

RI19.0C-2	4	2	0.1	9663	15.38
RI19.0C-2	20	2	10	8728	17.83
RI19.0C-2	20	2	1	5328	24.34
RI19.0C-2	20	2	0.1	2799	31.41
RI19.0C-2	40	2	10	2372	33.89
RI19.0C-2	40	2	1	946	36.07
RI19.0C-2	40	2	0.1	355	33.98
RI19.0C-2	4	3	10	16597	8.5
RI19.0C-2	4	3	1	13052	11.08
RI19.0C-2	4	3	0.1	9636	15.12
RI19.0C-2	20	3	10	8833	17.49
RI19.0C-2	20	3	1	5384	24.17
RI19.0C-2	20	3	0.1	2822	31.63
RI19.0C-2	40	3	10	2305	33.71
RI19.0C-2	40	3	1	890	36.58
RI19.0C-2	40	3	0.1	296	36.76
RI19.0C-3	4	1	10	12938	9.84
RI19.0C-3	4	1	1	9873	12.99
RI19.0C-3	4	1	0.1	7007	17.48
RI19.0C-3	20	1	10	6702	19.35
RI19.0C-3	20	1	1	3896	26.2
RI19.0C-3	20	1	0.1	1951	33.11
RI19.0C-3	40	1	10	1699	32.95
RI19.0C-3	40	1	1	649	34.41
RI19.0C-3	40	1	0.1	225	34.03
RI19.0C-3	4	2	10	13487	9.37
RI19.0C-3	4	2	1	10415	12.44
RI19.0C-3	4	2	0.1	7479	16.88
RI19.0C-3	20	2	10	6598	19.71
RI19.0C-3	20	2	1	3856	26.61
RI19.0C-3	20	2	0.1	1941	33.29
RI19.0C-3	40	2	10	1652	35.65
RI19.0C-3	40	2	1	594	38.49
RI19.0C-3	40	2	0.1	202	36.76
RI19.0C-3	4	3	10	12674	8.87
RI19.0C-3	4	3	1	9938	11.74
RI19.0C-3	4	3	0.1	7206	16.06
RI19.0C-3	20	3	10	6464	19.06
RI19.0C-3	20	3	1	3826	25.83
RI19.0C-3	20	3	0.1	1946	32.59
RI19.0C-3	40	3	10	1592	34.05

RI19.0C-3	40	3	1	597	35.74
RI19.0C-3	40	3	0.1	211	33.78
RI19.0C-4	4	1	10	15919	9.28
RI19.0C-4	4	1	1	12185	12.17
RI19.0C-4	4	1	0.1	8831	16.23
RI19.0C-4	20	1	10	8318	17.99
RI19.0C-4	20	1	1	4999	24.4
RI19.0C-4	20	1	0.1	2654	31.14
RI19.0C-4	40	1	10	2453	31.69
RI19.0C-4	40	1	1	1014	34.09
RI19.0C-4	40	1	0.1	386	32.77
RI19.0C-4	4	2	10	14776	9.46
RI19.0C-4	4	2	1	11406	12.03
RI19.0C-4	4	2	0.1	8272	15.82
RI19.0C-4	20	2	10	7735	18.22
RI19.0C-4	20	2	1	4656	24.58
RI19.0C-4	20	2	0.1	2437	31.27
RI19.0C-4	40	2	10	1948	34.02
RI19.0C-4	40	2	1	760	36.63
RI19.0C-4	40	2	0.1	267	35.82
RI19.0C-4	4	3	10	15641	8.96
RI19.0C-4	4	3	1	12096	11.83
RI19.0C-4	4	3	0.1	8710	15.88
RI19.0C-4	20	3	10	7965	18.62
RI19.0C-4	20	3	1	4746	25.08
RI19.0C-4	20	3	0.1	2455	31.88
RI19.0C-4	40	3	10	1992	34.45
RI19.0C-4	40	3	1	766	37.04
RI19.0C-4	40	3	0.1	262	36.06
RI19.0C-5	4	1	10	17194	8.81
RI19.0C-5	4	1	1	13452	11.52
RI19.0C-5	4	1	0.1	9843	15.61
RI19.0C-5	20	1	10	8799	18.3
RI19.0C-5	20	1	1	5266	25.05
RI19.0C-5	20	1	0.1	2724	31.79
RI19.0C-5	40	1	10	2284	34.56
RI19.0C-5	40	1	1	875	36.86
RI19.0C-5	40	1	0.1	292	35.81
RI19.0C-5	4	2	10	16972	8.84
RI19.0C-5	4	2	1	13192	11.73
RI19.0C-5	4	2	0.1	9573	15.81

RI19.0C-5	20	2	10	8573	18.73
RI19.0C-5	20	2	1	5093	25.34
RI19.0C-5	20	2	0.1	2612	32.08
RI19.0C-5	40	2	10	2185	34.48
RI19.0C-5	40	2	1	829	36.55
RI19.0C-5	40	2	0.1	280	35.06
RI19.0C-5	4	3	10	16144	9.2
RI19.0C-5	4	3	1	12474	12.15
RI19.0C-5	4	3	0.1	9028	16.33
RI19.0C-5	20	3	10	8454	18.51
RI19.0C-5	20	3	1	5031	25.26
RI19.0C-5	20	3	0.1	2577	32.43
RI19.0C-5	40	3	10	2189	34.63
RI19.0C-5	40	3	1	836	36.8
RI19.0C-5	40	3	0.1	286	35.36
RI19.0C-6-1	4	1	10	16630	9.6
RI19.0C-6-1	4	1	1	12737	12.24
RI19.0C-6-1	4	1	0.1	9399	15.52
RI19.0C-6-1	20	1	10	9455	17.51
RI19.0C-6-1	20	1	1	5899	22.47
RI19.0C-6-1	20	1	0.1	3365	27.41
RI19.0C-6-1	40	1	10	2745	31.9
RI19.0C-6-1	40	1	1	1242	34.66
RI19.0C-6-1	40	1	0.1	517	34.31
RI19.0C-6-1	4	2	10	18368	8.84
RI19.0C-6-1	4	2	1	14485	11.08
RI19.0C-6-1	4	2	0.1	10857	14.06
RI19.0C-6-1	20	2	10	9623	16.85
RI19.0C-6-1	20	2	1	6075	22.27
RI19.0C-6-1	20	2	0.1	3525	27.35
RI19.0C-6-1	40	2	10	2876	31.44
RI19.0C-6-1	40	2	1	1305	34.03
RI19.0C-6-1	40	2	0.1	548	33.63
RI19.0C-6-1	4	3	10	18333	8.56
RI19.0C-6-1	4	3	1	14538	10.54
RI19.0C-6-1	4	3	0.1	11014	13.6
RI19.0C-6-1	20	3	10	9267	17.82
RI19.0C-6-1	20	3	1	5775	22.84
RI19.0C-6-1	20	3	0.1	3340	27.39
RI19.0C-6-1	40	3	10	2713	31.37
RI19.0C-6-1	40	3	1	1236	34.07

RI19.0C-6-1	40	3	0.1	503	33.99
RI19.0C-6-2	4	1	10	11968	10.64
RI19.0C-6-2	4	1	1	8930	13.23
RI19.0C-6-2	4	1	0.1	6331	16.73
RI19.0C-6-2	20	1	10	5421	20.84
RI19.0C-6-2	20	1	1	3118	26.03
RI19.0C-6-2	20	1	0.1	1688	30.11
RI19.0C-6-2	40	1	10	1568	32.25
RI19.0C-6-2	40	1	1	652	34.43
RI19.0C-6-2	40	1	0.1	246	35
RI19.0C-6-2	4	2	10	11094	11.36
RI19.0C-6-2	4	2	1	8226	14.26
RI19.0C-6-2	4	2	0.1	5878	17.82
RI19.0C-6-2	20	2	10	5658	20.63
RI19.0C-6-2	20	2	1	3276	25.9
RI19.0C-6-2	20	2	0.1	1758	30.51
RI19.0C-6-2	40	2	10	1582	32.47
RI19.0C-6-2	40	2	1	651	34.82
RI19.0C-6-2	40	2	0.1	246	34.83
RI19.0C-6-2	4	3	10	11357	10.43
RI19.0C-6-2	4	3	1	8521	13.1
RI19.0C-6-2	4	3	0.1	6062	16.43
RI19.0C-6-2	20	3	10	5452	19.97
RI19.0C-6-2	20	3	1	3192	25.08
RI19.0C-6-2	20	3	0.1	1748	29.29
RI19.0C-6-2	40	3	10	1616	30.72
RI19.0C-6-2	40	3	1	714	32.32
RI19.0C-6-2	40	3	0.1	320	31.13

Direct Tension Cyclic Fatigue Test Results

Table 51 and Table 52 present summaries of the direct tension cyclic fatigue test results for the tested RS9.5C samples and tested RI19.0C samples, respectively.

Table 51. Direct Tension Cyclic Fatigue Test Results (RS9.5C)

Sample	Specimen	|E*| Fingerprint (MPa)	DMR	N_f	D^R
RS9.5C-1	1	9029	1.1	25250	0.64
RS9.5C-1	2	8662	1.0	29290	0.64
RS9.5C-1	3	8121	0.9	21170	0.59
RS9.5C-2	1	4900	0.9	8370	0.66
RS9.5C-2	2	4857	0.9	7150	0.65
RS9.5C-2	3	5245	1.0	2320	0.61
RS9.5C-3	1	5638	1.1	7580	0.61
RS9.5C-3	2	5794	1.1	13020	0.71
RS9.5C-3	3	5603	1.1	4170	0.64
RS9.5C-4	1	6220	1.1	11280	0.67
RS9.5C-4	2	6365	1.1	16020	0.70
RS9.5C-4	3	6207	1.0	7140	0.64
RS9.5C-7	1	5659	1.1	5860	0.65
RS9.5C-7	2	5407	1.0	10370	0.67
RS9.5C-7	3	5629	1.1	4260	0.64
RS9.5C-9	1	6367	1.0	14170	0.67
RS9.5C-9	2	6545	1.0	16350	0.68
RS9.5C-9	3	6762	1.1	7400	0.61
RS9.5C-10	1	7198	0.9	17970	0.65
RS9.5C-10	2	7271	0.9	29070	0.66
RS9.5C-10	3	7311	0.9	29370	0.68

Table 52. Direct Tension Cyclic Fatigue Test Results (RI19.0C)

Sample	Specimen	|E*| Fingerprint (MPa)	DMR	N_f	D^R
RI19.0C-1	1	11587	1.05	4620	0.488819
RI19.0C-1	2	11736	1.06	7140	0.436325
RI19.0C-1	3	10588	0.96	12180	0.440411
RI19.0C-2	1	9775	1.04	3380	0.442962
RI19.0C-2	2	10153	1.07	5090	0.501296
RI19.0C-2	3	10558	1.12	6400	0.524595
RI19.0C-3	1	7007	0.99	3620	0.459078
RI19.0C-3	2	7742	1.09	15330	0.449944
RI19.0C-3	3	7462	1.06	7500	0.368036
RI19.0C-4	1	8744	1.01	2260	0.519217
RI19.0C-4	2	9391	1.08	32120	0.410045
RI19.0C-4	3	8986	1.04	16260	0.478213
RI19.0C-5	1	9228	0.99	13090	0.445095
RI19.0C-5	2	9631	1.03	12030	0.480911
RI19.0C-5	3	9616	1.03	19600	0.445314
RI19.0C-6-1	1	9704	0.95	6890	0.525719
RI19.0C-6-1	2	9637	0.94	3400	0.598697
RI19.0C-6-1	3	10411	1.02	3410	0.600281
RI19.0C-6-2	1	6573	1.12	4400	0.633881
RI19.0C-6-2	2	6053	1.03	2480	0.631572
RI19.0C-6-2	3	5918	1.01	17470	0.561838

Stress Sweep Rutting Test Results

Table 53 and Table 54 present summaries of the stress sweep rutting test results for the tested RS9.5C samples and tested RI19.0C samples, respectively.

Table 53. Stress Sweep Rutting Test Results (RS9.5C)

Sample	Specimen	Temperature (°C)	Cycle	Permanent Strain
RS9.5C-1	1	29	600	0.0032
RS9.5C-1	2	29	600	0.0036
RS9.5C-1	3	50	600	0.0116
RS9.5C-1	4	50	600	0.0128
RS9.5C-2	1	29	600	0.0086
RS9.5C-2	2	29	600	0.0082
RS9.5C-2	3	50	600	0.0659
RS9.5C-2	4	50	600	0.0527
RS9.5C-3	1	29	600	0.0085
RS9.5C-3	2	29	600	0.0068
RS9.5C-3	3	50	600	0.0473
RS9.5C-3	4	50	600	0.0450
RS9.5C-4	1	29	600	0.0056
RS9.5C-4	2	29	600	0.0054
RS9.5C-4	3	50	600	0.0259
RS9.5C-4	4	50	600	0.0258
RS9.5C-7	1	29	600	0.0065
RS9.5C-7	2	29	600	0.0077
RS9.5C-7	3	50	600	0.0406
RS9.5C-7	4	50	600	0.0403
RS9.5C-9	1	29	600	0.0049
RS9.5C-9	2	29	600	0.0047
RS9.5C-9	3	50	600	0.0230
RS9.5C-9	4	50	600	0.0214
RS9.5C-10	1	29	600	0.0041
RS9.5C-10	2	29	600	0.0047
RS9.5C-10	3	50	600	0.0183
RS9.5C-10	4	50	600	0.0202

Table 54. Stress Sweep Rutting Test Results (RI19.0C)

Sample	Specimen	Temperature (°C)	Cycle	Permanent Strain
RI19.0C-1	1	26	600	0.0023
RI19.0C-1	2	26	600	0.0023
RI19.0C-1	3	46	600	0.0090
RI19.0C-1	4	46	600	0.0085
RI19.0C-2	1	26	600	0.0023
RI19.0C-2	2	26	600	0.0026
RI19.0C-2	3	46	600	0.0128
RI19.0C-2	4	46	600	0.0128
RI19.0C-3	1	26	600	0.0036
RI19.0C-3	2	26	600	0.0041
RI19.0C-3	3	46	600	0.0276
RI19.0C-3	4	46	600	0.0256
RI19.0C-4	1	26	600	0.0032
RI19.0C-4	2	26	600	0.0028
RI19.0C-4	3	46	600	0.0177
RI19.0C-4	4	46	600	0.0175
RI19.0C-5	1	26	600	0.0030
RI19.0C-5	2	26	600	0.0030
RI19.0C-5	3	46	600	0.0169
RI19.0C-5	4	46	600	0.0151
RI19.0C-6-1	1	26	600	0.0024
RI19.0C-6-1	2	26	600	0.0022
RI19.0C-6-1	3	46	600	0.0061
RI19.0C-6-1	4	46	600	0.0067
RI19.0C-6-2	1	26	600	0.0046
RI19.0C-6-2	2	26	600	0.0055
RI19.0C-6-2	3	46	600	0.0178
RI19.0C-6-2	4	46	600	0.0161